

Superconducting Magnets for CLAS12

R. Fair^{a,1}, R. Banchimanchi^a, G. Biallas^b, V. Burkert^a, L. Elouadrhiri^a, P. K. Ghoshal^a, J. Hogan^a, D. Kashy^a, R. Legg^a, C. Luongo^c, J. Matalevich^a, J. Meyers^a, O. Pastor^c, S. Philip^a, R. Rajput-Ghoshal^a, N. Sandoval^a, S. Spiegel^a, M. Wiseman^a, G. R. Young^b

^aThomas Jefferson National Accelerator Facility, Newport News, VA, 23606, USA

^bThomas Jefferson National Accelerator Facility, Newport News, VA, 23606, USA (Retired)

^cInternational Thermonuclear Experimental Reactor Organization (ITER), St. Paul-lez-Durance 13067, France.

ARTICLE INFO

Keywords:

Superconducting, magnets, torus, solenoid, quench, mapping , toroid

ABSTRACT

As part of the Jefferson Lab 12 GeV upgrade, the Hall B CLAS12 system requires two superconducting iron-free magnets – a torus and a solenoid. The Physics requirements to maximize space for the detectors guided engineers towards a particular coil design for each of the magnets which in turn led to the choice of using conduction cooling methodology. The Torus consists of 6 trapezoidal NbTi coils connected in series with an operating current of 3770 A. The Solenoid is an actively shielded 5 Tesla magnet consisting of 5 NbTi coils connected in series operating at 2416 A. Within the hall, the two magnets are located in close proximity to each other and are completely covered both inside and outside by particle detectors. Stringent size limitations were imposed for both magnets and introduced particular design and fabrication challenges. This paper describes the design, construction, installation, commissioning and finally operation of the two magnets.

¹ The Manuscript received XXXXXX.

This work was supported by Jefferson Science Associates, LLC, under U.S. DOE Contract DE-AC05-06OR23177. The U.S. Government retains a non-exclusive, paid-up, irrevocable, world-wide license to publish or reproduce this manuscript for U.S. Government purposes.

R. Fair, R. Banchimanchi , G. Biallas, V. Burkert, L. Elouadrhiri, P. K. Ghoshal, J. Hogan, D. Kashy, R. Legg, C. Luongo, J. Matalevich, J. Meyers, O. Pastor, S. Philip, R. Rajput-Ghoshal, N. Sandoval, S. Spiegel M. Wiseman, G. R. Young

Corresponding author: R Fair (e-mail: XXXX@jlab.org)

Color versions of one or more of the figures in this paper are available online at XXXXXXXX

Digital Object Identifier (inserted by Publisher)

I. PHYSICS REQUIREMENTS AND TECHNICAL SPECS

Tables I and II summarize the Physics requirements for the Torus and Solenoid superconducting magnets respectively **Figure 1 [1]**, while **Table III** provides a summary of the key design parameters for the two magnets.

TABLE I
CLAS12 HALL B - TORUS PHYSICS REQUIREMENTS

Parameters	Requirement
Angular coverage	$\Theta = 5^\circ - 40^\circ$ $\Delta\Theta = 50\text{-}90\%$ of 2π
$ B _{dl}$ @ nominal current	2.83 T.m @ $\Theta = 5^\circ$ 0.6-1.0 T.m @ $\Theta = 40^\circ$
No obstruction sideways	Open access to field volume
Uniformity of B-field in Θ	Limit distortions from toroidal field

TABLE II
CLAS12 HALL B – SOLENOID PHYSICS REQUIREMENTS

Parameters	Requirement
B_0	5T
$L=1/B_0 B _{dl}$	$L = 1$ to 1.4 m
Field Uniformity in Target Area	$\Delta B/B_0 < 10^{-4}$ in cylinder 0.04 m length x 0.025 m (100 ppm)
Field at HTCC PMTs location	$B < 35$ Gauss (for the four HTCC PMT locations)
Field at TOF PMTs location	$B < 1200$ Gauss (for the two TOF PMT locations)

TABLE III
CLAS12 HALL B - SOLENOID AND TORUS MAGNET PARAMETERS

PARAMETER	DESIGN VALUE	
	SOLENOID	TORUS
Number of Coils	4 + 1	6
Coil structure	Layer wound	Double Pancake potted in Aluminum Case
Total Number of turns	5096 (2 x 840 + 2 x 1012+1392)	1404 (117 x 2 x 6)
NbTi Rutherford cable	SSC 36 strands	SSC 36 strands
Nominal current (A)	2416	3770
Central field (T)	5	N/A
Conductor Peak Field (T)	6.56	3.6
Field homogeneity in $\phi 25\text{mm} \times L 40\text{ mm}$ cylinder	1×10^{-4}	N/A
Inductance (H)	5.89	2
Stored Energy (MJ)	17	14
Warm bore (mm)	780	124
Outer Diameter x Length	2.16 m x 1.8 m	N/A
Inner bore length /opening angle	0.897 m/ 41°	N/A
Coil Case thickness	-	Originally 100mm changed to 125mm
Total weight (KG)	18800	25,500
Cooling mode	Conduction cooled	Conduction cooled
Supply temperature (K)	4.5	4.5
Temperature margin	1.5	1.5
Stabilized conductor	W17 mm x T2.5 mm copper channel	W20 mm x T2.5 mm copper channel
Turn to Turn Insulation	0.004" Glass Tape ½ Lap	0.003" Glass Tape ½ Lap
Heat Shield Cooling	Helium boil-off	LN2 Thermo-Siphon

The torus magnet, its service tower (TST) and cryogenic distribution box were designed and assembled at Jefferson Lab (JLab) while the coils were fabricated at the Fermi National

Accelerator Laboratory (FNAL), USA [2,3]. It provides a bending field for high energy (>1.5 GeV to 8GeV) charged particles and mechanical support for 3 regions of drift chambers. The solenoid magnet was designed and fabricated by Everson Tesla Inc., USA (ETI), while its service tower (SST), and cryogenics were designed and fabricated by JLab. The magnet provides a field to bend low energy (400MeV to 1.5 GeV) energy charged particles. The field also provides focusing and shielding for Moeller electrons which allows the detector system to run at high data rates. A homogeneous field at the magnet center is needed for Polarized targets. The magnets differ in their cooling schemes from that of more conventional bath-cooled superconducting magnets by using conduction-cooling methodology in order to comply with tight physical space requirements. These requirements imposed certain size limitations on the design of the torus and solenoid magnet coils, which led to each magnet having their own unique issues for design, fabrication and installation. Leftover superconductor from the Superconducting Super Collider (SSC) project (which was terminated in 1993) was modified by soldering into a copper channel and then used to wind the coils for the torus and solenoid.

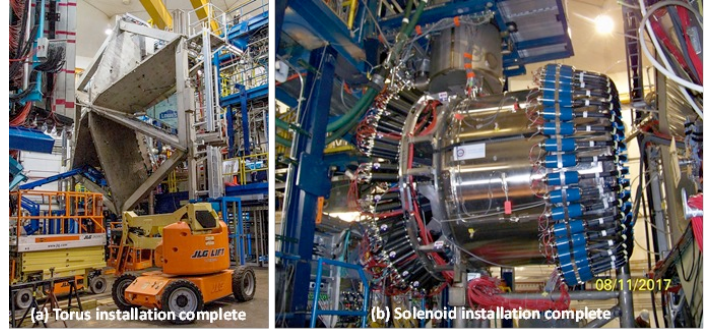


Fig.1 Magnets installed in Hall B – (a) Torus (before drift chambers are installed between the coils), (b) Solenoid (with some detectors installed)

II. RISK MITIGATION

All critical tasks for both the magnet systems were subjected to a detailed Risk Assessment and Mitigation (RAM) process. The process was used to evaluate the overall magnet design and the robustness of its protection system and commissioning process. The magnet risk assessments were developed via a series of electromagnetic and electromechanical analyses which included induced eddy currents, Lorentz forces, thermal loading, magnet-to-magnet interactions and an assessment of magnet performance while in proximity to ferromagnetic structures. A Magnet Task Force was formed to pool critical resources and skills at the laboratory. The risk mitigation approach was based on a Failure Modes and effects Analysis (FMEA) carried out for each phase of the project: design, fabrication, installation, and commissioning [4]. FMEA is a tool used to eliminate or mitigate known potential failures, problems, and errors within systems. A failure mode is defined as the way a component could fail to meet its performance requirements or to function. More than 400 risk items were identified, categorized, and ranked; mitigation avenues were investigated for all risks, and implemented when warranted, either because the risk was deemed to be high, or implementation was easily achieved.

The potential failure modes are evaluated based on a Risk Priority Number (RPN) which is the product of three factors: the Severity ranking (S), the probability of Occurrence (O), and the probability of Detection (D). The RPN is used as a measure of overall risk and helps to identify and rank the risks of the potential failure modes. The end results of failures that lead to unsafe conditions or significant losses in functionality are rated high in severity. Larger RPNs indicate the need for corrective action or failure resolution. The FMEA process was used to assist in identifying potential failure modes early in the design phase.

Several of the key risks for the torus and solenoid (indicated by larger RPNs) are listed below and were addressed during the project:

- The system does not satisfy the physics requirements
- Defects in the build and manufacture of thermal insulation (e.g. standoffs, multi-layer insulation)
- Insufficient Helium mass flow in the cooling channel
- Vacuum vessel cannot maintain required vacuum
- Break down of the electrical insulation of magnet system
- Loss of control of the magnet power supply system
- Loss of magnet protection due to a fault in the quench detection and protection system

Some of the mitigation actions stemming from the FMEA included:

- Extensive use of mock-ups and practice builds for all quality-critical activities (e.g. conductor soldering into channel, conductor splices, distortion of vacuum jackets during welding, connection of hex beams to coils, mounting of instrumentation)
- Development of written procedures, before and in conjunction with the practice builds
- Safety and risk-awareness meetings prior to each critical operation
- Extensive use of in-process quality assurance (QA) checks
- Detailed weekly and daily planning of installation activities in the hall
- Vendor oversight by JLab staff

Safety reviews as well as Director's Reviews and Department of Energy Reviews played a crucial role in developing the RAM process at JLab. Safety Reviews in particular comprise two key sub-reviews - Pressure System Reviews (a check against relevant design codes like ASME and to that ensure all relevant documentation is in place), and Experimental Readiness Reviews (Cooldown and Power-up reviews) before the magnet systems are signed over to the Physics Division for operation.

III. DESIGN AND ANALYSIS

The coils for the two magnets utilize surplus Superconducting Super Collider (SSC) outer dipole conductor consisting of 36 strands of 0.6 mm diameter multi-filamentary NbTi superconductor with a Cu:Sc ratio of 1.8 : 1, manufactured as a flattened Rutherford cable and soldered into a nominally dimensioned 2.5 mm × 20 mm OFHC copper channel for the torus and a 2.5mm x 17 mm channel for the solenoid (Figure 2 and Table IV). This Rutherford conductor had been in storage for many years, so sample lengths of conductor from each spool were tested to check for any degradation in performance. The

superconductor for the magnets has a tested short sample performance of better than 11000 A at 4.2 K at 5 T and showed no discernable degradation when compared to its original specifications.

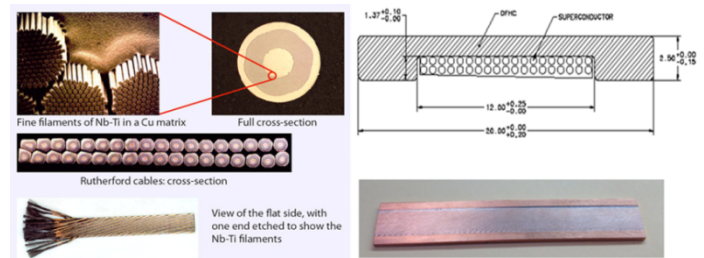


Fig 2 SSC Outer Dipole NbTi Rutherford Cable and cross-sectional view of the conductor with critical dimensions

TABLE IV
TORUS CONDUCTOR SPECIFICATION

Parameter	Details
Rutherford type of cable (Superconductor)	NbTi
Conductor material (NbTi + Cu)	Cu-(NbTi) in Cu Channel
Number of strands in the cable	36
Number of NbTi filaments in each strand	4600
Strand bare diameter (mm)	0.648
Copper to non-Copper ratio	1.8
Twist pitch (mm)	15
Conductor size (bare) (mm x mm)	20 x 2.5
Conductor size (insulated) (mm x mm)	20.2 x 2.7
Short sample current at 4.22 K, 5 T (kA)	11
RRR Cu (Cu-NbTi) – Strand	100
RRR Cu Stabilizer (design purpose)	200 (70)

TORUS

Torus Magnet design

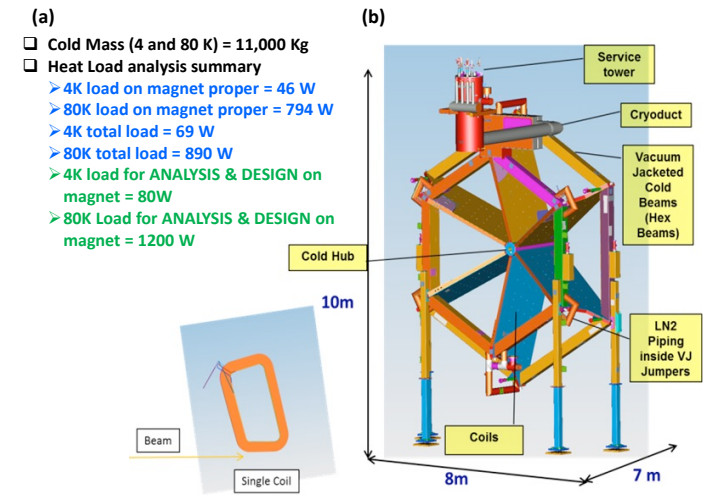


Fig 3 The Torus Magnet (a) Design heat loads, (b) Key features and dimensions

The torus magnet has 6 double-pancake coils wound with copper-stabilized NbTi Rutherford cable, which are then vacuum impregnated with epoxy, wrapped with copper cooling sheets, assembled in aluminum cases and then repotted, to produce a coil cold mass (CCM) which will operate at 4.5 K. Pre-formed multi-layer insulation (MLI) blankets are then fitted to each CCM. Aluminum thermal shields, (cooled to 80 K by a liquid nitrogen thermo-siphon), are installed around each CCM before

themselves being covered with additional MLI blankets. The whole assembly is enclosed within a stainless steel vacuum jacket which is welded shut. The 6 independent CCMs are mechanically held together at a cold hub positioned along the axis of the torus. The CCMs are connected to each other on their outer extremities via 12 hex beams operating at 4.5 K. There are two hex beams per sector, upstream and downstream (Figure 3). The six coils are electrically connected in series using soldered joints or splices. A liquid filled (4.5 K, 1.4 atmosphere) helium re-cooler is mounted to each upstream beam, to which the conduction-cooled inter-coil splices are anchored. All six coils share a common vacuum space with two vacuum pumping systems being operated continuously - at the top and bottom of the torus magnet.

Torus Superconducting Coil Design

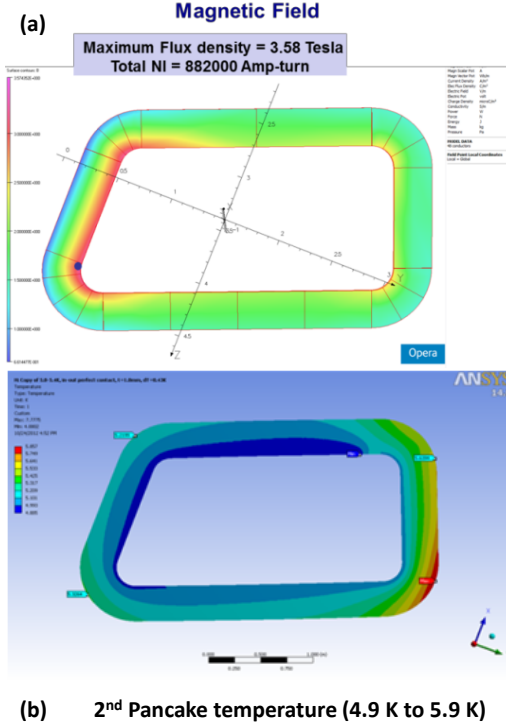


Fig 4 (a) Magnetic field distribution on torus coil surface with magnet at 3770 A, (b) Steady state temperature distribution on torus coil surface (assuming 3x design heat load)

The Torus magnet coils generate a toroidal magnetic field. Figure 4a illustrates the magnetic field distribution on the coil surface. The peak field of 3.6 T is located at the coil inner surface and at a small radius. The magnetic flux density is about two times lower at the coil's outer radius. Figure 4b indicates the temperature distribution across the coil, the 'warmest' part of coil having the highest thermal radiation heat load near the lead exit due to the extended surface of the coil case at the hex rings.

Figure 5 summarizes the performance of the superconducting Rutherford cable used for both the torus and solenoid magnets in the form of a set of critical current curves at varying operating temperatures. The load lines for the torus and solenoid magnets are displayed as straight lines labeled I_{coil} .

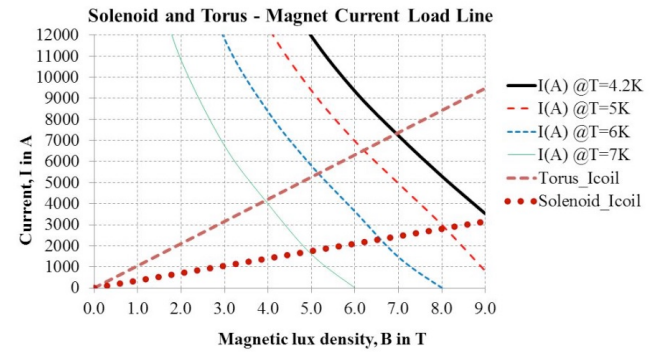


Fig.5 Superconducting Rutherford cable critical current – Solenoid and torus magnet load lines (I_{coil})

TABLE V
SUMMARY OF TORUS CONDUCTOR STABILITY ASSESSMENT [9]

Operating Scenario (Hall B Torus)		
Conductor temperature T_{top} (K)	5.3	K
Maximum field in the coil B_{max} (T)	3.58	T
Operating current I_{top} (A)	3770	A
I_c (at B_{max}) (A) at T_{top}	9836	
Summary		
Short sample performance (SSP)	< 40%	38.33%
Stable for T_{cs} value (Margin)	Yes	> 1.5 K
Stable for Beta (Adiabatic stability)	Yes	
Adiabatic flux jump stability	Yes	
Dynamic stability	Yes	
Adiabatic self-field stability	Yes	
Stable in term of twist pitch	Yes	
Stable for finite element size	Yes	

As can be seen from Figure 5 and Table VI, the torus coil design has a more than adequate temperature margin ΔT which in all cases exceeds the usual design guidance of 1.5 K, strongly suggesting that the magnet coils are somewhat tolerant of temperature variations.

TABLE VI
TORUS MAGNET MARGIN AND SSP

Case	B_{max} (T)	I_c (at B_{max}) (A) at T_{top}	I_{top} (A)	% SSP	T_{top} (K)	T_c (K)	T_g (K)	ΔT (K) = $T_g(K) - T_{top}(K)$
1	3.58	12076		31.22	4.7	7.86	6.87	2.17
2	3.58	11332		33.27	4.9	7.86	6.88	1.98
3	3.58	9836	3770	38.33	5.3	7.86	6.88	1.58
4	3.58	9285		40.60	5.3	7.86	6.82	1.52
5	1.5	11467		32.88	5.9	8.75	7.81	1.91

The magnet coils are protected via an externally-located dump resistor which is permanently connected across the magnet terminals. This resistor has a center tap which then feeds a ground-fault indicator. The presence of this center tap produces an expected maximum voltage during a typical quench scenario of 250 V. However, in the unlikely event that the center tap is lost, the voltage across the magnet terminals could increase to a peak of 500 V and this value together with a safety factor was used to determine the overall recipe for the coil turn insulation, pancake-to-pancake insulation and the Turn-to-Ground insulation (Figure 6 and Table VII). A similar approach was used to define the solenoid coil insulation.

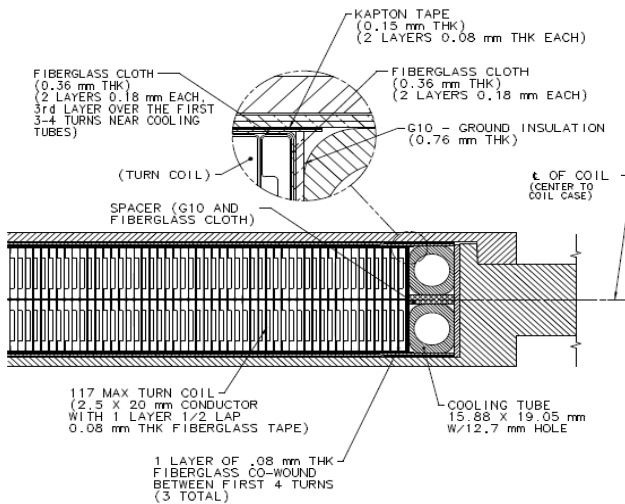


Fig. 6 Construction detail for the Torus coils, showing conduction cooling mechanism and coil winding details. The coil cross section inside of the aluminum case is 353 x 45 mm.

TABLE VII
TORUS COIL ELECTRICAL INSULATION BREAKDOWN VOLTAGE [5]

Material	E-Glass with Epoxy Thickness (mm)	G10 Thickness (mm)	Kapton Thickness (mm)
Insulation Region			
Turn to Turn Insulation (T-T)	0.3048	0	0
Turn to Turn Insulation (P-P)	0.3048	0.38	0
Turn to Ground (GND)	0.508	0	0.1524
Location	Turn to Turn	Pancake-Pancake	Turn to GND
Breakdown Voltage (kV)- Calculated	7.01	15.75 kV	21.74 kV
Factor of safety	10	10	5
Breakdown voltage (kV) with Safety factor used for design	0.7	1.58	2.17
Torus Magnet 12GeV (V) expected	< 10	< 120	< 250 (500*)

* Rare fault case resulting in 500V

Additional analyses were carried out to ensure that the coil pack and coil case stresses were within acceptable limits during normal operation (Table VIII) [5],[6-10].

TABLE VIII
TORUS STRESS SUMMARY

Component	Primary Limit (MPa)	Primary + Secondary Limit(MPa)	EM+Gravity		Cooldown+EM	
			Peak	General	Peak	General
Case	184	552	350	70	380	300
Cover	184	552	130	45	430	350
Conductor	94	282	-	68	-	-181
Coil Pack Shear	15	45	5	13	40	20
Coil Pack Radial	94	282	-	-30	-	-120

Primary stresses were limited to the lesser of 2/3 times the yield strength or 1/3 times the ultimate tensile strength. Primary plus secondary stresses were limited to 3 times the primary stress allowable.

Torus Splice Design

The magnet consists of six trapezoidal (race track) coils connected in series, with an operating current of 3770 A. The

magnet coils are cooled by 4.6K supercritical helium whereas the joints connecting the coils (splices) are all conduction cooled by 4.6 K liquid helium.

The key drivers for the splice design were minimization of contact resistance and quench protection. All conductors which are not within the main coil winding, (splices between the individual superconducting magnet coils, between coils and current leads and long runs of superconducting bus bar), have additional copper stabilizer to manage temperature rises during a quench event. The conductor that exits the coil case also has stabilizer that runs to the outermost turn of each pancake. To design a ‘quench-tolerant’ splice, the amount of copper has to be large enough to minimize peak temperatures during a quench event but also small enough to allow the development of a resistive voltage that can be detected and used to trip the fast dump interlocks to prevent the superconductor from burning out. This ‘balancing act’ is a critical part of the design of the quench protection system of any superconducting magnet. The Oxygen Free High Conductivity (OFHC) copper stabilizer bars, extend over the entire splice length and are soldered to the assembly in the same operation that solders the splice.

The splice has been designed for low temperature operation at about 5 K to allow for some margin. Each splice was required to have a resistance of no higher than $7 \times 10^{-9} \Omega$ thus imposing a joule heating limit of no more than 100 mW, (based on CERN design criteria for the superconducting magnets on the Large Hadron Collider). This corresponds to operation at 3770 A at 4.6 K and in magnetic fields in the region of 0.3 T (to allow for the magnetoresistance effect). The splice was cooled via copper braids soldered to the helium re-cooler units located inside the upstream cold hex beams. The splice design was also constrained by the available space on the re-cooler units and electrical insulation requirements (similar to the coils).

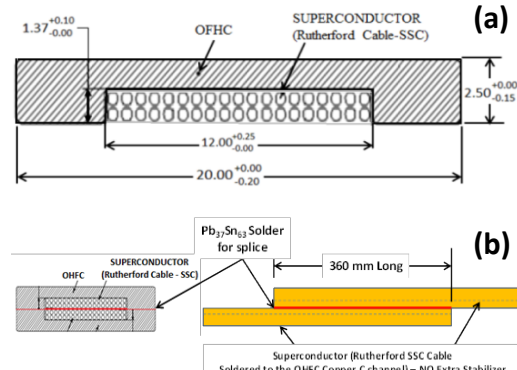


Fig. 7 (a) Torus conductor - SSC outer cable soldered into copper channel (Dimensions in mm), (b) Typical layout of the test splice for joint resistance evaluation (without additional copper stabilizer)

The key risk to the joint is the lack of even solder distribution and the creation of voids within the solder & between the cables being joined. The cables are placed with the SSC cables facing each other and the keystone edges of the mating conductors lying on opposite sides of the joint to ensure a minimum gap between the cables. Several splice mock-ups were made and destructively tested to qualify the fixture and fabrication procedure. A portion of the lip of the copper channel along the mating surfaces of the two conductors was removed to reduce

the likelihood of void formation since the groove in the channel is deeper than the thickness of the Rutherford cable (Figure 7).



Fig 8 (a) Temperature controlled Aluminum block splicing rig. Cut-outs in the side of the rig allowed for visual inspection of solder flow, (b) Splice mock-up end-on view of the sectioned splice cut lengthwise showing void free construction. NbTi strands and solder can be seen in the copper matrix. Outer-wrap is Polyimide film and epoxy.

$\text{Sn}_{60}\text{Pb}_{40}$ solder was used to bond the Rutherford cable into the copper channel. It has a liquidus of 188 °C to 190 °C (and melts above 200 °C). Soft solder paste $\text{Sn}_{63}\text{Pb}_{37}$ (with an eutectic melting point of 183 °C) was used for the splice. Delamination of the Rutherford cable from the copper channel was avoided by careful control of the temperature during the soldering process using thermocouples for monitoring. The design of the soldering rig shown in Figure 8 included open zones for direct viewing of the conductors during soldering which allowed visual inspection of solder flow during the splicing operation.

The insulation system is designed to accommodate a 2.5 kV standoff to Ground using polyimide film and a minimum tracking length of 1/2 inch. For improved thermal performance, any physical gaps in the assembly are filled with two-part blue Stycast 2850 FT epoxy. The assembly was Hi-Pot tested to 1 kV in air to validate electrical isolation and integrity.

Test splices with 360mm long soldered joints were prepared at JLab and critical current (I_c), n-value and V-I data measurements were carried out at the University of Durham, UK up to 2000 A in one of two 15 T magnet systems (Table IX). With the limitation of the measurement set up to accommodate the length of the splice in the magnet, the resistance across the splice was also measured at a lower current and in an elevated magnetic field at LHe temperature. This measurement was carried out in order to characterize splices that would be located in higher fields (up to 4 T) for the Hall B solenoid magnet system which employs similar conductor and splices. Typical resistances measured for sample DR4686 are given in Table X.

TABLE IX

Critical Current and n-value Data for JLab Splice Sample# DR4562

Critical Current data			
E field Criteria	10.5 T	10.0 T	9.5 T
100 $\mu\text{V/m}$	254 A	851 A	1708 A
10 $\mu\text{V/m}$	165 A	656 A	1415 A
n-Value			
10-100 $\mu\text{V/m}$	5	9	12

TABLE X

Resistance Measured for DR4686 at Varying Magnetic Field at 4.2 K

Joint Length (mm)	Field at field Centre (T)	Field at the top of the joint (T)	Joint resistance ($\times 10^{-9} \Omega$)
260	0	0	≤ 0.1
	0.5	0.13	0.70
	1	0.25	0.66
	2	0.50	0.68

	3 4	0.75 1	0.68 0.7
--	--------	-----------	-------------

The resistance of the splices measured at elevated magnetic fields was less than 1 nΩ in LHe (4.2 K), the maximum allowed was 7.0 nΩ.

Torus Quench Protection

Various quench scenarios were analyzed utilizing the Vector Fields (Cobham) quench codes which incorporate the ELEKTRA 3D (transient analysis) and TEMPO 3D (thermal analysis) software modules. The analyses involved the examination of eddy currents generated within the coils themselves as well as nearby electrically-conductive components such as the aluminum coil cases and aluminum thermal shields and any subsequent forces produced by these eddy currents (Figure 9). These generated eddy currents can produce a phenomenon known as ‘quench-back’ – i.e. the eddy currents produce a heating effect which then reflects back into the superconducting coils thus speeding up the quenching of coils – in effect providing a secondary form of quench protection.

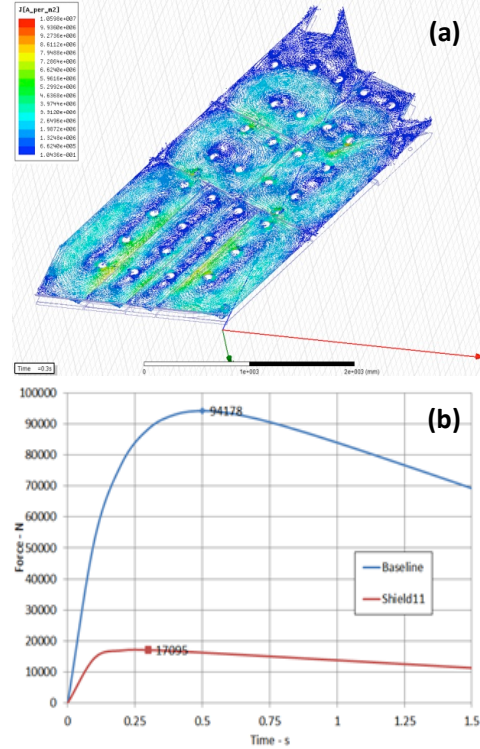


Fig 9 Torus segmented thermal shield performance during quench event – (a) current density vector plot, (b) Force reduction due to segmented shield design

The torus magnet is protected via an externally-located dump resistor which is permanently connected across the magnet terminals. This resistor has a center tap which then feeds a ground-fault indicator (Figure 10). Quench detection is via voltage taps located at either side of the splices between coils, thus allowing voltage detection across individual coils, splices and long runs of bus bar.

At the operating current of 3770 A and with a total inductance of about 2 H, the torus magnet has a stored energy of 14.2 MJ. With the 0.124 Ω dump resistor in circuit, any current decay under non-quench conditions will have a time constant of 16.7 seconds. It should be noted that during a quench event, nonlinear

superconductor normal zone growth and induced eddy currents in the aluminum cases and shields will decrease the effective discharge time due to the increase in effective resistance in the overall magnet circuit.

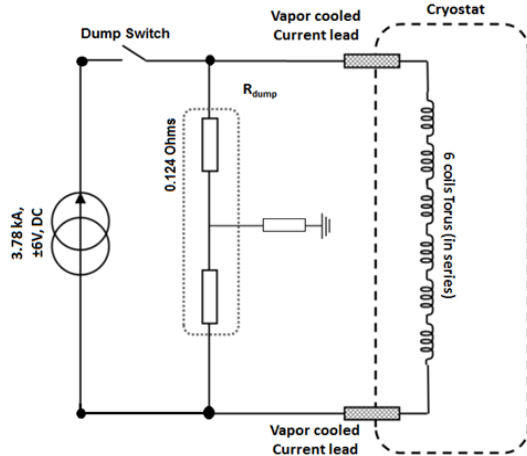


Fig. 10 Torus Magnet Protection Circuit

TABLE XI
TORUS - ANALYZED QUENCH AND NORMAL OPERATING SCENARIOS

	Quench Scenario	Observed Results	Mitigation
1	Normal magnet current decay from 3770 A with dump resistor connected across magnet terminals	The magnet system's 'normal' decay via the dump resistor (i.e. with-out a quench) will initiate a "quench back" after about 0.3 s which will then cause all the coils to quench. The thermal shield can experience high forces due to the induced eddy currents during a quench.	This has been mitigated at the design stage by slotting or segmenting the shield in multiple locations and using a combination of two different grades of aluminum in its construction – one to preserve mechanical strength and the other to improve thermal conductivity. Bumpers between the shield and the coil case and vacuum jacket have also been incorporated in the design. The segmentation of the shields reduces the current density from 9.5×10^6 to 2.5×10^6 A/m ² , with a corresponding reduction of out-of-plane forces from 94 kN to 17 kN.
2	One coil quench from 3770 A with full stored energy being dissipated amongst all 6 coils	Coil peak hot spot temperature = 53 K	None necessary as typical conservative design guidelines limit this peak hot spot temperature to no higher than 150 K
3	One coil quench from 3770 A with full stored energy being dissipated in only one coil	Coil peak hot spot temperature = 75 K	None necessary as typical conservative design guidelines limit this peak hot spot temperature to no higher than 150 K
4	A short in one coil which then causes the coil to quench (includes thermal stresses from cooling (395 K to 4 K), Lorentz forces due to a quench resulting from a single coil to ground short, and 110% gravity loading).	A single coil short followed by a quench will disrupt the symmetry of the magnetic field which can result in out-of-balance forces between the coils. The out of plane load generated by this load case is ~129 kN.	Damage to the cold mass that potentially could be caused by these non-symmetric forces has been mitigated by incorporating "coil case-vacuum vessel" bumpers. The vacuum vessel has also been designed to be capable of withstanding these forces.
5	Cool down stresses from 395 K to 4 K (includes stresses due to epoxy curing at 122°C).	The results from this analysis suggest that the coils are preloaded (compression) at room temperature. All stresses due to cool down are secondary stresses (self-limiting). Refer Table IX.	
6	Normal operation (includes cool down stresses from 395K to 4 K, Lorentz forces due to energization and 110% static gravity loading to allow for earthquake loads). Assumes perfect coil symmetry with no out of plane forces due to electromagnetic loads.	The stresses from this load case are both primary (EM and gravity) and secondary (cool down). Refer to Table VIII.	
7	Current imbalance (includes thermal stresses from cooling (395 K to 4 K), Lorentz forces due to a current imbalance condition, and 110% gravity loading). The current imbalance includes Lorentz forces from a 10% reduction of current (equivalent to losing ~12 turns in each pancake) in a single coil.	This current imbalance generates a ~70 kN out of plane force on the coil. This analysis is also used to verify stresses due to out of plane EM forces resulting from imperfect coil locations. The maximum out of plane force due to imperfect coil locations is ~7kN.	

Quenches normally start from the peak magnetic field region within a coil, (which is the inner coil surface for the torus), and then propagate through the coil to the outer radius causing the current in the series-connected coils to decay very rapidly. This rapid current decay in turn induces large eddy currents and therefore large forces in the aluminum coil cases and thermal shields. Initial analysis suggested that the forces on the thermal shield would cause excessive deflection and permanent bending of the shield. Multiple iterations of segmentation were analyzed to reduce the eddy currents developed during a quench. Figure 9a shows the final segmentation employed for the shield and Figure 9b shows the total force on the shield. The segmentation reduced the force by a factor of more than 5.0 [11].

The quench and normal operation scenarios analyzed, observed results and mitigating actions are summarized in Table XI [5,12].

SOLENOID

Solenoid Magnet design

The solenoid is an actively shielded 5 Tesla magnet designed and built by Everson Tesla Inc. (ETI) Pennsylvania, USA. The solenoid magnet has five coils in series (also wound with copper-stabilized NbTi Rutherford cable but with a slightly narrower copper channel, 17mm instead of 20mm as for the Torus); two main inner coils (Coils 1 and 2) shrunk-fit inside a thick-walled stainless steel bobbin, another two intermediate coils (Coils 3 and 4) wound into separate pockets milled into the outer surface of the same bobbin and one long thin shield coil (**Figure 11**). The shield coil is wound onto its own bobbin but electrically connected in reverse to the other four coils as an “active shield” to limit the extent of the stray field. This is important as there are many detectors mounted in close proximity to the solenoid which are sensitive to magnetic field (**Figure 12**). Using two split-pair coils and one solenoidal coil allowed the required field strength and homogeneity to be obtained in a compact magnet volume that also satisfied the placement and location of the various Physics detector packages [13].

All coils are supported via 8 radial and 8 axial supports and are conduction-cooled via copper cooling strips, which are potted with the coils and connected to a centrally located annular helium cooling channel. The magnet is cooled by a helium thermo-siphon connected to the magnet reservoir. Gas generated by the magnet is used to cool the thermal shield before being exhausted via the Solenoid Service Tower (SST).

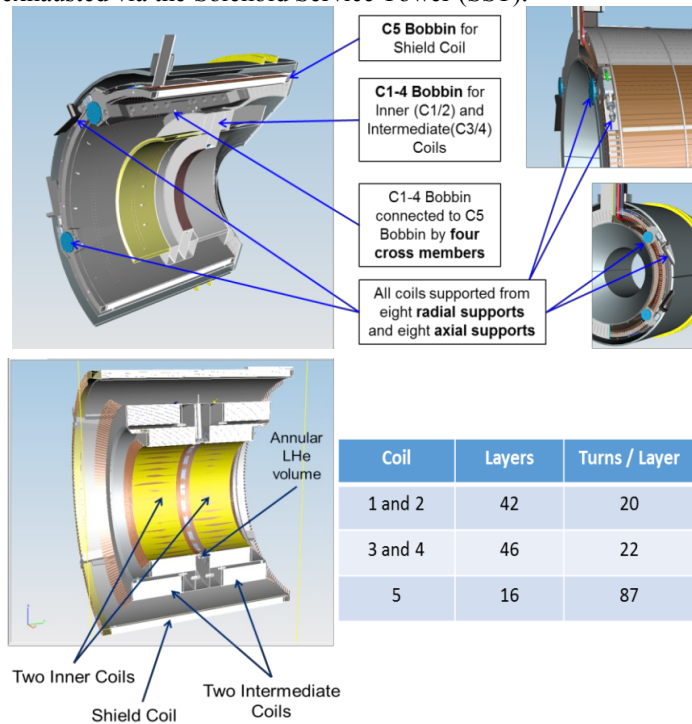


Fig. 11 Cross-sectional views of the internal construction of the solenoid together with the coil winding details

Coils “sticking and slipping” against their formers during current ramp-up, can cause spurious quenching, and necessitated

the incorporation of slip planes consisting of Kapton and Mylar sheets placed between Coils 3,4 and 5 and their respective bobbins to mitigate this problem. Forces and stresses encountered within the thermal radiation shield during quench events have been mitigated by slotting the shield. Temperature margins for each coil were quantified and resulted in improvements to the design and operation of the overall cryogenic cooling scheme.

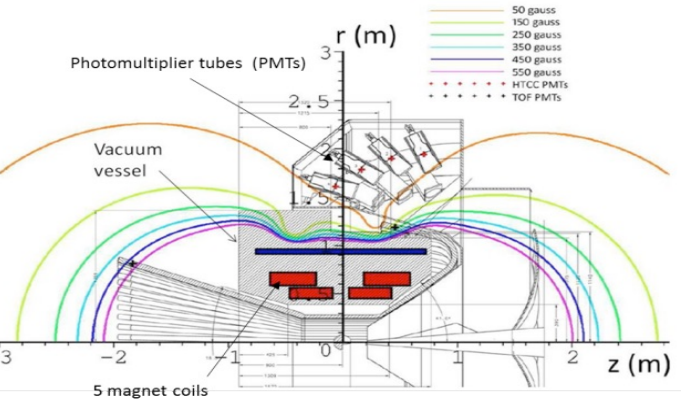


Fig. 12 Cross-sectional view through the side of the solenoid showing the location of the PMTs and the stray field lines

Coil manufacturing variations can degrade the magnetic field homogeneity from its required value of < 100 ppm (peak-to-peak) within a cylindrical volume of 25 mm diameter × 40 mm length located at the geometric center of the magnet. A proposed solution is to incorporate small superconducting shims (Z1, Z2, X, and Y) on the 1 K shield which surrounds the target within the bore of the magnet. To quantify manufacturing variations for the solenoid coils and to check on the effectiveness of the winding and epoxy impregnation processes, a half-size practice coil was successfully wound, potted and dissected.

Electromagnetic interactions exist between the Torus and the Solenoid. A fast dump of the Torus produces a voltage rise across the shield coil of the Solenoid which can trigger the solenoid’s quench protection system thus causing the solenoid to undergo a fast dump itself. While the electromagnetic analysis predicts the sum of the overall forces on each Torus coil to be zero, locally the load cells of the out-of-plane supports (OOPS) of the Torus coils do experience a force. These OOPS, which are located in the center of the race track coil show large changes in force when the Torus is at field and the Solenoid is energized. Electromagnetic analysis shows that the OOPS near the upstream leg of the Torus coil will see a force change in the opposite direction of the one near the downstream leg. The OOPS are instrumented to read up to 8.9 kN of force, their failure load is 44.5 kN. Load changes of up to 4 kN were recorded. These changes in load are repeatable and nicely match those predicted by the analysis in magnitude and direction. All the OOPS are operating well below the maximum read back value.

Solenoid Superconducting Coil Design

The initial design of the coils indicated that the innermost Coils 1 and 2 had the smallest temperature margin (1.28 K) where design guidelines suggest at least 1.5 K for better stability

(Figure 13 and Table XII). As a result, JLab made plans to enable operation of the magnet at sub-atmospheric pressures in order to obtain additional temperature margin and the complete magnet system was designed for this pressure. As it turned out, in practice the cooling of the coils was much better than had originally been predicted, so this mode of operation was not necessary.

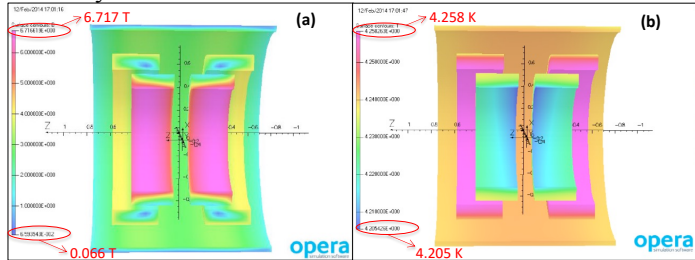


Fig. 13 (a) Magnetic field distribution on solenoid coil surfaces, (b) Temperature distribution in coils at end of ramp up to full field

TABLE XII

SOLENOID – FIELD AND TEMPERATURE MARGINS FOR COILS

JLAB Thermal report

Coil Number	T _{coil} (K)	B _{max} (T)	I _c (A)	SSP (%)	T _c (K)	T _{cs} (K)	ΔT (K)
1 and 2	4.68	6.56	6548	36.90	6.451	5.797	1.117
3 and 4	4.81	4.21	11022	21.92	7.578	6.971	2.161
5	5.62	3.05	10202	23.68	8.093	7.507	1.887

T_{coil}= Coil temperature, B_{max}= Maximum field in the coil, I_c= Critical current at B_{max} and T_{coil}, SSP= Short sample percentage, T_c= Critical temperature at B_{max}, T_{cs}= Current sharing temperature, ΔT= Temperature margin

Figure 14 illustrates the general protection scheme for the solenoid which was used as the basis for the quench and fault scenarios analyzed.

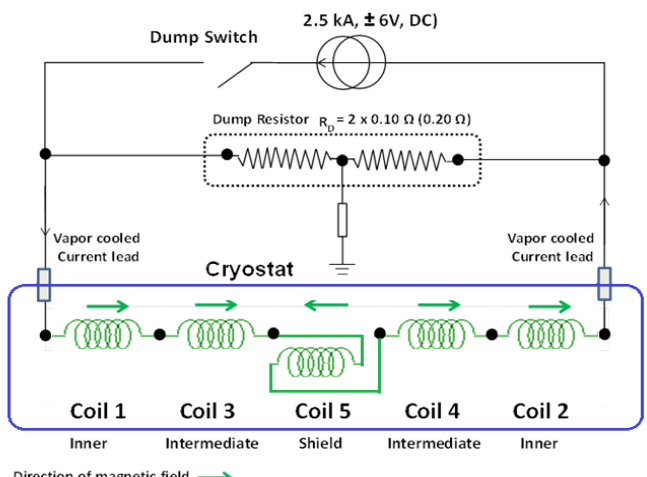


Fig. 14 Solenoid Magnet Protection Circuit

Table XIII summarizes all the analyzed quench and normal operating scenarios together with observed results and any appropriate mitigations.

TABLE XIII

SOLENOID - ANALYZED QUENCH AND NORMAL OPERATING SCENARIOS

	Quench Scenario	Observed Results	Mitigation
1	Quench initiating in C1, assuming presence of AC losses and electromagnetic coupling between coils	Peak temperature = 91 K, Peak voltage across coil = 102 V	No special mitigation was necessary as the coils are self-protecting and the coils are insulated for 1000V to Ground.
2	Quench initiating in C3, assuming presence of AC losses and electromagnetic coupling between coils	Peak temperature = 87 K, Peak voltage across coil = 108 V	No special mitigation was necessary as the coils are self-protecting and the coils are insulated for 1000V to Ground.
3	Quench initiating in C5, assuming presence of AC losses and electromagnetic coupling between coils	Peak temperature = 79 K, Peak voltage across coil = 156 V	No special mitigation was necessary as the coils are self-protecting and the coils are insulated for 1000V to Ground.
4	Quench initiating in C1, assuming all the stored energy is dissipated in only one coil – i.e. no electromagnetic coupling with other coils	Peak temperature = 108 K, Peak voltage across coil = 96 V	No special mitigation was necessary as the coils are self-protecting and the coils are insulated for 1000V to Ground.
5	Quench initiating in C3, assuming all the stored energy is dissipated in only one coil – i.e. no electromagnetic coupling with other coils	Peak temperature = 99 K, Peak voltage across coil = 101 V	No special mitigation was necessary as the coils are self-protecting and the coils are insulated for 1000V to Ground.
6	Quench initiating in C5, assuming all the stored energy is dissipated in only one coil – i.e. no electromagnetic coupling with other coils	Peak temperature = 99 K, Peak voltage across coil = 156 V	No special mitigation was necessary as the coils are self-protecting and the coils are insulated for 1000V to Ground.
7	Quench initiation in Coil 5 with all coil leads and splices between coils included	Peak temperature = 41 K	No special mitigation was necessary as the coils are self-protecting with quenches propagating faster due to the physical connections (splices) between coils
8	Quench initiation in a coil splice	Peak temperature = 42 K	No special mitigation was necessary as the coils are self-protecting with quenches propagating faster due to the physical connections (splices) between coils
9	Eddy current effects in the thermal shield due to a fast discharge of the magnet, the fastest rate being about 281 A/sec	High forces experienced by the Al-1100 thermal shield.	The shield was designed with multiple slots which significantly reduced eddy current formation and thus forces.
10	Training of the solenoid coils to full field	Preliminary analysis of the shield coil indicated that the potted conductor and epoxy were in tension and that this could potentially be a cause for multiple training steps to full field.	The shield coils (as well as Coils 3 and 4) were manufactured with slip planes between the coils and their formers (bobbins). Coil 5 (the shield coil) was also over-bound with multiple layers of glass cloth during the manufacturing process. As

		a result, there was minimal training of these coils to full field during commissioning. There were a total of 5 training quenches (C3: 937 A, C4:1014 A, C4:1035 A, C3:1059 A and C3:1066 A)
11	Torus-Solenoid electromagnetic interactions [14]. The following scenarios were analyzed: <ul style="list-style-type: none">▪ Solenoid alone under normal operating conditions▪ Solenoid and torus under normal operating conditions▪ Solenoid under fault conditions▪ Solenoid under fault conditions with various operating conditions of the Torus	i. The long straight sections of the torus coils experience a force in the presence of the solenoid coils. The force on the straight coil sections closer to the solenoid is almost 3 times the forces on the far straight sections and varies from 1 kN to 6 kN. This force is balanced by other coils (so the net force is zero). These forces are in the X and Y directions, there is no axial force on the torus coils. The forces and the X and Y directions explain the slight buckling of the torus coils. The direction of the buckling depends on the relative directions of currents in both the magnets. This buckling phenomenon can be observed from the load cell data‡. ii. Under certain fault conditions, the torus can exert very small torques on the solenoid magnet. iii. The worst but very improbable case (maximum torque) is for the torus with one of torus coils at 90% of full operating current (Fault #1) and no active shield in the solenoid, as a mitigation action solenoid was tested independent of torus magnet. iv. During subsequent post-commissioning runs, it was discovered that there is some low-level coupling between the torus magnet coils and the shield coil (Coil 5) of the solenoid. The mutual inductance has been estimated as being approximately 0.2 H. So if the Torus quenches or undergoes a fast dump, it is likely that the voltage across Coil 5 of the solenoid will rise and exceed the threshold for quench protection, thereby causing the solenoid to undergo a fast dump also. This has happened at least once without any ill-effects for either magnet – apart from all the Helium being lost from the reservoirs of both magnets.

‡ Initial electromagnetic studies between the two magnets show almost no interaction. However in this initial analysis each torus coil was modelled as one conductor and only the net force on that conductor was taken into account. A more detailed analysis was then performed modelling the torus coils as 8 sections: 2 long straight sections, 2 short straight sections and 4 corner sections. The results from this subsequent analysis match closely to that observed during normal operation of these magnets.

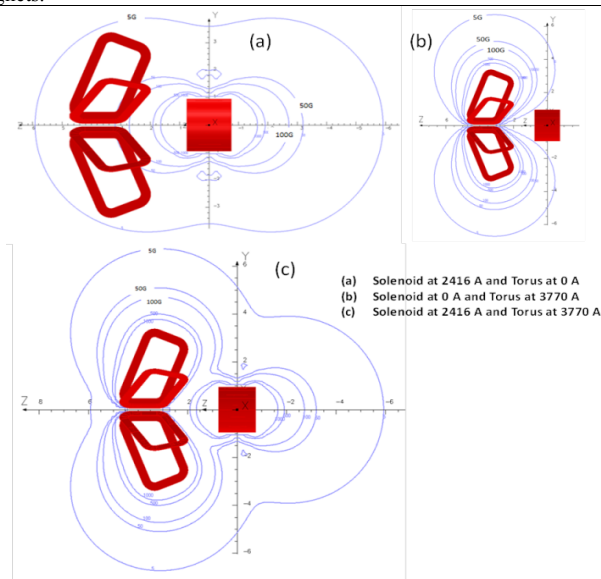


Fig. 15 Solenoid and torus stray field maps under different operating conditions

Figure 15 illustrates the combined stray field maps of the torus and solenoid for various operating conditions.

Additional analyses included assessment of forces on the coils due to the proximity of ferromagnetic components – for example the structural space-frame within the hall, the walkway that spans the left and right halves of the space-frame and the BAND detector located close to the bore of the magnet with its multiple iron-shielded photomultiplier tubes. Eddy current analyses were also performed to verify and mitigate forces on electrically conductive components located within the bore of the solenoid – for example the copper heat exchanger for the Silicon Vertex Tracker (SVT). The results from the analyses were used to either confirm that there was minimal or no risk of damage to the magnet or the components in question, or to facilitate a re-design of the components to reduce the risk of damage. The CTOF shields exert a net force of about 5kN. The magnet vendor (ETI) was provided with the detail of the CTOF shields and designed the z-restraints for a 4.9 kN force. The CND shields exert a net force of about 400 N. The other components are the Hall structure and tubes in the MVT and SVT inserts. The forces on the coils due to the Hall structure depends on the magnet

position; in the operational position the coil forces are about 500 N. Most of the material in the MVT and SVT inserts is non-magnetic. To counteract the 4.9 kN force from the CTOF detector shielding, an iron compensating ring has been installed on the downstream end of the solenoid – bolted to the vacuum jacket's end closure plate. This compensating ring reduces the forces on the coils from the CTOF detector by about 3.6 kN. The total forces on the coils in the presence of all the components are summarized in **Table XIV** indicating a resultant axial force on the coils (in the beam line direction) of about 2.4 kN with the compensating ring installed.

TABLE XIV

SOLENOID – FORCES ON COILS DUE TO PROXIMITY OF FERROMAGNETIC OBJECTS

Components close to the Solenoid Magnet	Fz (N)
Torus Magnet	0
CTOF	4884
CTOF + Compensating Ring	1239
CND	414
HTCC	-35
Hall Structure	499
SVT mounting tube (Stainless Steel part)	196
SVT mounting Tube (Aluminum part) during quench	22
SVT region 4 mounting tube (Aluminum part) during quench	76
Total without Compensating Ring	6056
Total with Compensating Ring	2411

The common supply and return lines from the refrigerator supplies both magnets and a buffer dewar. These lines can in theory produce coupling between the torus, solenoid, buffer dewar and target, in particular the warm return piping. Passive and active control elements have been put in place to minimize the potential for damaging the magnets due to these cryogenic coupling phenomena – for example check valves on the vapor-cooled leads prevent reverse flow, automated vent valves allow flow to continue in the event of a pressure rise to prevent leads from warming and remain open until a magnet completes a controlled ramp down. There are also check valves in the torus and solenoid supply and return u-tubes to prevent back flow of hot gas from either magnet going into the other. These check valves also delay the instantaneous pressure rise that back flow would cause. Operational experience has shown that either magnet can be fast dumped that the system design allows the other not to be effected cryogenically.

IV. POWER SUPPLY, CONTROLS AND INSTRUMENTATION

Superconducting Magnet DC Power Supply [15-17]

Each magnet is charged using identical superconducting magnet power supplies (MPS). This was a bespoke design from Danfysik based on their model 8500/T854 power supply. The MPS DC output is low voltage, high current, designed for near zero resistance loads; however, the impedance seen at the magnet/power supply output terminals can go from pure inductive to an almost pure resistive state during a quench. Due to the requirements for high stability and low drift on a static magnetic field, a linear series-pass regulation topology was selected. The MPS output utilizes two-quadrant operation allowing for smooth and continuous ramping of the current into the magnet. The power supply is programmed to sweep magnet currents at predetermined rates at different current levels without user intervention. The MPS incorporates features designed to

mitigate or prevent failure modes during magnet operation. These features include: controlled current ramping (up or down), fast dump switch and dump resistor (124 mΩ and 200 mΩ for the torus and the solenoid respectively) to de-energize the magnet, integrated polarity reversal switch, slow dump capability, and redundant DC current transducers for current based interlocks. Additionally, a separate rack mounted PLC-based controller allows the programming of current ramp rates, monitors interlocks and the overall health of the magnet. Salient MPS and energy dump specifications are given below (**Table XV**).

The power supply is designed to detect a quench and switches off power automatically. The hard-wired quench detection subsystem acts directly on the dump switch as part of the primary protection system. The quench protection system is capable of detecting quench-induced voltages at multiple points on the magnet, namely magnet coils, bus-bars and splices within the cryostat. The quench fault thresholds are set to the expected quench voltages derived from simulations. The voltage thresholds and the inductance of the magnet set upper limits on the MPS current ramp rate, in order to avoid false trips.

The power supplies' default factory settings meant that there was a total time delay of about 750 ms between when the quench set threshold voltage was exceeded to the time when the dump switch was fully opened during a fault condition. Although this delay time would have been adequate for the torus and solenoid, operational experience with similar designs of power supply within the laboratory suggested that reducing this time delay would provide a larger safety margin in terms of minimizing peak hot spot temperatures within the coils. The delay time consists of three components - (a) T_q is the time between quench initiation and when the quench voltage threshold is exceeded, (b) T_{qi} is the time between when the quench voltage threshold is exceeded and the quench-interlock relay contact opens, which is a constant attributed to the associated electronics, and (c) T_{dsu} is the subsequent time for the dump switch to fully open. The control circuit for the dump switch was modified following consultations and instructions from the power supply vendor and the resulting total delay time has now been reduced to about 120 ms.

TABLE XV
 TORUS - DC POWER SUPPLY AND FAST ENERGY DUMP SPECIFICATIONS

Description	Specification
Output current/voltage	± 4000 A / ± 6 VDC
Ramp rate	Variable: ± 0.2 to ± 3.0 A/s
Supply voltage	480 V/3-Φ/60 Hz.
Ambient temperature	15-35 °C
Cooling water (flow, temperature)	60 l/m, 15-35°C
Pressure	300 psig
Ground Isolation	>1.0 MΩ
Quench protection	Fast DC output breaker
Absolute accuracy	-0/+100 ppm
Stability (30 min)	$<\pm 5$ ppm
Stability (8 hours)	$<\pm 10$ ppm
Magnet	I _{OP} (A)
Torus	± 3770
Solenoid	± 2416
L _{TOT} (H)	E _{ST} (MJ)
2.0	14.21
6.0	17.50
V _{DUMP} (V)	R _{DUMP} (Ω)
< 500	0.124
< 500	0.200
T _{MAX} (°C)	
	<350

Magnet Current Leads and Ice-Management System

Water-cooled leads are used to connect each magnet power supply to the respective magnet's vapor-cooled leads. Air-cooled multi-stranded (flexible) copper jumpers are used to transition between the hard connection points at the power supply end as well as at the magnet end (Figure 16).

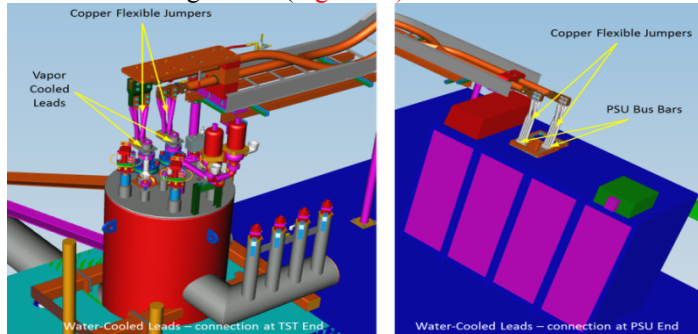


Fig. 16 Torus – water-cooled leads, flexible jumpers and vapor-cooled leads. The set-up for the solenoid is similar.

The tables below summarize the main features of these current transfer components (Table XVI, XVII, XVIII).

TABLE XVI
WATER-COOLED LEADS SPECIFICATIONS

Description	Torus	Solenoid
Operating current	4000 A	3000 A
Cable cross sectional area	2000 MCM	2000 MCM
Voltage drop per lead pair @ 4000 A (Torus) @ 3000 A (Solenoid)	1.1 V @ 50°C	1.3 V @ 50°C
D.C. resistance for both leads connected in series	274 $\mu\Omega$	475 $\mu\Omega$
Input water temperature	40°C	40°C
Output water temperature	50°C	50°C
Max. operating pressure rating	300 psig	300 psig
Test pressure	400 psig	350 psig
Insulation to Ground voltage rating	2 kV	3 kV
Minimum allowable water flow @ 4000A (Torus) @ 3000A (Solenoid)	1.2 gpm	3.2 gpm

TABLE XVII
AIR-COOLED JUMPER SPECIFICATIONS

Description	Torus	Solenoid
Maximum Design Current	4000 A	3000 A
Jumper cross sectional area	3000 MCM	3150 MCM
Voltage drop for jumpers per lead @ 4000 A (Torus) @ 3000 A (Solenoid)	One jumper pair = 0.06 V @ 70°C	One jumper pair = 0.014 V @ 70°C
D.C. resistance for jumpers per lead @ 70°C	One jumper pair = 15 $\mu\Omega$	One jumper pair = 4.7 $\mu\Omega$

TABLE XVIII
VAPOR-COOLED LEADS SPECIFICATIONS

Description	Torus	Solenoid
Rated Operating current	5000 A	2500 A
Operating helium consumption @ 5000 A	20 liters/hr. per pair	7 liters/hr. per pair
Standby helium consumption	15 liters/hr. per pair	6 liters/hr. per pair
Minimum recommended lead gas flow per lead @ 5000 A / 4000 A (Torus), @ 2500 A (Solenoid)	118 SLPM / 112 SLPM	42 SLPM

Maximum allowable voltage drop per lead @ 5000 A (Torus) and @ 2500 A (Solenoid)	100 mV	100 mV
Allowable operating time with no gas flow	150 sec	150 sec

Band and cartridge heaters are installed at the top of the vapor-cooled leads where they exit the magnet service towers to keep ice-formation to a minimum (Table XIX).

TABLE XIX
LEAD HEATER SPECIFICATIONS

Description	Torus Specification (per lead)	Solenoid Specification (per lead)
Upper heater set – No. of heaters / Power / Voltage	1/ 400 W per heater / 120 VAC (Mica band heater 3" ID, 1.5" width)	2/ 150 W per heater / 115 VAC (cartridge heaters)
Central heater set – No. of heaters / Power / Voltage	2 / 300 W, 600W / 115 VAC (heater tapes) - proposed	1 / 600W / 115 VAC (Mica band heater)
Lower heater set – No. of heaters / Power / Voltage	1 / 600W / 115 VAC (heater tapes) - proposed	2 / 300 W, 600W / 115 VAC (Mica band heaters)

In case of heater failure an ambient vaporizer is installed between the VCL and the warm return piping. The piping between the VCL and the vaporizer is vacuum jacketed. These features keep water from dripping onto the detectors which is critical for the detector system.

Controls and Instrumentation

Depending on where instrumentation was mounted on the magnet, all selected sensors had to be compatible with cryogenic temperatures and magnetic fields with regards to reliability and reproducibility of read-outs with all detectors in their final locations.

The cycling of large currents in the superconducting magnets during ramp-up and ramp-down operations results in heat loads caused by eddy current effects. This phenomenon, together with the level of ambient noise within the experimental hall, guided some of the instrument choices. The risk analysis also identified the various forces that arise during operation of the torus and solenoid magnets viz. eddy current forces, Lorentz forces, thermal loading, and also the electromagnetic and cryogenic interaction between the torus and solenoid magnets. For safe magnet operation, it is necessary to monitor and control all the following parameters - temperatures, pressures, pressure drops, liquid levels, mass flows, vacuum levels, voltages, strains, loads (Table XX) [18,19]. Extensive instrumentation was used to verify the design under various operating conditions during commissioning and to allow flexible, reliable and safe control of all sub-systems by non-expert personnel post-commissioning.

Instrumentation is monitored using the following key electronic sub-systems:

- a. JLab-designed sensor excitation electronics + National Instruments Compact Real-Time Input Output controller or cRIO (Slow DAQ refers to Slow Data Acquisition) - Magnet temperatures and strains
- b. National Instruments cRIO (Fast DAQ refers to Fast Data Acquisition) – Magnet-related voltages
- c. Cryo-Con readout units – Cryogenic system temperatures (Cryo-Con refers to Cryogenics Control Systems Inc.)
- d. PLC – Cryogenic system pressures, vacuum levels

Monitoring and control of the entire system (including valves and flow indicators) was performed by Allan Bradley PLCs.

The design of the sensor read back chassis was based on the requirements of the torus and solenoid instrumentation in terms of quantity and types. Commercially available read out boxes for sensors are usually limited to a certain number of channels and the multi-functional capability of these devices usually means that these devices are expensive. The motivation to accommodate all the sensor types (temperature, pressures, strains, loads, magnetic field – termed ‘slow data’) that would be used on both magnets together with a reduced set of functions, (i.e. to only meet the required control system needs of the magnets and no more), led to a Jefferson Lab-designed and developed FPGA-based multi-sensor-excitation-low-voltage (MSELV or simply LV) chassis which sets the excitation current or voltage for a sensor and also provides read back [20]. The data read back would then be routed to a NI-cRIO (the slow DAQ system) which would pass data to the PLC for control of the various sub-systems and interlocks. The majority of instruments are powered and read out via the LV chassis:

1. The MSELV sends the unscaled raw readouts to the NI-cRIO via individual RS232 ports. Each port is typically divided

based on instrument type, temperature, strain, etc. The NI-cRIO takes the raw data for each instrument and converts it to engineering units from specified calibration tables. This ‘slow’ data is sampled at 1 Hz.

2. The cRIO device puts scaled sensor readouts into arrays, based on instrument type, and sends these arrays to the PLC via Ethernet.
3. The PLC then takes this data along and uses prescribed routines (cool down, power up, etc.) to force action on valves, heaters, power supplies, etc. The PLC also transfers this data to an EPICs IOC (input-output controller) to allow for archiving and site wide system control (e.g. the cryo compressor in the End Station Refrigerator can use one of our cryogen liquid levels to help determine cryogenic heat load).
4. In parallel another cRIO (fast DAQ) uses its 24-bit ADC’s to monitor the voltage taps. This cRIO directly sends 10 kHz data to the EPICs IOC for off-line analysis. In parallel, it also sends the voltage tap data to the PLC at a rate of 5Hz for the redundant (secondary) protection system.

TABLE XX
TORUS AND SOLENOID MAGNET SYSTEM SENSORS AND VOLTAGE TAPS

(A) TORUS Magnet System

Measurement	Voltage		Temperature (4 K)		Temperature (77K)		Strain		Load cell		Hall sensor		
Sensor/Wiring Type	8mil Kapton insulated-multi-strand copper wire (pair)		Cernox™(1070) – 4 wire		Calibrated PT100 – 4 wire (Omega F2020-100-B)		Cryogenic series 350 Ω (CFLA-6-350) 4-wired/3-wired for measurement		LOAD CELL - FUTEK FSH02239 (2000 LBS), 4 wire, 300 K		Cryogenics hall generator (axial), HGCA-3020, 4 wire		
# sensors/wiring	Magnet	23	Magnet	54	Thermal shield	60	Coil Cold Mass (CCM)	24	OOPS	26	Vacuum Vessel 6		
	Zero-Flux Current Transducer	2	Cooling Tube	12	Current - Leads	2+2	Axial sup	6	FMEA result	3 (Hub)			
	FMEA Result	1 (Power supply- One bus bar)	Splices	6+2	Axial sup	3	Vert sup	8					
	Line-GND/Dump Resistor	1	VCL in Cryostat	2+2	Vert sup	4	FMEA result	24 (Hex)					
Wire material	Copper		Constantan harness		Constantan harness		Constantan harness		Copper	Copper			
Lead gauge	24 AWG		36 AWG		36 AWG		36 AWG		28/32 AWG	28/32 AWG			
Signal amplitude	Magnet	300 V pk	3 mV (300K) to 50 mV (4.2K)	0.1 V (77K) to 0.5 V (300K), actual excitation Current = 2.5 mA	0-5 V for resistance measurement the variation is 0-0.5 Ω or 10 μV – 1 mV (CFLA-6-350)	~ 2.0 mV/V	~ 1.00 mV/kG (at 298 K)						
	Dump R	250/500 Vpk											
	ZFCT	50 mV											
	PSU	6V											
Sampling rate	> 2 kHz		100 Hz		100 Hz		100 Hz		100 Hz	100 Hz			
Excitation current/Voltage	n/a		0.20-20 μA		1-5 mA		0-10 V (2.5 V)		0-10V (2.5 V)	100 mA			
No. of channels	24		71		61		38		26	12			
Multiplexed	YES / NO		Y		Y		Y		Y	Y			
Control	Primary-Hard wired to Quench detection/Secondary - PLC		PLC		PLC		PLC		PLC	PLC			
Fast DAQ	FPGA		FPGA		FPGA		FPGA		FPGA	FPGA			

(B) SOLENOID magnet System

Measurement	Voltage		Temperature (4 K)		Temperature (77K)		Load cell		Hall sensor						
Sensor/Wiring Type	8mil Kapton insulated-multi-strand copper wire (pair)		Cernox™ – 4 wire (4.2 – 325K)		Calibrated PT100 – 4 wire		LOAD CELL, 4 wire, 300 K (Force)		Cryogenics hall generator (axial), HGCA-3020, 4 wire						
# sensors/wiring	Magnet	21	Magnet	26	Thermal shield	18	8 (LCM307) 0-10 kN (axial)		Vacuum Vessel 3						
	Zero-Flux Current Transducer, Power supply Bus	4					8 (KMR300kN) 0-165 kN (radial)								
Wire material	Constantan/Manganin/Copper		Constantan harness		Constantan harness		Copper		Copper						
Signal amplitude	Magnet	718 V pk	3 mV (300K) to 50 mV (4.2K)	0.1 V (77K) to 0.5 V (300K), actual excitation Current = 2.5 mA	~ 2.0 mV/V	~ 1.00 mV/kG (at 298 K)									
	Dump R	250/500 Vpk													
	ZFCT	50 mV													
	PSU	6V													
Sampling rate	> 2 kHz		100 Hz		100 Hz		100 Hz		100 Hz	100 Hz					
Excitation	n/a		0.20-20 μA		1-5 mA		0-10V (2.5 V)		100 mA	100 mA					

current/Voltage					
Control	Primary-Hard wired to Quench detection/Secondary - PLC	PLC	PLC	PLC	PLC
Fast DAQ	FPGA	FPGA	FPGA	FPGA	FPGA

Analog data collection from other devices not listed above are: Pressure transducers, EV electric valves, PV pneumatic valves, RV pressure relief valves, VCL lead heaters, VCL lead flow indicators, Vacuum pump control (gauges and gate valve), Bus-bar water flow switches, Magnet power supply water flow and temperature monitors.

Magnet Quench Protection and Control [14]

The magnet Quench Protection System (QPS) was developed for both magnets based on the analysis of several quench scenarios and comprises primary and secondary sub-systems. Parallel path voltage taps from multiple locations throughout the magnet (magnet coils, splices, bus-bars, leads, etc.) feed both these sub-systems. The voltage taps feeding the primary protection sub-system are hardwired directly from the magnet to the Danfysik Quench Detector units – i.e. with no electronics or any software manipulation in between.

The secondary quench protection sub-system is also fed from the same voltage tap locations but this time the information is acquired by a fast data acquisition system (Fast DAQ), using a National Instruments cRIO device, and then routed to a PLC which performs summations and subtractions of various voltages to provide back-up for the hard-wired primary sub-system. A quench-induced voltage which exceeds pre-set voltage thresholds will trigger the primary system closely followed by the secondary system.

Each hardwired Quench Detection (QD) module consists of four differential input channels, i.e. an upper and lower channel. The voltage signals are fed into the lower and upper channels and then subtracted from each other. The resultant voltage is compared with the pre-set voltage threshold (i.e. set by the operator). If the resultant voltage is higher than this threshold and remains above this threshold for a pre-set time period, then the QD will trip and fast dump the magnet—i.e. the dump switch will open and the magnet will run down through the external dump resistor. [Figure 17](#) illustrates a set of typical voltage taps for the solenoid magnet, feeding both the primary QPS (i.e. to the quench detector units, QD-U) and also to the secondary QPS (DAQ).

The secondary QD system routes voltage tap data from the magnet via Knick isolation amplifiers (iso-amps) [21,22] to a second dedicated NI-cRIO having eight four-channel N9239 24-bit analog input modules. The voltage tap data are then manipulated by the PLC to produce summed and subtracted voltages which are then routed to the various interlocks.

Two sets of thresholds are employed here - one set to initiate a controlled ramp down and a second set which is deployed as a

backup for the hardwired QD and also acts directly on the fast dump contactor.

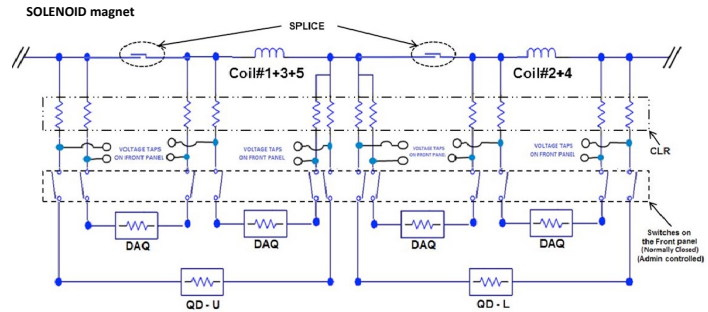


[Figure 17](#) Schematic arrangement of a typical section of the solenoid magnet for impedance-matching simulations – Current Limiting Resistor (CLR), Op-Amp, QD board

Upon detection of a quench via voltage taps (VTs), a mechanically operated dump switch is opened to isolate the MPS from the magnet coils. Between 43-63% of the stored energy within the magnet is extracted and dissipated in the external dump resistor. The remainder of the energy is dissipated within the magnet coils and cryogenic system itself. The designs of the quench protection and voltage tap sub-systems were driven by the anticipated levels of voltages developed during a magnet quench.

The quench protection provides valuable data during a quench event via data capture of the voltage and temperature waveforms. The magnets are continuously monitored during ramp up, steady state operation and also ramp down—i.e. the QPS is always active—so inductive voltages across coils during ramp up and down operations are also captured and have been used during the commissioning process to ensure the correct balancing of voltages between the various coils and thus QD channels.

The same cRIO also feeds VT waveform data to EPICS at 10 kHz for online review via parallel Ethernet communications. The primary and secondary voltage thresholds for the torus and solenoid are summarized in [Table XXI](#), which also provides the full list of interlocks that are managed by the control system.

TABLE XXI
 TORUS AND SOLENOID MAGNET HARDWARE AND SOFTWARE INTERLOCK THRESHOLDS

TORUS Magnet system			
	Acceptable operating Range	Actual Trip Limit	Expected Threshold
Hardwire Interlocks (FAST DUMP)			
Liquid Helium Level (SC probe)	21-110%	<20%	<20%
Liquid Helium Level (Diff Press)	21-110%	<20%	
Vapor Cooled Lead Temp	4.5-15 K	>15 K	>10 K
Danfysik QD's	>200mV, 100mV(VCL), >2250 mV		Varies across sections identified
PLC Interlock - I (Fast Dump)			
Current Limit (Hard coded)	Not to exceed ± 3880 A	3850 A	± 3880 A
Software Quench, 2nd Threshold	Coil voltages are compared>350mV, VCL >125 mV		Coil voltages are compared>350mV, VCL >125 mV
PLC Interlock - II (Controlled Ramp Down)			
CCM Load Cell	Top 600lbs, bottom 1300lbs	Top 600lbs, bottom 1300lbs	Top 600lbs, bottom 1300lbs
Vertical Support	-9500lb		-9500lb
Coil Compartment 1st Threshold	Coil voltages are compared>250mV		Coil voltages are compared>250mV
Vacuum	>5x10^-5 ATM		>5x10^-5 ATM
Pressure Helium Tank	PT8120<2.3 ATM		PT8120<2.3ATM
Supercritical Helium Pressure	2.4-3.0 ATM	<2.3 ATM	
Pressure Nitrogen Tank	<2.0ATM		<2.0ATM
LL Helium Tank	<90%		<90%
LL Nitrogen Tank	<90%		<90%
VCL Flow	± 15 SLPM of SP		± 15 SLPM of SP
VCL Temp	>10 K		>10 K
VCL Voltage	80 mV		80 mV

SOLENOID Magnet system

	Acceptable operating Range	Actual Trip Limit	Expected Threshold
Hardwire Interlocks (FAST DUMP)			
Liquid Helium Level (SC probe)	21-110%	<20%	<20%
Liquid Helium Level (Diff Press)	21-110%	<20%	
Vapor Cooled Lead Temp	4.5-20K	>20 K	<15 K
Danfysik QD's	>200mV, 100mV(VCL), >1500 mV		Varies across sections identified
PLC Interlock - I (Fast Dump)			
Current Limit (Hard coded)	Not to exceed ± 2500 A	2500 A	± 2500 A
Software Quench, 2nd Threshold	Coil voltages are compared>350mV, VCL >125 mV		Coil voltages are compared>350mV, VCL >125 mV
PLC Interlock - II (Controlled Ramp Down)			
Axial Support	0-8000 Lbs		
Radial Support	0-18000 Lbs		
Coil Compartment 1st Threshold	Coil voltages are compared>250mV		Coil voltages are compared>250mV
Vacuum	>5x10^-5 ATM		>5x10^-5 ATM
Pressure Helium Tank	PT8120<2.3 ATM		PT8120<2.3ATM
Supercritical Helium Pressure	2.4-3.0 ATM	<2.3 ATM	
LL Helium Tank	<90%		<90%
VCL Flow	± 15 SLPM of SP		± 15 SLPM of SP
VCL Temp	4.5 - 15 K		>17 K
VCL Voltage	80 mV		80 mV

V. FABRICATION AND ASSEMBLY

TORUS - The six coils make up a hexagonal assembly where the hex beams carry the elements to make the hydraulic and electrical connections between coils; they also contain re-coolers (Figure 18a). The re-coolers re-cool the helium that exits each coil before it enters the next and also provides cooling for the inter-coil splices (Figure 18b). The design is a coiled tube in a shell and work well both during cooldown and at steady state at 4K. During cooldown variable temperature gas is transferred into the shell side. At steady state the shell side is filled with liquid helium by thermosiphon from the reservoir in the TST. All coils, hex beams and the service tower share a single vacuum space which is pumped by two 8 inch turbo pumps.

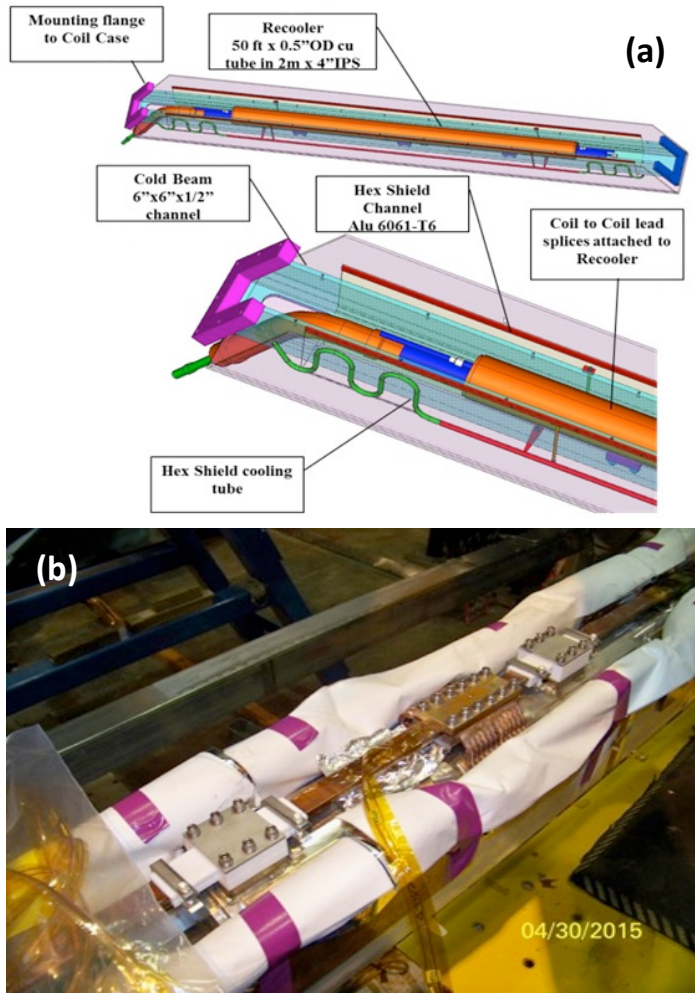


Fig.18 (a) Typical Hex beam detail, (b) Coil splice (soldered joint) attached to re-coolers

The individual coils are housed in an aluminum case that is approximately $2 \times 4 \times 0.05$ m [23]. The conductor is insulated with fiberglass tape and each of the coils is wound as a double pancake. Each coil is conductively cooled by supercritical helium supplied at 4.6 K from cooling tubes located on the coil inner diameter. Two layers of copper are soldered to the cooling tubes on each side of the double pancake and completely encase the coil, providing the main path for conduction-cooling. To allow for visual inspection of the coil potting quality the coils

are first potted without the copper sheets. Ground plane insulation was then added followed by the installation of the copper sheets. The coil is then positioned and potted for a second time in its aluminum case (Figure 19).

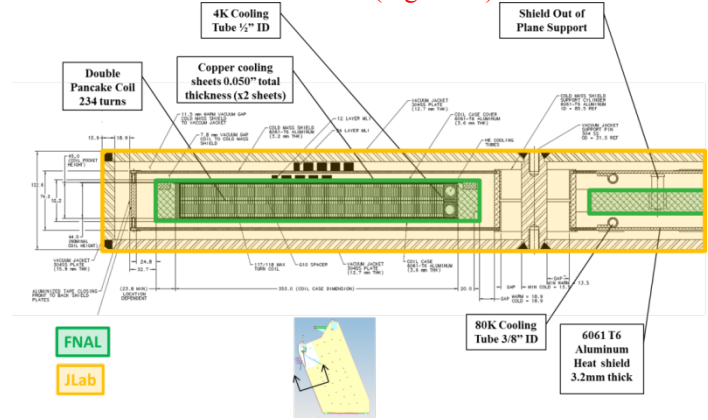


Fig.19 Coil and cryostat design (FNAL – components fabricated by Fermi Lab, JLab – components fabricated by JLab)

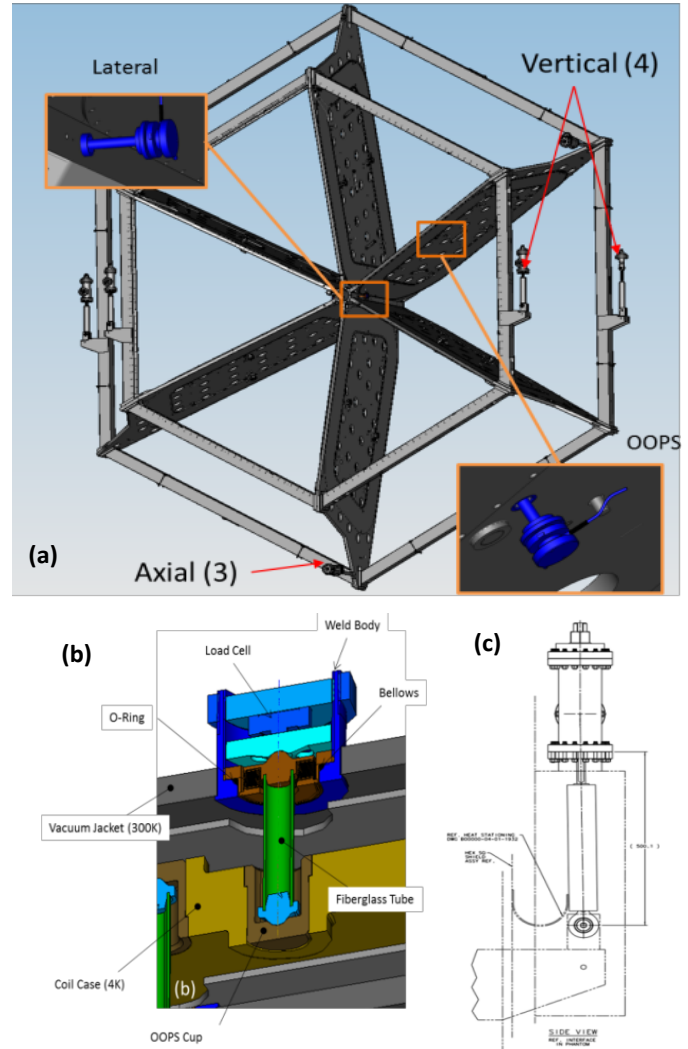


Fig.20 (a) Cold mass support system, (b) Out-of-Plane support, (c) Vertical support

The coil case is shielded from the vacuum jacket by a 3mm thick 80K thermal shield. The shield is actively cooled by

thermo-siphon driven liquid nitrogen circulating through tubes welded to the shield. The shield is supported off of the coil case by bumpers and thin walled support arms. The shield is constructed of Al-6061 with Al-1100 strips epoxied to the shield at maximum temperature regions in the shield. The 6061 provides mechanical strength to the shield while the 1100 strips add additional cooling where needed. The shield has been segmented to reduce the effects of eddy currents generated during a rapid discharge of the magnet coils.

The entire torus cold mass is supported by 3 axial supports (i.e. in the beam direction), 4 vertical supports, 2 lateral out-of-plane supports (OOPS), and 24 coil OOPS supports (Figure 20). The coil OOPS eliminate the sag in the coil due to gravity and react any out-of-plane forces due to misalignments and forces that arise from energization of the solenoid. The OOPS design consists of a fiberglass tube epoxied to spherical bearings. The bellows at the vacuum case maintains vacuum, allows adjustment in the out of plane direction and force leveling between upstream and downstream OOPS. Bellows also allow movement of the coil during cool-down. The assembly includes a room temperature load cell connected to the data acquisition system so that the out-of-plane force seen by each coil is always known. The axial and vertical supports are stainless steel links with strain gauges mounted near the warm end. Each end has a spherical bearing rod-end; they connect the cold mass to the vacuum jacket. The vertical supports take the entire gravity load for the 25 Ton cold mass, while the axial supports react-to any loads in the beam direction to adjust the magnet in the pitch and yaw directions and to handle the seismic loads.

TABLE XXIII
A SUMMARY OF THE KEY MANUFACTURING STEPS - TORUS

Manufacturing Step	Location
1 Superconducting Rutherford cable soldered into C-shaped copper channel	Advanced Engineering Systems (AES) LLC, PA, USA
2 Clean and inspect conductor (supplied by JLab)	
3 Wind cooling tube and apply ground insulation	
4 Insulate conductor	
5 Wind first pancake layer, set coil dimensions	
6 Turn to turn short tests	
7 Install ground insulation on coil OD	
8 Install layer-to-layer insulation	
9 Wind second layer, set dimensions, repeat tests	
10 Install ground insulation, and molding hardware	
11 Push into potting mold and flip assembly	Fermi National Accelerator Laboratory (FNAL)
12 Install ground insulation on first pancake	
13 Form leads	
14 Close and seal the mold	
15 Vacuum impregnate the coil, cure the epoxy.	
16 Remove from the mold – full coil electrical test	
17 Survey conductor location on both sides	
18 Solder copper cooling sheets on each side of coil	
19 Position coil in Aluminum Case	
20 Vacuum epoxy impregnate and cure	
21 Final electrical test	
22 Ship to JLAB	
23 Apply multi-layer insulation (MLI) to coil case	JLab
24 Fit thermal shield and insulate with MLI	
25 Fit vacuum jacket and transport to hall	
26 Install torus	
27 Fabricate and distribution box	
28 Fabricate torus service tower (TST)	
29 Install distribution box	

30	Install TST
31	Commission torus

Jefferson Lab contracted with AES to solder the Rutherford cable into a copper channel for the two magnets. Soldering required bonding the cable to the channel and also bonding the two layers of the key-stoned cable. Bonding between the strands adjacent to the channel was nearly perfect, but the bonding between the layers was more difficult. With a Minimum Quench Energy (MQE) of 47 mJ for the torus magnet the following limits were set as requirements based on a factor of safety of 10 or 4.7mJ. An acceptable void area was determined to be about 82mm² which implied a 9mm diameter or approximately 4x20mm void. Similarly, the solenoid MQE is 20 mJ and an acceptable void area is 30 mm², which translates to a 6.2 mm diameter or 5.5 mm x 5.5mm void. A continuous void monitoring system was attempted with varying levels of success and thus process control was the only solution. Control of overall dimensions was also extremely important, so wiping the exterior surfaces free of solder was a key step in the fabrication process. Another key element of the process was to make each production length of conductor as a single run thus removing the issues with quality during the line starting and stopping. This required multiple shifts to keep the line running around the clock. To check the quality, cables were peeled from the channel and then strands removed from one layer to expose the center solder joint. Once the process was optimized each soldered length of conductor had several meters removed, about 50m in from its beginning and end, and inspected to ensure that quality soldering was being achieved. The flux used was SUPERIOR #75 warmed to 38°C together with 60/40 Tin/Lead solder. After soldering, the surface solder layer is removed from the copper using buffering wheels on 4 sides to improve epoxy bonding and then the completed conductor was shipped to FNAL.

Because of the large size of the coils, FNAL had to develop new tooling and processes to support coil production operations [3]. At FNAL the conductor was de-spooled, cleaned once again before being wound onto a specially prepared spool (Figure 21). These spools were also electrically insulated so that the conductor could be hi-pot tested during insulation application. The conductor was then insulated with an automated machine that applied ½ lap 0.08 mm fiberglass tape insulation around the conductor immediately prior to the start of winding. Coils were wound by first winding the 2 turns of cooling tube around the winding mandrel, followed by winding the coil. The coil is wound as a double pancake by winding 117 turns of the first layer with the second layer cable supported above the coil, then winding the second layer for a total length per coil of ~2000 m (Figure 22). There is a 0.38 mm thick sheet of G10 placed in between the coil pancakes. The ground insulation between the conductor and copper cooling tubes or copper foil varies but has a minimum of 4 layers of 0.18 mm glass cloth. After each coil layer was wound, shims were installed between the cooling tube and the first turn at the hub and the first 0.7 meter of the upstream and downstream straight sections; shims were not applied along the radii at the corners near the hub. The primary purpose was to ensure coil to coil uniformity in the high field area and to push the extra material caused by dog-boning to the outer portions of the coil where it has little effect on the field or physics of the CLAS12 detector system. After potting the coils

were removed and the FNAL survey team used photogrammetry to provide JLAB with actual locations of the conductors around the perimeter of each coil (discussed later).



Fig. 21 (a) The conductor being cleaned from right to left. The aluminum spool with conductor from the soldering company is positioned on the winding table at right. The cleaning station (inset), is located between the two wooden spools. The tensioner with the FNAL aluminum spool is on the left, (b) Partial view of the coil fabrication shop at Fermilab showing a coil being wound, the second spool is seen above the winding table.

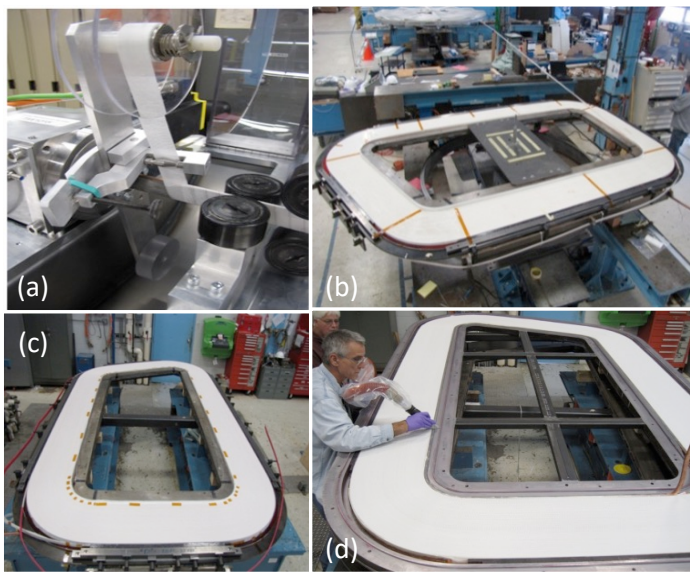


Fig. 22 (a) Conductor being insulated, (b) The start of the 2nd pancake winding, (c) After 2nd pancake winding, (d) Coil in the potting mold

During winding, the coil was also subjected to a turn-to-turn short test measurement capable of detecting both ‘hard’ and ‘soft’ (of about 1 ohm) shorts between adjacent turns. Additional copper stabilizer was added to the leads before an initial Vacuum Pressure Impregnation (VPI) in a sealed mold with CTD-101k epoxy. The impregnation procedure was designed, and qualified, for proper degassing, and to prevent outgassing of the epoxy during impregnation. The temperature of the coil and of the mold was driven and maintained through resistive heating of the coil itself. Temperature uniformity was guaranteed via sensors mounted along the mold. The coil was then allowed to soak for 24 h at 58°C before the cure cycle began. The cure cycle took place over 3 days with a gel stage, cure, and post-cure. A layer of polypropylene mesh was incorporated between the mold and a peal ply adjacent to the coil, to allow a uniform epoxy flow over the surface of the coil as well as act as a route for trapped and evolved gases to escape to one of the 3 main vacuum pump-out ports (Figure 23).

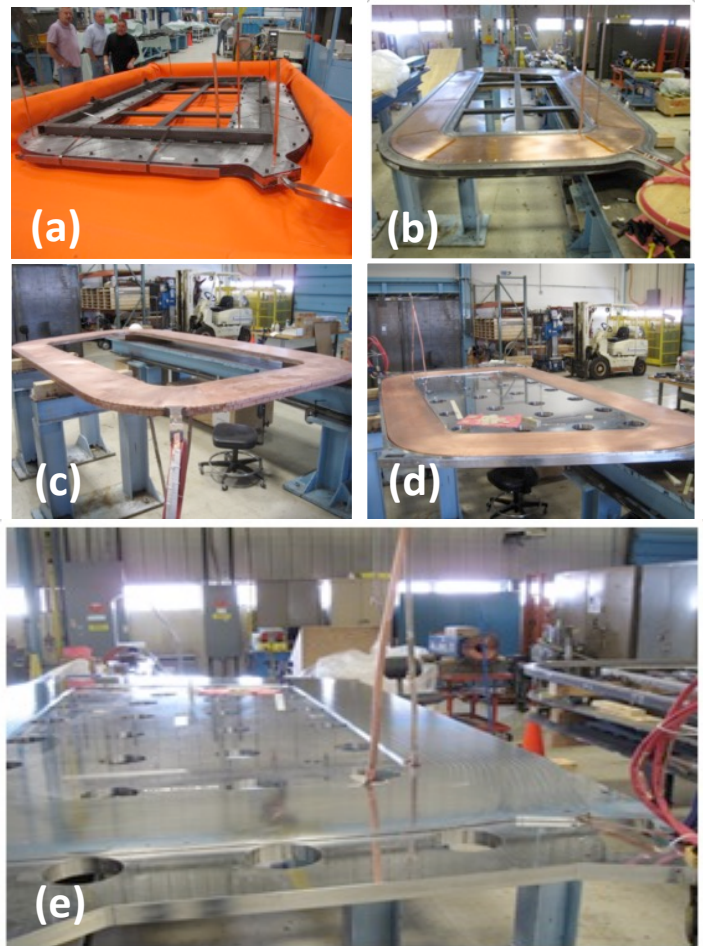


Fig. 23 (a) Potting mold closed up ready for potting, (b) copper sheets were positioned after removal from the coil potting mold, (c) Coil cleaned up and ready for cooling sheet attachment, (d) Coil aligned in coil case, (e) Case cover fit up with coil and case

Upon removal from the mold, a thorough visual inspection was carried out of both sides of the potted coil to check potting quality. After initial potting, two sheets of 0.635 mm of annealed OFE copper are soldered to the cooling tubes on each side of the coil and then folded over the outside of the coil. Two layers of .006” Kapton are installed on the inner layer of copper

for ground insulation and an additional layer of glass is installed between the Kapton and coil to aid in epoxy flow between the two during the second coil potting. The coil is then placed into its 6061-T6 aluminum coil case and a second impregnation step is carried out using the same basic procedures as developed for the first potting (Figure 23e). The difference in thermal expansion between aluminum and copper ensures an adequate preload on the coils after cool down. After the second potting, the coil case modules had their cooling tubes formed, received their final round of quality control tests and were then shipped to JLab for installation into their vacuum vessel and ultimate assembly in Hall B.

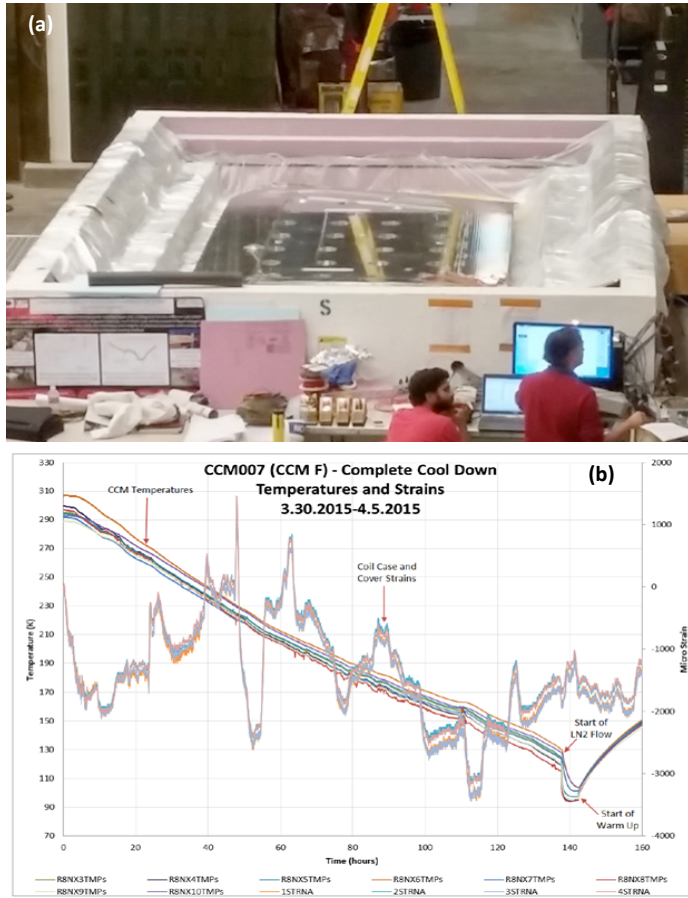


Fig.24 (a) Coil placed in large ‘foam’ box being prepared for the 80 K test, (b) Cool down curve during 80 K test

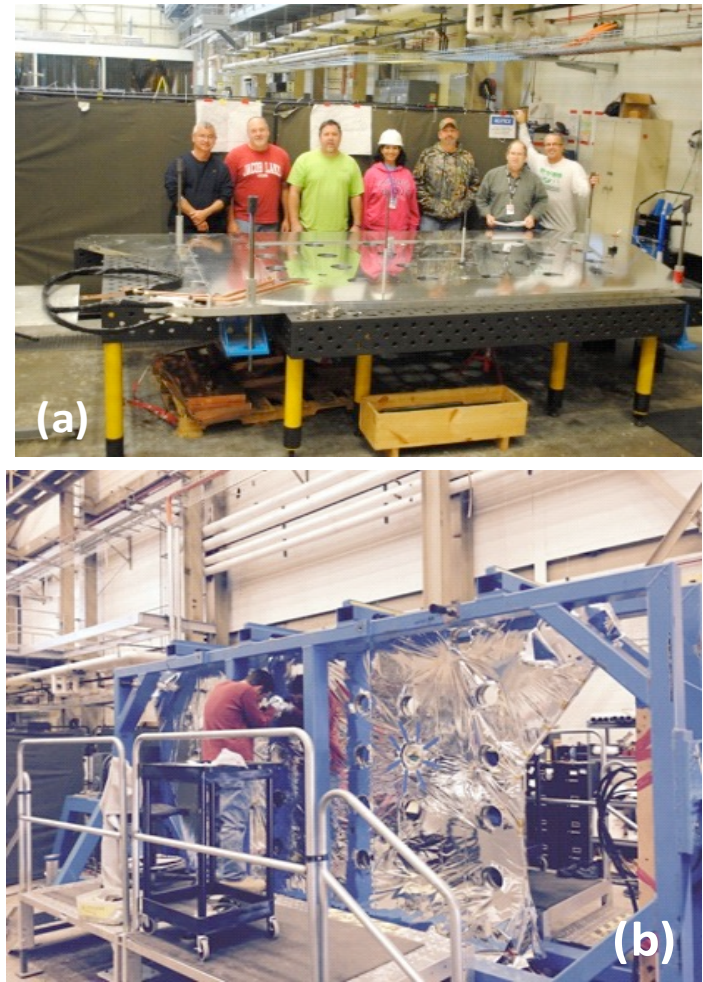
TABLE XXII
80K DATA CORRELATION TO CALCULATED RESULTS

LOCATION	80 K Test	80 K Test	4 K Scaled	4 K Scaled	4 K
	Result Front	Result Back	Result Front	Result Back	ANSYS FEA
Temperature difference at Hub (bore) K	4.00	3.10	0.12	0.09	0.251
Temperature difference at Downstream HEX K	7.20	4.80	0.22	0.15	0.834

A “Cryostat Factory”, set up at JLab, facilitated the assembly of each coil as it arrived from FNAL. Upon arrival, each coil was inspected, instrumented with temperature sensors and strain gauges and underwent a cool down test to 80 K (Figure 24) to assess the robustness of the coil’s electrical insulation and its structural integrity as well as to test the efficacy of the employed

conduction cooling method [24]. Table XXII summarizes the results obtained from the 80 K test, extrapolation to 4 K and comparison with results obtained from finite element analysis. The results indicated that the conduction-cooling system was indeed functioning as designed with more than adequate safety margin.

The CCM was then wrapped in multi-layer insulation (MLI), fitted with its MLI-covered nitrogen-cooled thermal shield (Figure 25) and vacuum jacket before being moved to the experimental hall for final system assembly (Figure 26). As part of the Quality Assurance plan a practice coil was made by FNAL and delivered to JLAB. Following the 80 K test on the practice coil and a subsequent dissection, the coil was discovered to have several “dry” areas where the epoxy had not penetrated fully (Figure 27). A team was formed to investigate and address this problem and included experts from the USA and overseas organizations. Over a four month period, this team reviewed the impregnation process and carried out multiple trial runs on coil samples. An improved impregnation process was implemented and resulted in the successful production of 6 coils and two spares. The improvements to the impregnation process were also shared with the vendor for the solenoid magnet.



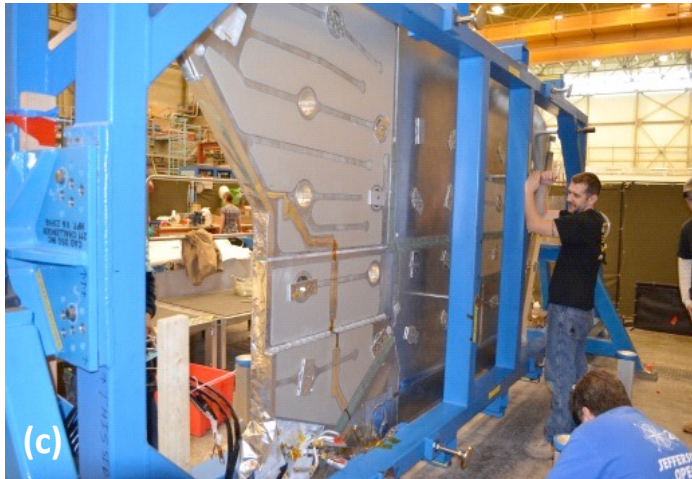


Fig. 25 (a) First production coil in its case received from FNAL, (b) Applying Multi-Layer Insulation (MLI) to coil case, (c) coil with thermal shield installed and in rotatable jig (to allow fitting of instrumentation on the other side)

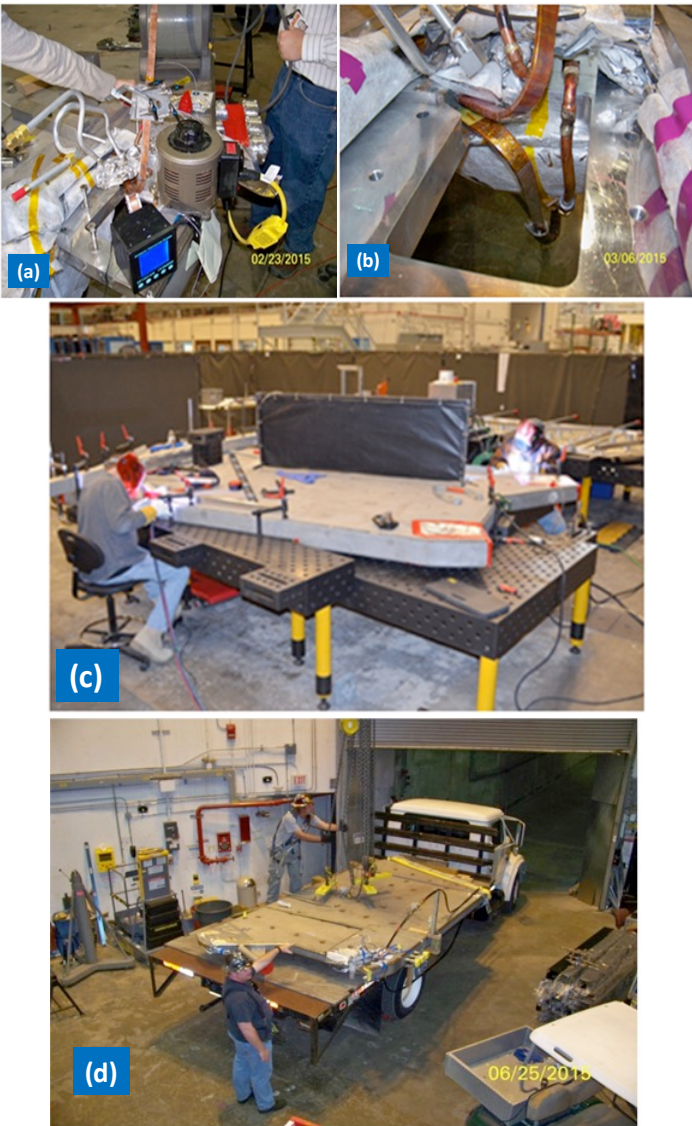


Fig. 26 (a) Soldering additional copper stabilizer to the leads as they exit from the vacuum jacket, (b) Stabilized leads bent to required shape and insulated – ready for transport to the hall, (c) Welding shut the vacuum jacket, (d) Last coil to be delivered to the hall from the JLab Cryostat Factory

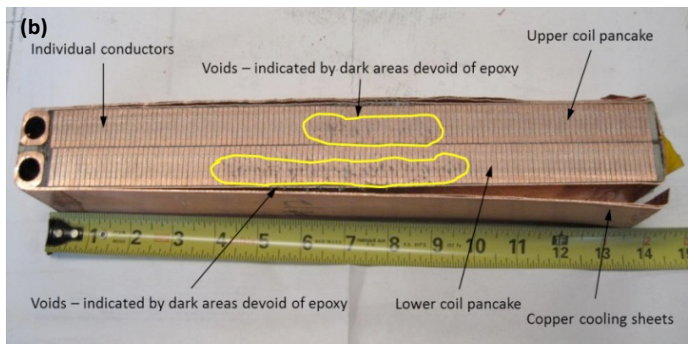
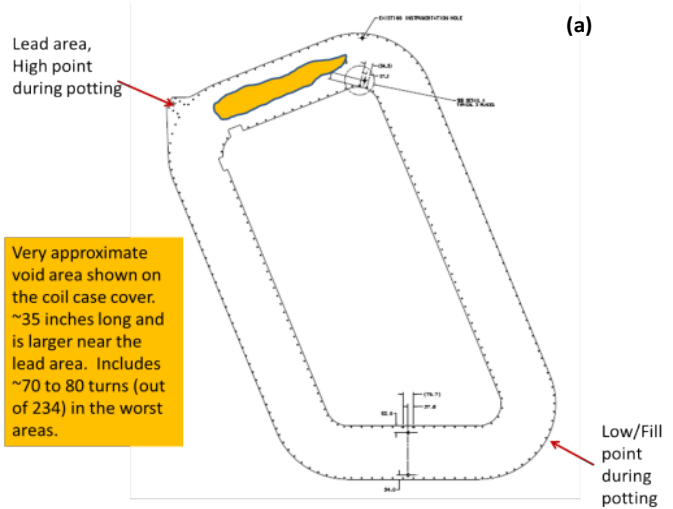


Fig 27 (a) Voids identified on practice coil, (b) sectioned coil indicating problem areas

Key changes for the torus included:

1. Changing of the sequence assembly by attaching the copper cooling sheets after first potting thus allowing complete visual inspection
2. Adding material (polypropylene mesh and peel ply) in the coil potting mold to take up the space left by the copper and ground plane and to allow resin distribution and removal of the spacer
3. Fine tuning of resin degassing and infusion process

Consistent with the program risk mitigation approach of practicing every quality or schedule-critical procedure, the Cryostat Factory practiced cryostating a full-scale empty coil case, which was later disassembled and returned to FNAL for use on a production CCM. This early practice allowed refinement of the assembly procedures and construction time estimates.

Solenoid

A top-level pictorial view of the manufacturing and build sequences with a summary ([Table XXIV](#)) of the overall magnet construction at the solenoid vendor (ETI) follows ([Figure 28-33](#)):

TABLE XXIV
A SUMMARY OF THE KEY MANUFACTURING STEPS - SOLENOID

Manufacturing Step	Location
1 Superconducting Rutherford cable soldered into C-shaped copper channel	Advanced Engineering Systems LLC, PA,

		USA
2	Conductor inspected and cleaned	Everson-Tesla Inc (ETI), PA, USA
3	Conductor insulated with glass-cloth and wound onto bobbin (coil former)	
4	Leak check and pressure test of C1-4 bobbin cooling channels and pipe work	
5	Wind Coil 1 (inner coil) and epoxy pot	
6	Wind Coil 2 (inner coil) and epoxy pot	
7	Wind Coils 3 and 4 (intermediate coils) on common C1-4 bobbin and epoxy pot	
8	Wind Coil 5 (shield coil) and epoxy pot	
9	Cool down Coils 1 and 2 (using LN2 boil-off) and shrink-fit into C1-4 bobbin	
10	Assemble Coil 5 over C1-4 bobbin using 4 cross-member beams	
11	Rivet and solder thermal ‘copper fingers’ between all coils	
12	Assemble thermal shield and C1-4 bobbin into vacuum jacket	
13	Fit suspension links	JLab
14	Leak check and pressure test of internal circuits	
15	Weld shut vacuum jacket	
16	Leak check	
17	Ship to JLab	
18	Fabrication of solenoid service tower (SST)	
19	Installation of SST and solenoid	
20	Commissioning of solenoid	

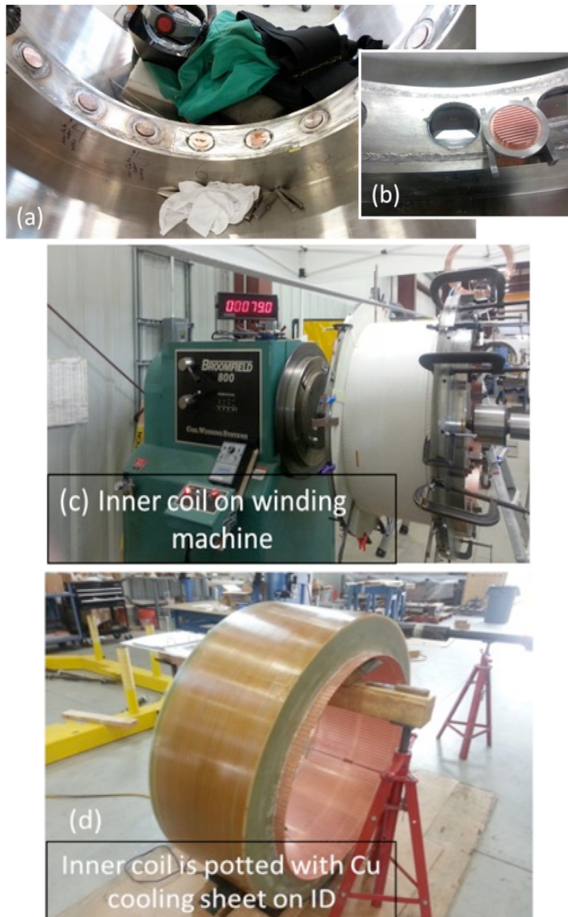


Fig. 28 Left to right: (a) central cooling channel with Helium ‘buttons’ installed’, (b) inset picture showing a helium button before welding into channel, (c) one of the two inner coils being wound, (d) One of the two inner coils after epoxy potting is complete (the slotted copper cooling sheet can be seen potted in with the coil on its inner surface

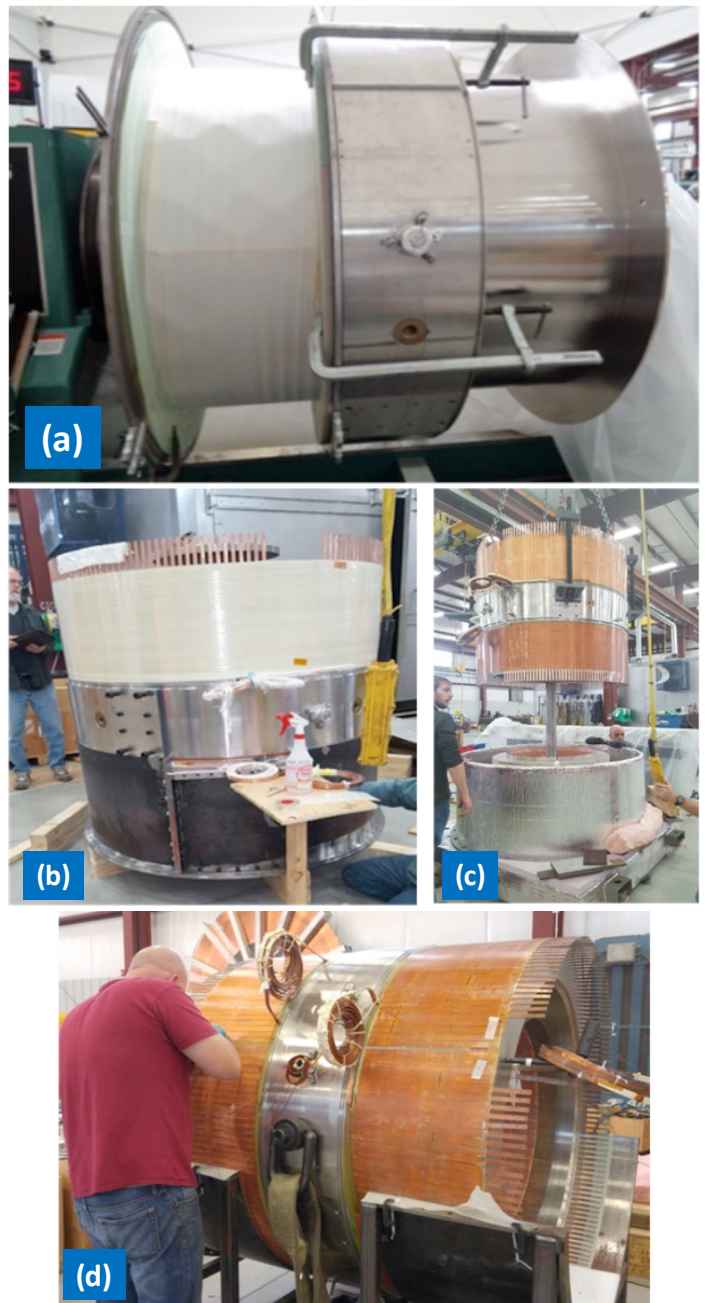


Fig. 29 Left to right: (a) Coil 3 being wound into its pocket on the Coil 3-4 bobbin, (b) Coil 4 (lower coil in the picture) having its potting mold being fitted around it in preparation for epoxy potting, (c) the Coil 3-4 bobbin being lowered over one of the two inner coils for the shrink fit operation (the copper fingers can be seen potted in with coils 3 and 4 on their outer surfaces), (d) Coils 1 and 2 assembled within the Coil 3-4 bobbin and coils 3 and 4 being instrumented with CERNOX temperature sensors



Fig. 30 (a) Coil leads being routed on the outside of Coil 5, (b) Additional copper stabilizer being soldered to leads



Fig. 31 Left to right: (a) Styrofoam being painted onto the outer diameter of Coil 5 after epoxy potting, (b) Inserting Coils 1-4 into the Coil 5 bobbin, (c) All five coils assembled together

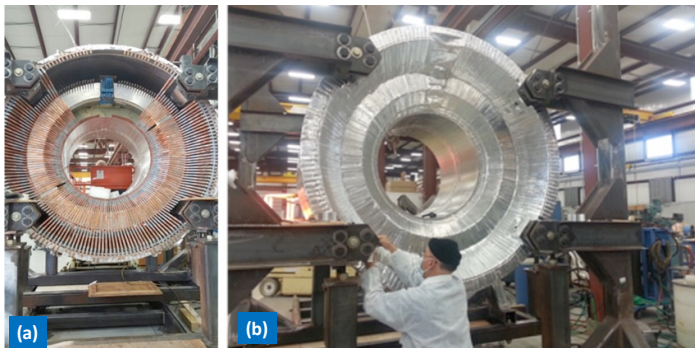


Fig. 32 (a) Copper cooling ‘fingers’ being riveted and soldered across all coils – these fingers provide the conduction cooling path from the central helium annular channel to each individual coil, (b) Fingers being taped over with aluminum tape



Fig. 33 Left to right: (a) Cold mass inserted into vacuum jacket, (b) Thermal radiation shield end cap being installed, (c) Solenoid in shipping cradle and transport fixture being loaded onto air-ride low-loader truck bed at vendors

VI. INSTALLATION

Torus - Installation in the hall was based on the “spit” method (Figure 34a). Individual coils assembled in their individual vacuum cases, (with a portion of the vacuum case open to enable attachment to the central hub, Figure 34b), were transported into the experimental hall. After the first coil is attached to the hub, its hex beams are attached before the next coil is brought in and connected to the hex beams and so on until all 6 coils were assembled (Figure 35). This whole sub-assembly is freely rotatable around the hub to allow critical operations (like splicing or welding), to be performed at a convenient and safe location and orientation.

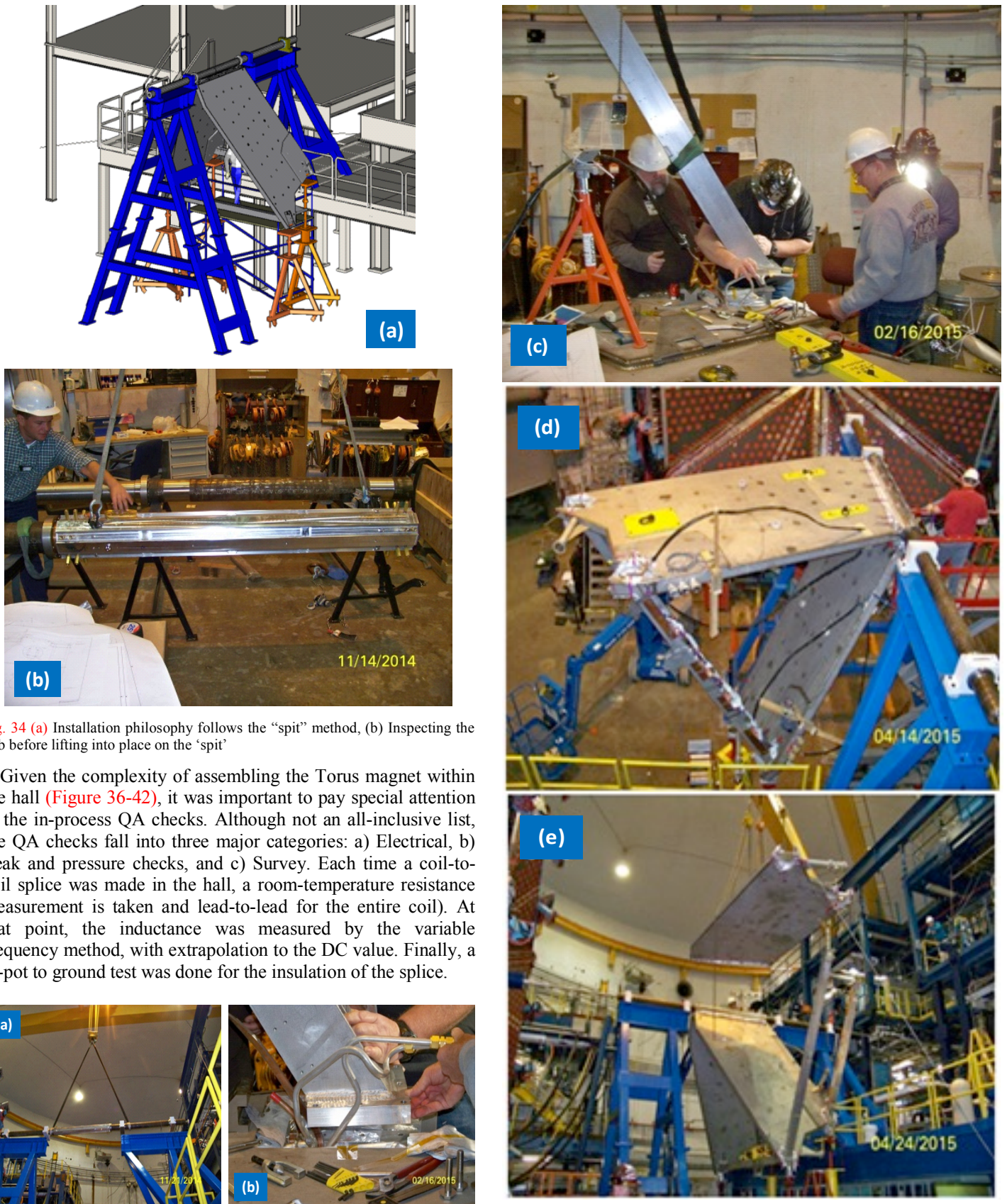


Fig. 34 (a) Installation philosophy follows the “spit” method, (b) Inspecting the hub before lifting into place on the ‘spit’

Given the complexity of assembling the Torus magnet within the hall (Figure 36-42), it was important to pay special attention to the in-process QA checks. Although not an all-inclusive list, the QA checks fall into three major categories: a) Electrical, b) Leak and pressure checks, and c) Survey. Each time a coil-to-coil splice was made in the hall, a room-temperature resistance measurement is taken and lead-to-lead for the entire coil. At that point, the inductance was measured by the variable frequency method, with extrapolation to the DC value. Finally, a hi-pot to ground test was done for the insulation of the splice.

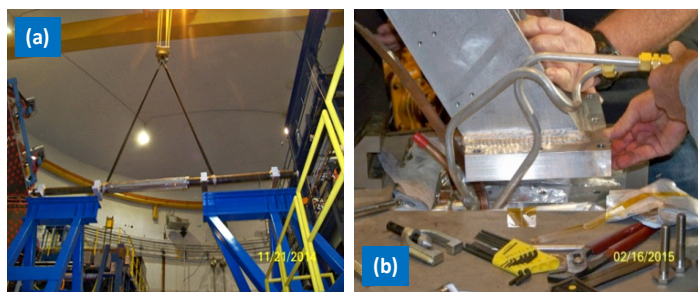




Fig. 35 (a) Installing the hub, (b) and (c) Trial fit of a hex beam to a coil (d) hex beams end to the coils (e) Third coil on the crane with torus rotated and hex beams installed to accept it, and (f) upstream hex beam in horizontal position to allow for convenient and safe working

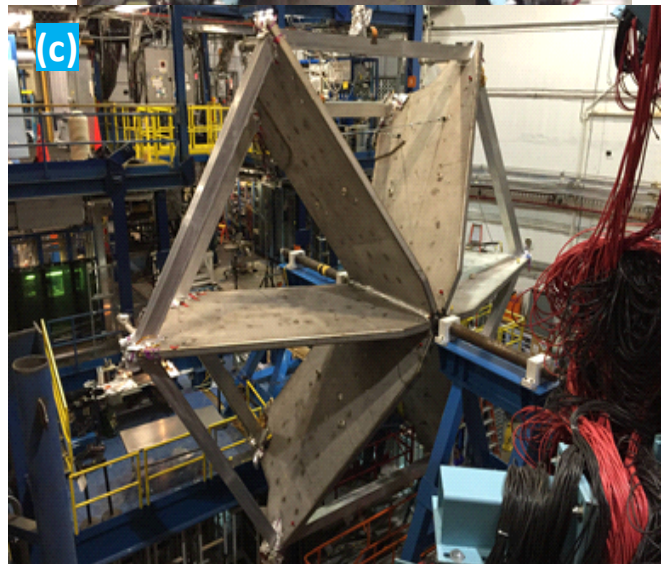
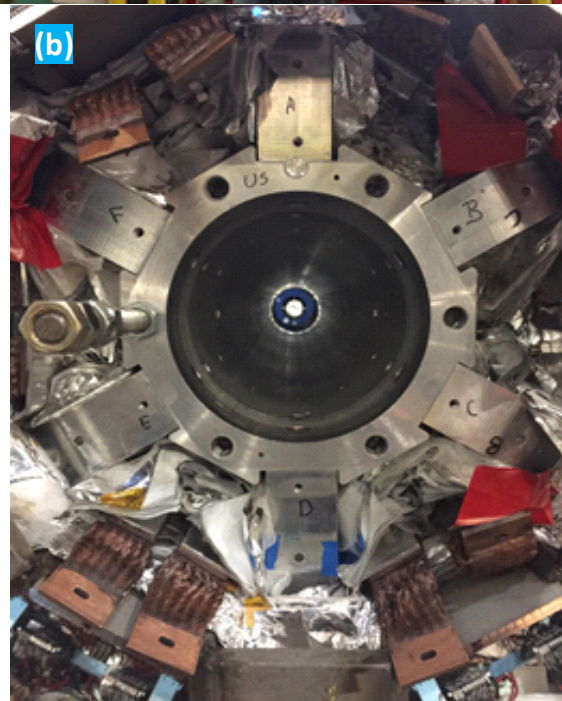
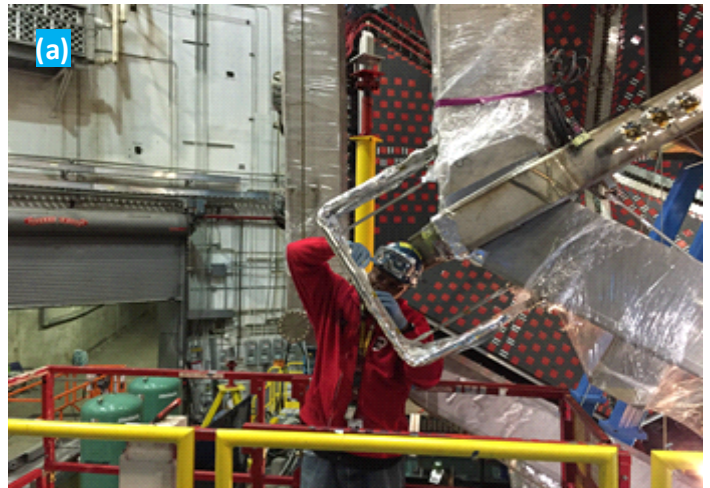


Fig. 36 (a) Splice soldering using purpose-built temperature-controlled heating rig, (b) Applying MLI to the splice joints, (c) Load testing an axial support

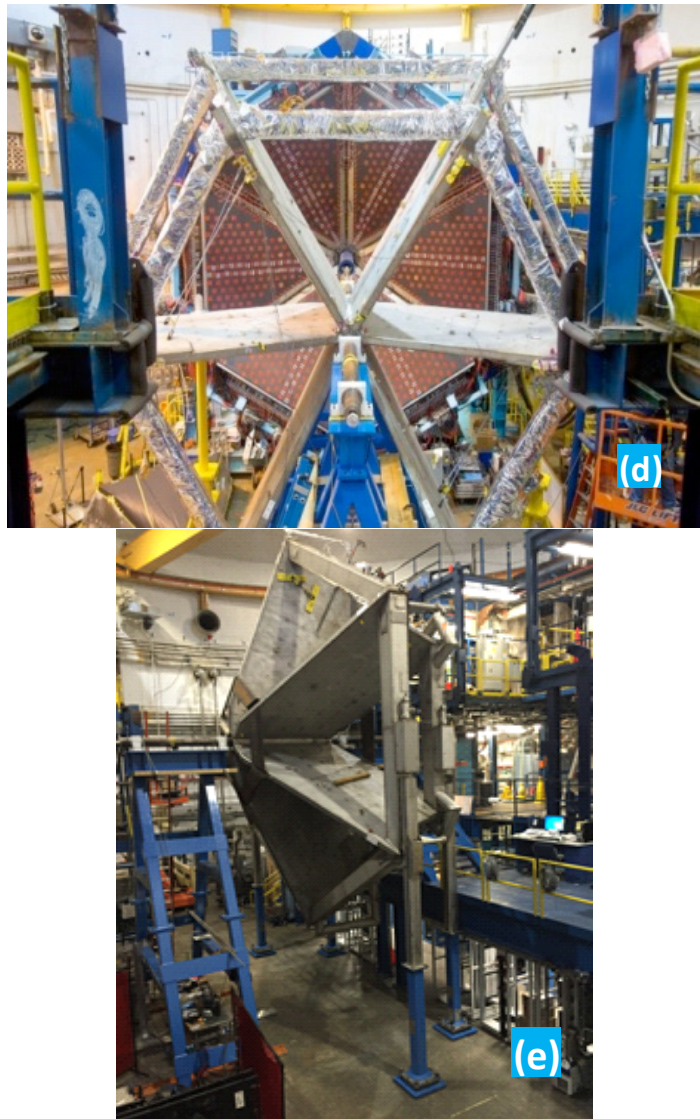


Fig. 37 (a) Insulating a cryogenic ‘jumper’ between hex beams, (b) Aligning and shimming the coils on the hub, (c) All torus coils and hex beams installed, (d) Hex beams wrapped in MLI, (e) Torus rotated to final position and legs installed

Likewise instrumentation checks are carried out routinely at the completion of each hex beam fitting, and each time the coils are rotated. All connections of each cooling circuit between coils within the vacuum jacket were made by either welding or brazing. Aluminum welds and copper brazes received a liquid nitrogen cold shock but stainless steel welds were exempt. Once each circuit that joined the 6 coils was completed it was pressure and leak tested prior to burying it in MLI. Surveys for alignment are also carried out after attaching each coil to the hub, and a global survey was done at the completion of the hexagon. Torus leak testing did not find any internal leaks, even with the pressure testing. For the external leak testing we employed two leak detectors, one at the TST and one at coil D (6 O’clock position). This arrangement were sufficient to find external leaks and upon completion of testing, no sign of any leaks on the most sensitive scale of the leak detectors.

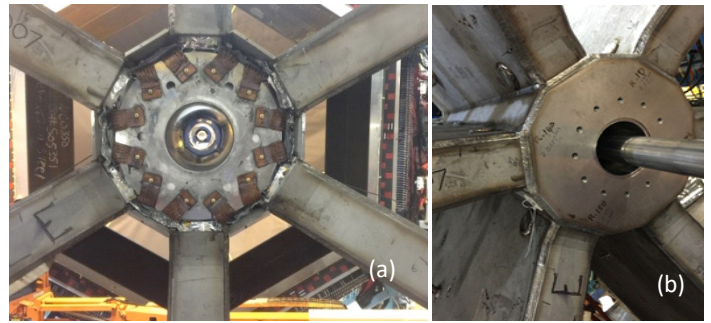


Fig. 38 (a) Aluminum thermal shield inside the bore installed with copper thermal straps attached, (b) Hub vacuum jacket ready to be welded shut

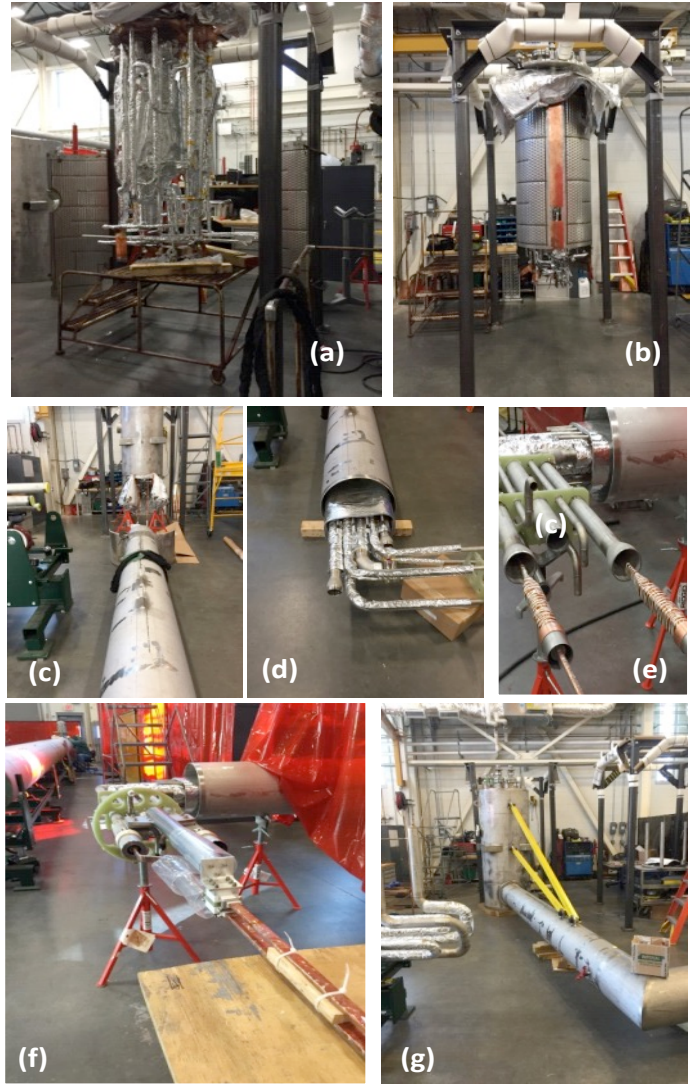


Fig. 39 (a) Torus Service Tower (TST) internals insulated with MLI, (b) Thermal shield fitted, (c) Preparing the cryo-duct for attachment to the TST, (d) Cryo-duct pipework insulated with MLLI, (e) Superconductor splice joints and leads at the helium-vacuum interface, (f) Insulated leads, (g) Cryo-duct welded to TST body

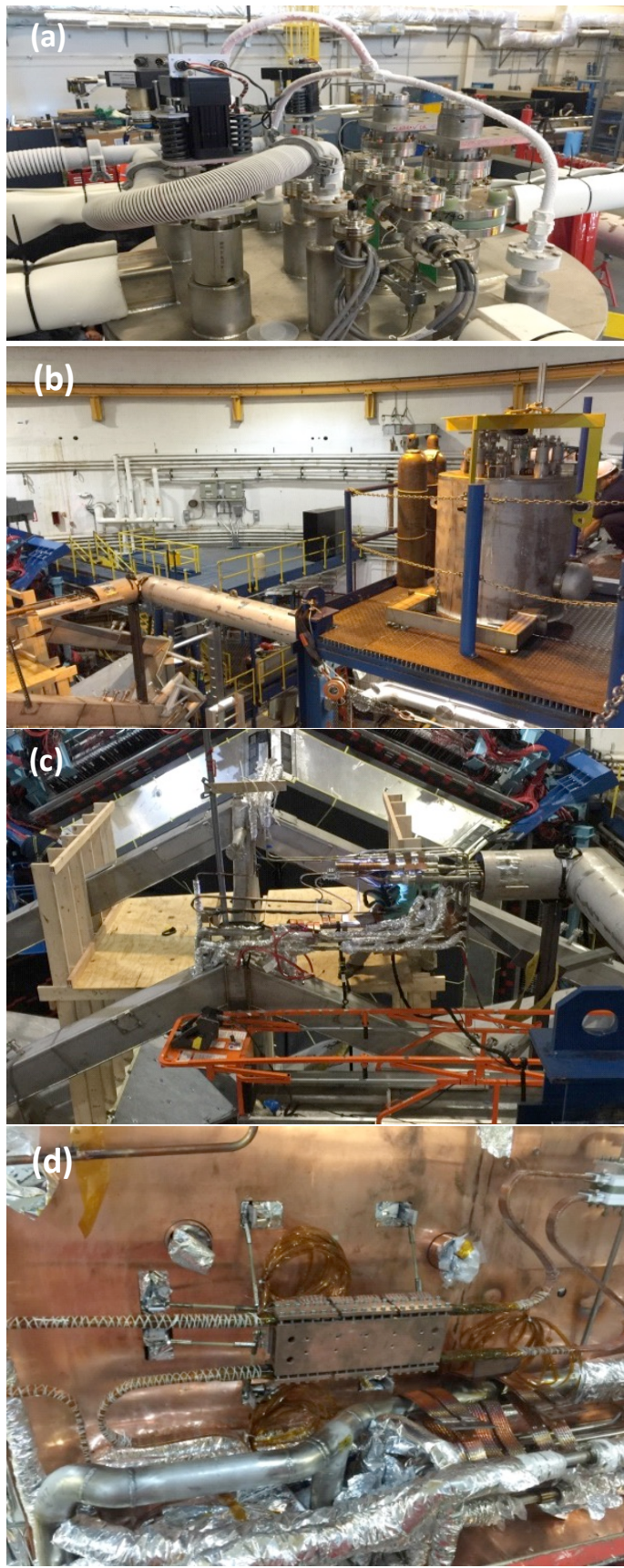


Fig. 40 (a) Cold testing TST pipework, (b) TST in place on the space-frame, (c) Cryo lines connected between the TST and the Torus, S-shaped conductor splices completed, (d) Conductor splices in the Torus 'Chimney'

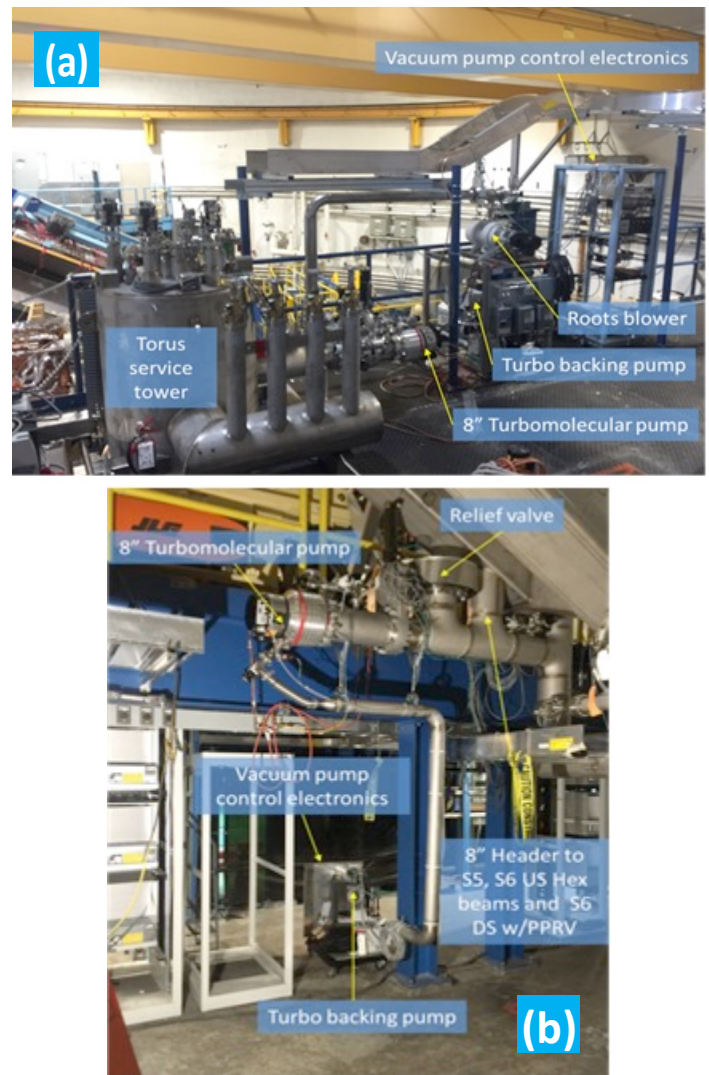
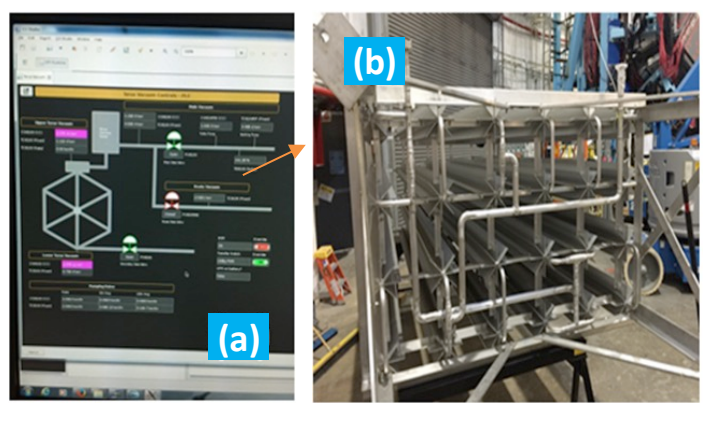


Fig. 41 (a) Primary pumping system mounted on service tower, (b) Supplemental pumping system mounted on torus hex beam



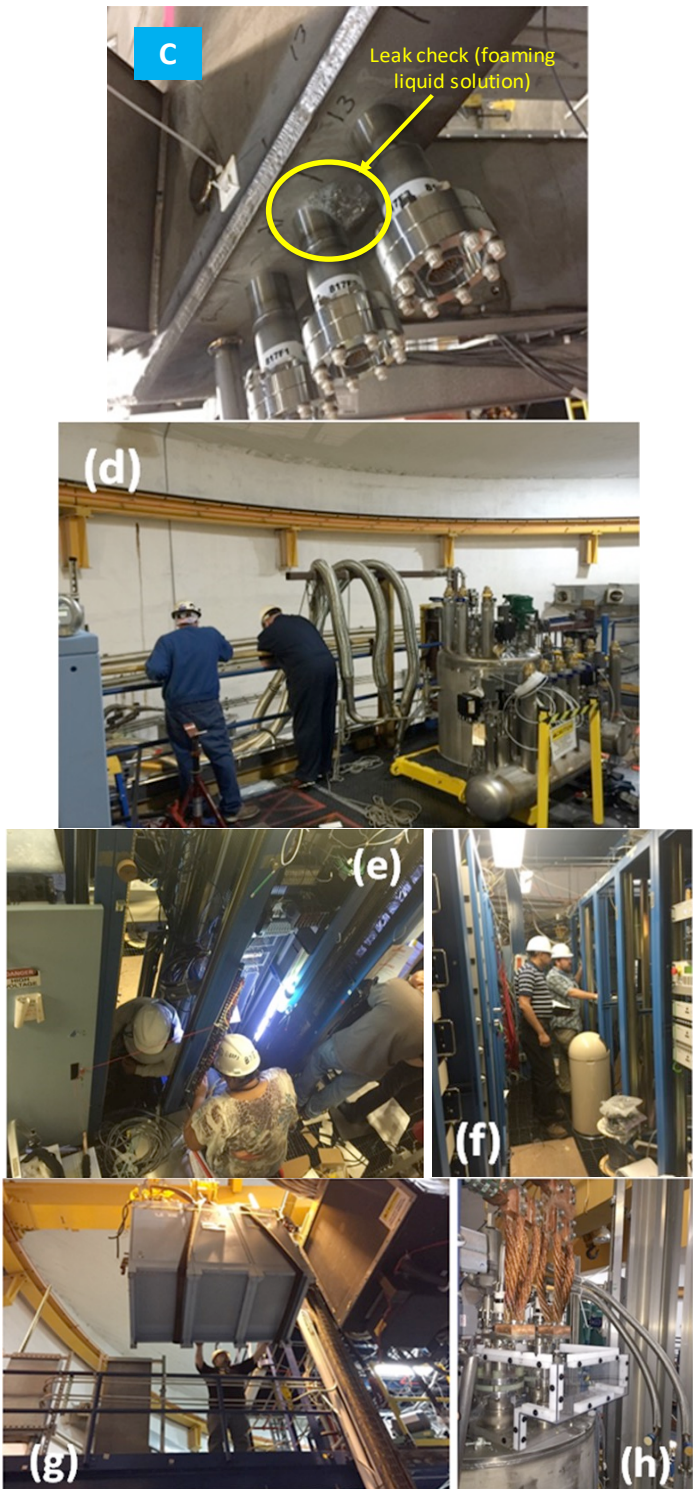


Fig 42 (a) Vacuum control screen for the Torus, (b) Modifications to an ambient vaporizer from CLAS to reduce pressure drop, (c) Leak checking with foaming liquid solution, (d) Distribution can in place in Hall B, (e) Wiring up instrumentation racks, (f) Running checks on the instrumentation, (g) Lifting a magnet power supply into position (h) Flexible copper jumpers connecting the torus water-cooled leads to the magnet vapor-cooled leads

Solenoid - The magnet was built by ETI, and transported by road to JLab using a purpose built shipping cradle and vibration isolation transport fixture (**Figure 43**). To assure safe transport several dummy runs between ETI and JLab were done and data on the acceleration loads was collected. This data was used for

analysis of the magnet structure with temporary shipping supports.

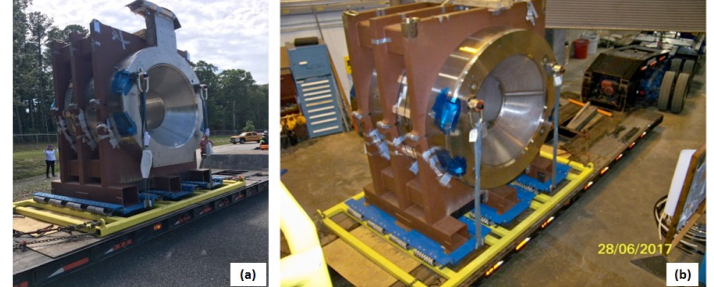


Fig. 43 (a) Solenoid in shipping cradle and transport fixture arrival at JLab, (b) solenoid arrival in Hall B at JLab

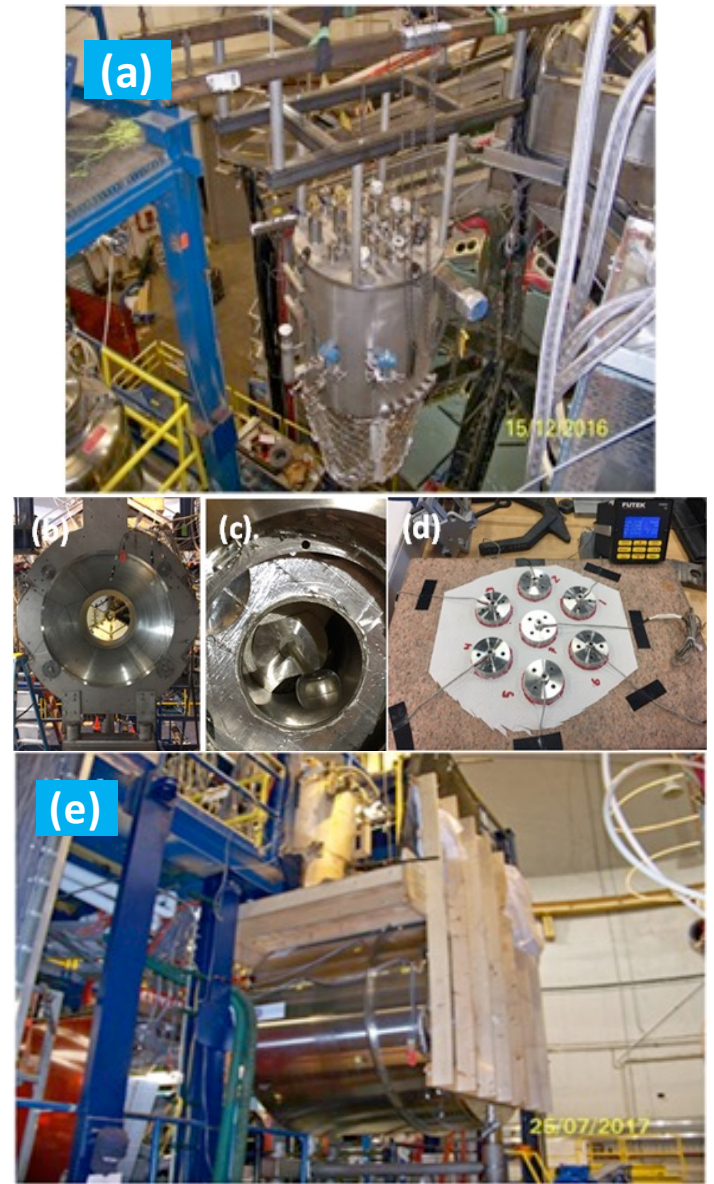


Fig 44 (a) The solenoid service tower being lifted into place on the space-frame within the hall to await the arrival of the magnet, (b) Solenoid on its cart awaiting removal of axial support shipping fixtures and installation of axial support rods, (c) one of eight axial support rods being installed, (d) Axial support load cell readings being checked for consistency prior to installation, (e) Solenoid in position on its 'cart' with a temporary wooden platform installed to allow welding of the service tower to the main magnet

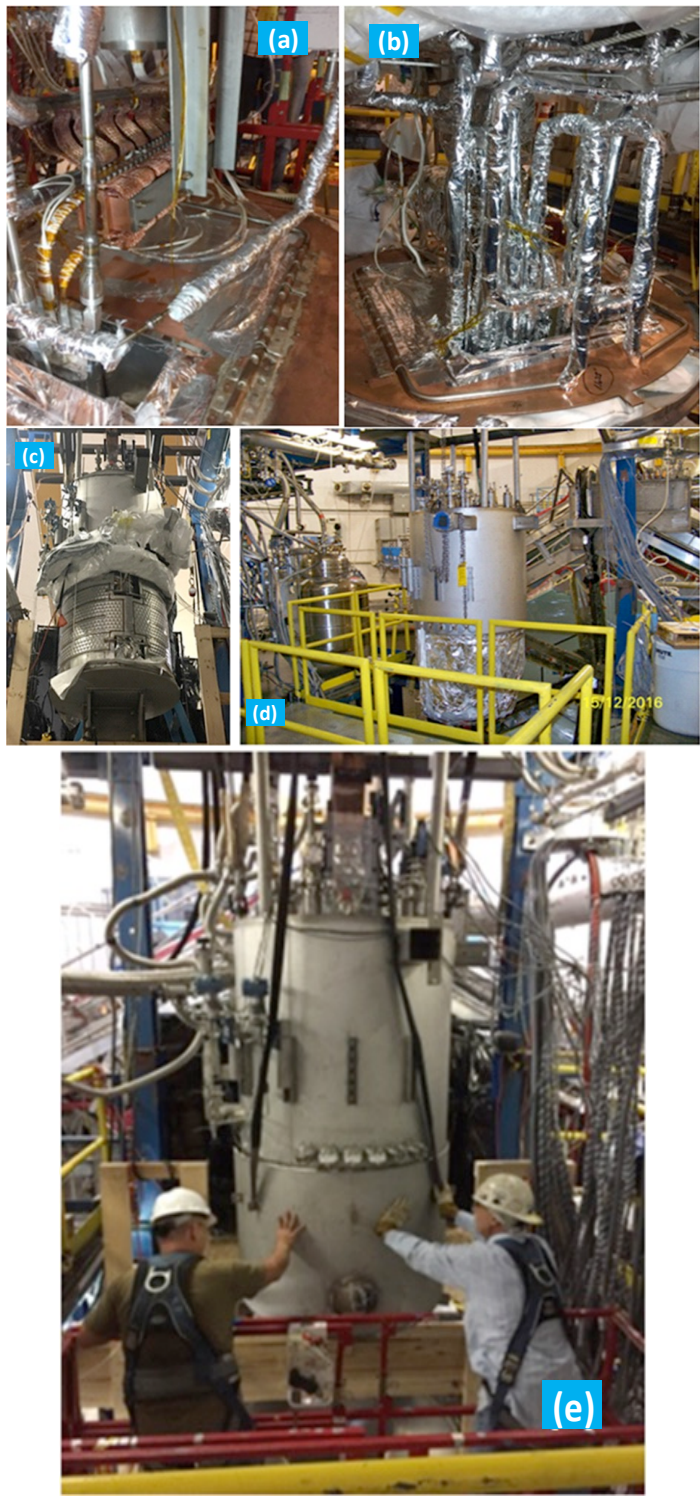


Fig 45 (a) Splices completed to join the magnet start and end leads with the vapor-cooled leads in the SST, (b) Splice block and cryogenic pipework wrapped in MLI, (c) Service tower thermal shield welding completed, (d) Service tower – ready to have its vacuum jacket closed up, (e) Fitting the SST vacuum jacket prior to final welding

Upon arrival at JLab, a visual inspection was completed along with testing of internal sensors and their wiring. The magnet was then lifted by the crane and attached to the installation cart on the beam line in Hall B. It was rough aligned by the JLab survey and alignment team and the temporary shipping braces were

replaced with the final supports and load cells. The solenoid service tower (SST), built by JLab was ready several months before the Solenoid arrival, and was already in Hall B and roughly positioned upon the space frame above the beamline. With the Solenoid on the beamline the SST was then aligned to the solenoid. The two splices that connect the SST to the magnet were completed and instrumented with voltage taps and temperature sensors before the internal welding commenced. Pressure and leak tests followed, similar to the Torus. Finally the multi-layer insulation blankets were applied and the vacuum jacket was welded shut ([Figure 44](#)).

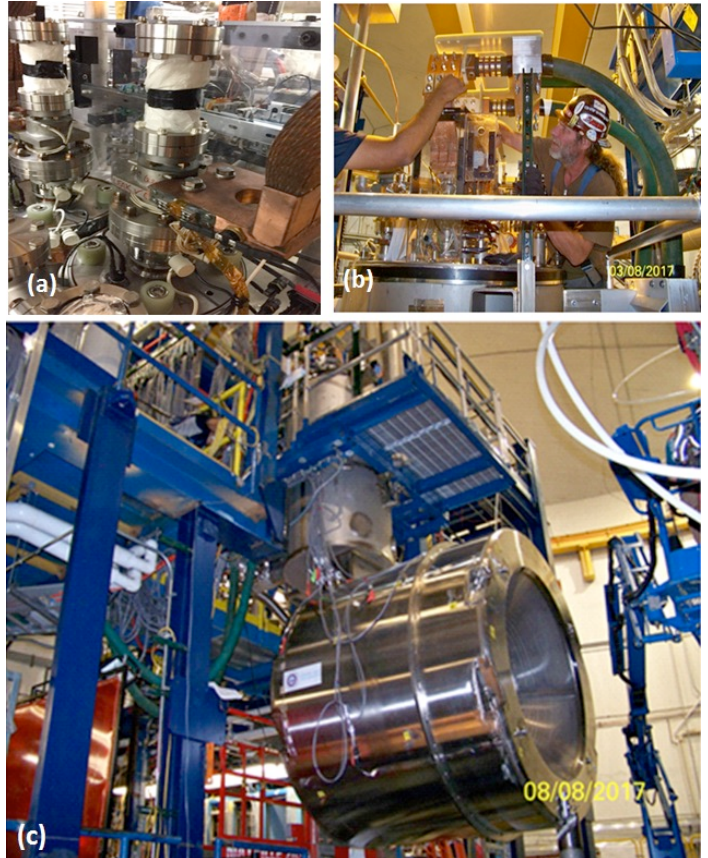


Fig.46 (a) Ceramic break fitted to top of vapor -cooled leads, (b) Connecting up the water-cooled leads to the vapor-cooled leads at the top of the SST, (c) Solenoid magnet installation complete with ‘crow’s nest’ service platform installed around the SST

VII. COMMISSIONING AND TEST RESULTS

System tests were carried out at predefined excitation currents to confirm that the overall system response was as designed. The electromagnetic and cryogenic parameters were monitored during the tests in order to validate the thermal/cryogenic circuit design features. Additionally the magnet was ramped to low currents to minimize its stored energy level before a controlled fast discharge was initiated. This allowed the JLab team to check that all system protection mechanisms were operating as designed, thereby mitigating any further risk when the torus was run at its nominal current of 3770 A. The torus magnet reached its full operating current without any quenches in November 2016 while the solenoid reached its full operating current of 2416 A in September 2017 with 5 training quenches in Coils 3

and 4.

Each magnet has its own cryogenic service tower which is fed from a common cryogenic distribution box. The monitoring, control, protection, power, vacuum and cooling sub-systems are similar but independent for each magnet. Although the systems are separate, a cryogenic ‘event’ in one magnet can affect the other and vice versa since both magnets share the same distribution box, as addressed previously.

Torus

Pump Down - Before the final vacuum pump down proceeded, all the OOPS were properly set to allow for vacuum jacket deflection. The pump down started gradually at about 2psig/hour for the first 7 hours to alleviate any coil-case ‘ballooning’ effects and to minimize any movement of the MLI. The roots blower followed by turbo-molecular pumps were used to reduce the pressure to about 10^{-4} Torr before initial cool down and several backfills with gaseous nitrogen were used to assist with the removal of water within the system. The pressure in the system reached about 5×10^{-5} Torr after cool down started.

Purification -A purification process using gaseous nitrogen (GN₂) and gaseous helium (GHe) was used to clean the nitrogen and helium circuits. The nitrogen circuit only needed to be free of water and flow purged with warm GN₂. The helium circuits needed to be free of water as well as all other contaminate gases.

The initial purification of the Torus included purification of the entire Hall B cryogenic system. This included all the warm gas piping, ambient vaporizers, cryogenic transfer lines, distribution box (DBX), U-tubes that interconnect the DBX to the 500liter helium buffer dewar, U-tubes that interconnect the DBX to the Torus, the Buffer Dewar and the Torus. There are 3 cold connections at the End Station Refrigerator (ESR) that are used, 4K helium supply, 4K helium return and LN2 supply. There are two warm gas connections to the ESR, 300K 4atm helium and 1 atm 300K return helium.

Cold connection U-tubes at ESR were not installed, Warm connection valves were closed. Where possible each circuit was purged with room temperature boil off nitrogen gas for several days to drive off moisture. The warm helium supply line could not be purged this way because there is no vent on the ESR end. It is also noted that care was taken to be sure not to pressurize the helium circuits above 1 atm with nitrogen, to keep from contaminating the operating ESR. The nitrogen circuits were then pumped and backfilled between .5 atm and .1torr 3 times and backfilled with nitrogen. At this point the N2 circuits are considered clean.

The helium circuits were pumped and backfilled through the same pressure range but 5 times. Pumping and backfilling allows access to the small dead end ranges of the circuits such as pressure transducer lines and relief valve lines. After pumping and backfilling the helium circuits, purging through the system was done using clean helium from the ESR and sending it back to the refrigerator helium recovery system. This recovery system has nitrogen contamination monitors to verify the level of contamination in the return gas. After the pump and backfills, the return gas to the recovery system showed little to no contamination was returned, thus our N2 purge and helium pump and backfills were successful. Similar process but on a

much smaller scale was done for the Solenoid

Cool Down – The unique nature of the Torus structure with a cold hub and cold beams made it especially critical to minimize temperature differences between the beams and the coils. Detailed FEA were done and showed that a maximum DT of 50K between them could be tolerated during the cooling process at temperatures between 300 and 100K for the 4K mass. The independent nature of the LN2 shields did not have this physical requirement. The piping of the supercritical circuit is nearly 200m long with most of it split equally between tubes in the coils and re-coolers. Due to this long length limited flow at room temperature can be pushed through this circuit with the 4atm helium supplied to the Hall at room temperature. To achieve the required cool down time of 3 weeks, the re-coolers were also designed to be used and performed well during cool down.

The cool down of the Torus was done using variable temperature helium gas provided by the distribution box. Inside the distribution box are two heat exchangers that cool one stream of helium to 80K. This 80K helium was mixed with room temperature helium to allow variable temperature gas to be fed to the super critical circuit and also the shell side of the re-coolers. This then allowed the even cooling of all the coils and the hex beams. During the cool down the maximum difference between the average coil temperature and the average Upstream Hex beam temperature was 12K and it averaged about 10K. For the downstream beams vs the coils the max difference was 25K at the beginning but once the flows were balanced it averaged about 2K. With these achieved values we were very safe versus our allowable difference of 50K. For safety we had the PLC programed to shut off all cool down flow if the differences ever exceeded the maximum allowable.

To gently cool the heat shield we took 80K boil off from the LN2 pot in the distribution box and with an electrical heater in the U-tube between it and the TST heated the gas to give a controlled temperature gas to the shield. Again this was interlocked to shut the heater and the flow if the maximum difference between any of the six coil shield outlets and the shield supply reached 60K.

From room temperature to about 100 K the cool down rate of the Torus was 0.5-0.7 K/hour The cool down time from 300 K to about 4 K for the torus was calculated to be about 14 days assuming a maximum temperature differential across the cold mass of 30 K and helium flow rate of 7 g/s. In reality, the cool down took longer and was carried out in several steps. During the cool down process (average CCM temperature = 209 K), it was noted (via observation of strain gauge readings on the supports) that the four torus vertical supports were apparently bending. This necessitated a slow-down in the cooling process (to about 170 K) and finally a temporary halt while measurements and strain gauge calibrations were checked. It was discovered that although some of the strain gauges were not being adequately temperature-compensated, the vertical supports were indeed experiencing some level of bending. A risk review was convened to plan the path forward and four options were considered – which included a ‘worst’ case option that required a warm-up to room temperature to repair the vertical supports by cutting into the vacuum jacket. A spare vertical support was tested at liquid Nitrogen temperature and was demonstrated to

have a more than adequate strength safety factor under bending ([Figure 47](#)). It was thus determined that it was safe to continue with the torus cool down which was then resumed and the torus achieved its Helium operating temperature of 4.5 K without any further issues.

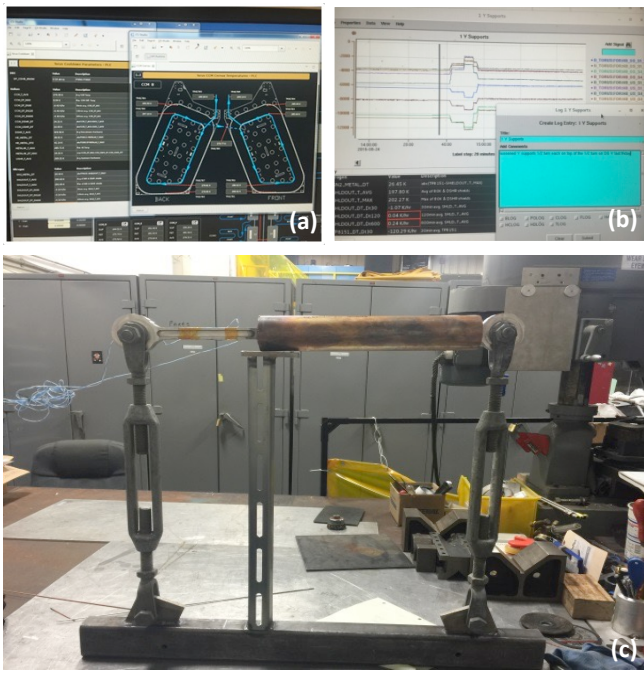


[Fig 47](#) (a) Monitoring coil temperatures during cool down, (b) Investigating strange bending behavior of vertical supports, (c) Monitoring forces on supports, (d) Bend testing a spare vertical support

Steady State Cooling - The US cold hex beams contain the cryogenic and electrical connections (splices) between coils as well as the re-cooler heat exchangers. The re-coolers contain liquid helium and are connected by large tubes to the helium reservoir at 1.3 atm. located within the Torus Service Tower (TST). Two small tubes originate at the bottom of the TST and run through the three re-coolers, exiting at the bottom of the re-cooler outer shell. Since the liquid in the small tube is denser than the heated fluid in the re-cooler's outer shell, a thermosiphon is established exchanging cooler reservoir liquid with the shell side fluid. The 1.3 atm. liquid helium cools 3.0 atm. helium, before entering each coil.

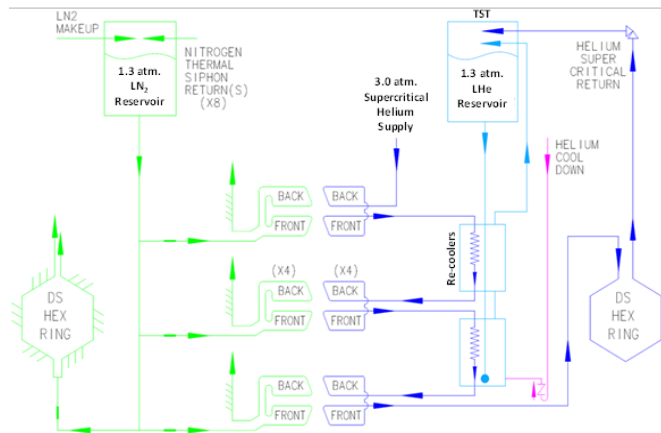


[Fig. 48](#) Simplified flow diagram of the CLAS12 torus helium and nitrogen cooling circuits

The cooling scheme ([Figure 48](#)) consists of three separate flow circuits as follows:

- 1.3 atm. Helium circuit* - helium fills the LHe reservoir (light blue) within the TST, it then flows down through the re-coolers to the blue dot. Thermal siphon flow returns back up through the re-cooler outer shells and the upstream hex beams.
- Supercritical helium at 3.0 atm.* - (dark blue) passes through a (recooler) coil in the TST helium reservoir, then through six coil/re-cooler sets, through tubes cooling the downstream cold beams, and through a final (Heat exchanger coil) coil in the TST helium reservoir prior to flowing through the Joule-Thompson valve that fills the TST reservoir.
- The 1.3 atm. LN₂ circuit* also utilizes a thermosiphon flow with one main feed separating into 8-parallel branches which keep each shield at ~80 K to reduce thermal radiation to the coils and cold hex beams ([Figure 49](#)). Out of 8 total branches, 2-feed into the downstream hex beam shields and 6-feeds into coil shields.

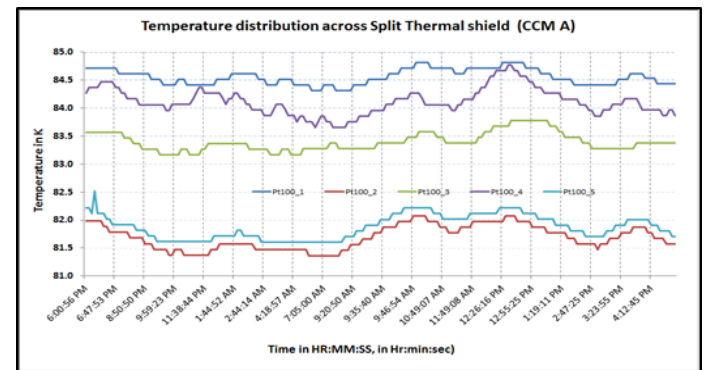


[Fig 48](#) (a) Steady state temperature distribution across one of the thermal shields

Solenoid

Pump down and Purification

Pump down of the solenoid was much faster and easier because the magnet has much less surface area, an overall smaller size and better conductance between the turbo pump and the magnet. Purification was done similarly to the torus using a gN₂ purge for several days, followed by 5 pump and back-fills then flowing to the purifiers while monitoring the contamination.

Solenoid Cooling

This five-coil magnet is also conduction cooled by 4.5 K helium but unlike the Torus coils the heat is directly transferred to liquid vs supercritical gas. The cool down system for the Solenoid is the same one as for the Torus and was used while the Torus was at 4.5K. Similar interlocks and controls were used to assure safe cool down. The magnet's liquid helium cooling channel is located between the two main inner coils and runs around the inner diameter of the bobbin. The thermal shields are cooled using the boil-off from the magnet LHe reservoir. The magnet is held at its operating temperature by conduction cooling via a thermosiphon helium circuit from the magnet reservoir ([Figure 50](#)). Adequate instrumentation with redundancy is provided to monitor and control the magnet cool down and steady state operation.

Pre-commissioning checks on all sub-systems, controls &

instrumentation are carried out for each magnet prior to starting the commissioning process.

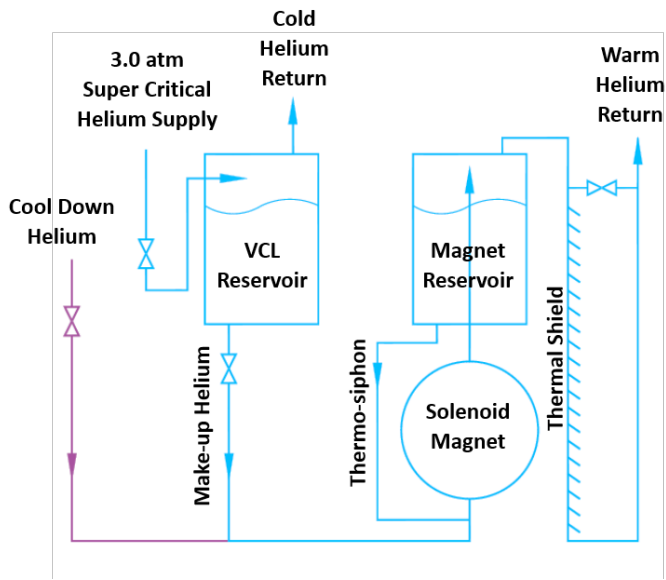


Fig 50 Simplified cooling circuit schematic for the solenoid

The torus and solenoid were cooled in 2-steps. Variable temperature gas was used to cool from 300 K-100 K followed by LHe to 4.5 K.

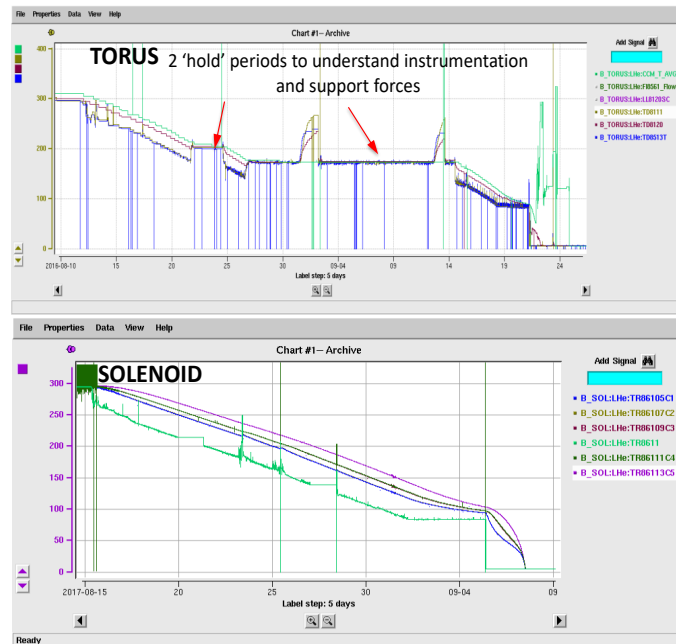


Fig. 51 Torus and solenoid cooldown (Torus Cooldown: Start-12Aug16; Complete-22Sep16 and Solenoid Cooldown: Start-5Aug17; Complete-07 Sep17)

Inlet temperature to the coil/s, average coil and outlet temp were monitored. The maximum cooling rate was limited to 2 K/hour (Figure 51).

- Total time = 43 days (Torus), 23 days (Solenoid)
- Cooling time = 19 days (Torus), 23 days (solenoid)
- Helium temperature controlled at 45 K below the maximum metal temperature for the Torus and between 35K and 60 K below maximum metal temp for the Solenoid

- Maximum allowed metal temperature differences in Torus was 40K and for the solenoid it was 46K. Because the cooling designs were robust the maximum differences were 25K for the Torus and 40K for the Solenoid.
- Cooldown Helium flow rate for the Torus was 6-7g/s and for the Solenoid it was 5-6 g/s

At steady state the solenoid magnet itself requires only 0.4g/s of liquid helium for its cooling. This flow was measured directly using a room temperature flow meter. This flow rate does not include the amount of flow needed for the VCL's, the lead reservoir or the primary supply and return U-tubes.

Torus process safety [25]

The operational protocol developed for the cryogenic process was guided by results of a study carried out by Ghoshal *et al*, which considered the worst-case scenario, of having a loss of vacuum (LOV) and magnet quench simultaneously.

In an LOV, quench, or Fast Dump the piping systems are protected from over pressure over pressure relief valves. Five relief valves placed along the 3.0 atm. cooling circuit. 3 valves, set to vent at 5.3 atm., are placed strategically along the path of CCM's and re-coolers and are located on the Hex Ring Vacuum Jackets and 2 valves are set to vent at 4.6 atm. And located on the TST. In the event of a fast dump, a check valve in the supply U-tube prevents any back pressure into the Distribution Box. The 1.3 atm circuit is protected by a 2.7 atm. Relief valve located on the TST.

During a LOV and magnet quench, the highest system pressure for this circuit will occur at the farthest point from the relief valve in the re-cooler piping. The majority of the energy imparted to the 1.3 atm. circuit comes from the LOV. The energy imparted from the magnet quench is much lower as it is indirectly transferred to the 1.3 atm system; (a) first to the 3.0 atm. helium flow, and (b) then into the 1.3 atm system through the re-coolers.

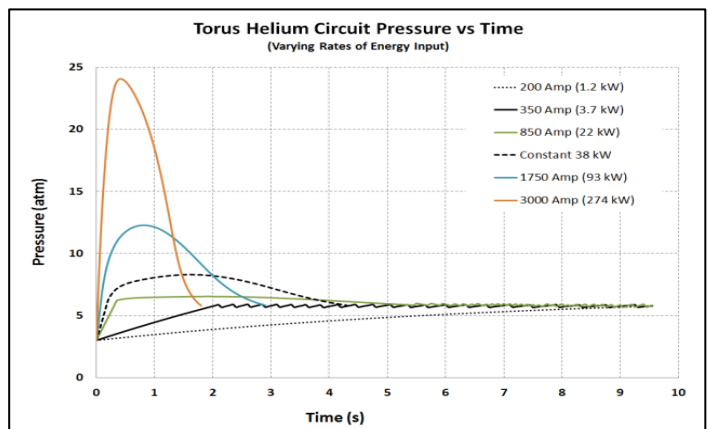
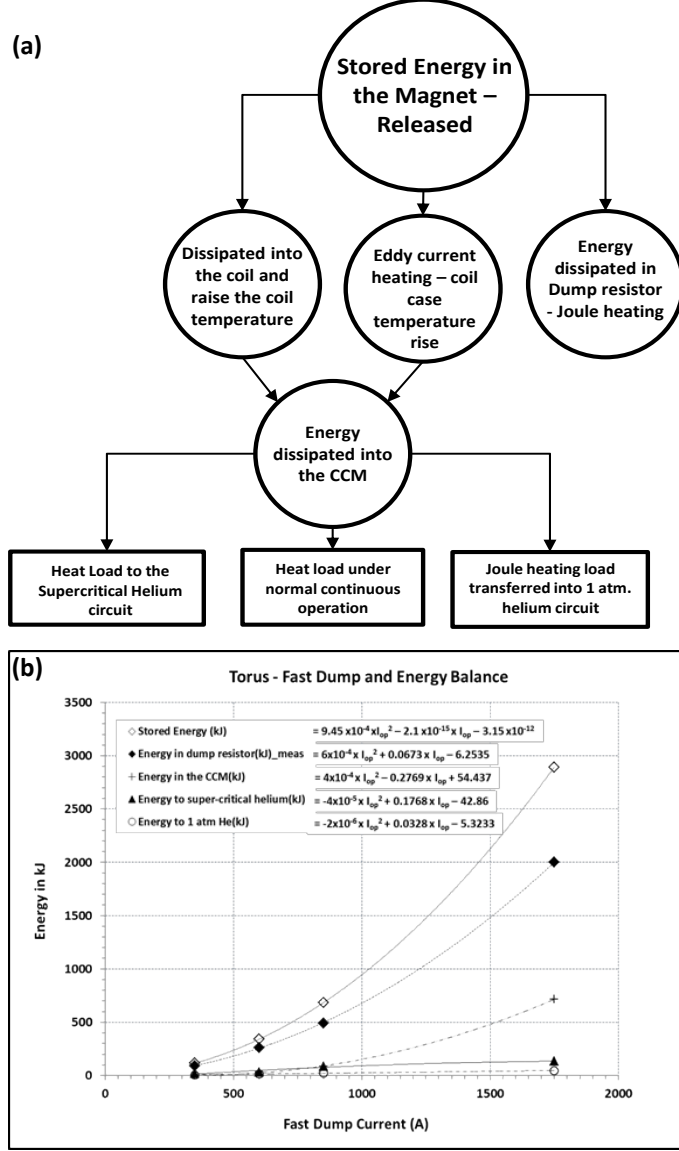


Fig. 52 Estimate of torus helium circuit pressure with time at increasing operating currents

However, in the 3.0 atm. circuit, during a relief event the highest system pressure is realized at a point in the circuit between relief valves, buried within the coils and re-coolers where flow may go both ways and the pressure is highest. Using the simple model to estimate the system pressure rise, (assuming all energy generated is transferred to the helium), the estimated

pressure rise (during a fast dump) is shown in [Figure 52](#). It is apparent that if all the energy from the 3000 A fast dump was transferred to the helium, the design pressure of 20.0 atm. of the system would be exceeded. However, using calculations from the detailed model, it was demonstrated that the 20.0 atm. pressure rating of the pipes would not be exceeded in the Torus circuit due to the distribution of energy throughout the entire system. Our commissioning tests have since validated the findings of this analysis.

Energy Dissipation during a Fast Dump



[Fig. 53](#) (a) Flow diagram representing the extraction of stored energy in the magnet during a fast dump or in the event of a quench, (b) Plots for the energy calculated based on the measured data during fast dump events at various operating currents up to 1750 A (approximated with a polynomial fit to the measured data points)

System Energy Balance Modelling - Before the commissioning tests, the system heat loads were estimated for each of the energization states to be carried out during commissioning. The estimates were developed using a Detailed Predictive Model (DPM), the details of which are calculated based on the Wilson model. The DPM assumes a fast dump releasing all the magnet-

stored energy ([Figure 53](#)). The DPM predicts that the torus was safe to operate for all energization states and fault scenarios up to the nominal operating current of 3770A.

After the initial testing, the magnet was ramped up to 3000 A and parked. During this period, an unexpected fast dump was triggered by the PLC comparator controls. Taking advantage of the captured data, the team evaluated the 3000A fast dump data and the results indicated that the magnet was safe to fast dump at 3770 A.

A maximum temperature (average for all CCM's) was recorded as <40 K during the 3000 A fast dump. The commissioning tests and analysis as carried out thus validated the pressure relief design and design assumptions for the torus cryogenic system confirming that the system was indeed safe.

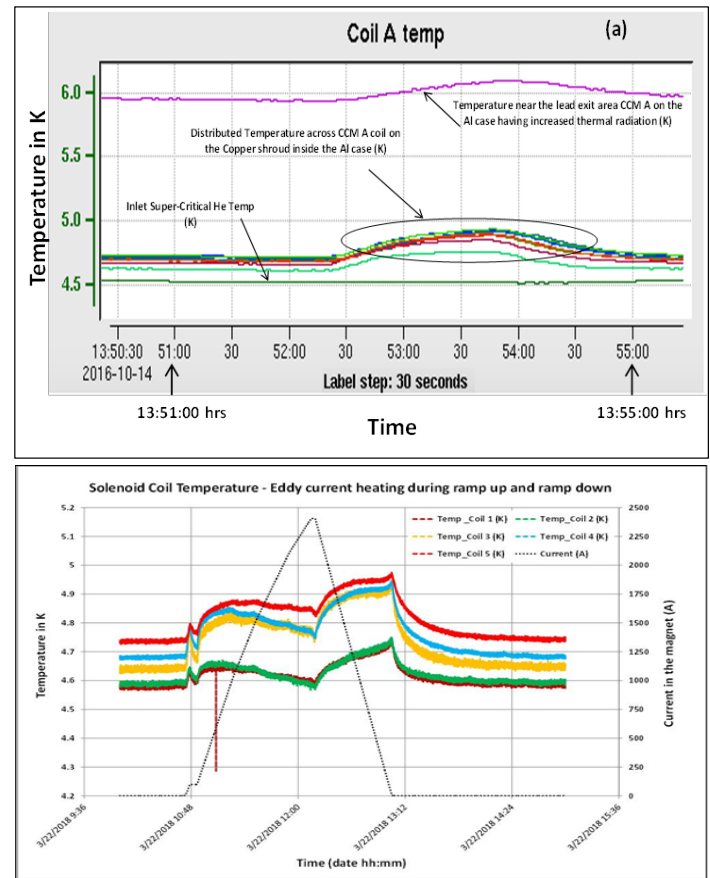


[Fig. 54](#) (a) Torus CCM B temperature rise during ramp to 150 A at 2 A/s due to eddy current heating, (b) A typical plot of temperature rise in the solenoid coils during normal ramp up and down

During commissioning, both the torus and solenoid were energized in steps to full operating current. Predetermined fast dumps were also carried out to check the instrumentation and magnet protection. Typical temperature rise of the torus and solenoid magnet coils during ramp up and down to full operating current is shown in [Figure 54](#) and are as a result of eddy current heating within the coils themselves. The temperature rises were modest (no higher than about 0.3 K) and well within the calculated 1.2 to 1.5K temperature margin of the coils but were nonetheless used to modify the ramp rates for both magnets to minimize eddy current heating.

As part of the commissioning process, several fast dumps

were carried out at low stored energies in the magnet and were found to match well with the predictive models. All tests carried out indicated that both magnets had more than adequate safety margins with regards to pressure relief of sub-systems and coil temperature rise. The coil temperatures recorded during a fast dump event, 3000 A (torus) and 2047 A (solenoid) are shown in Figure 55.

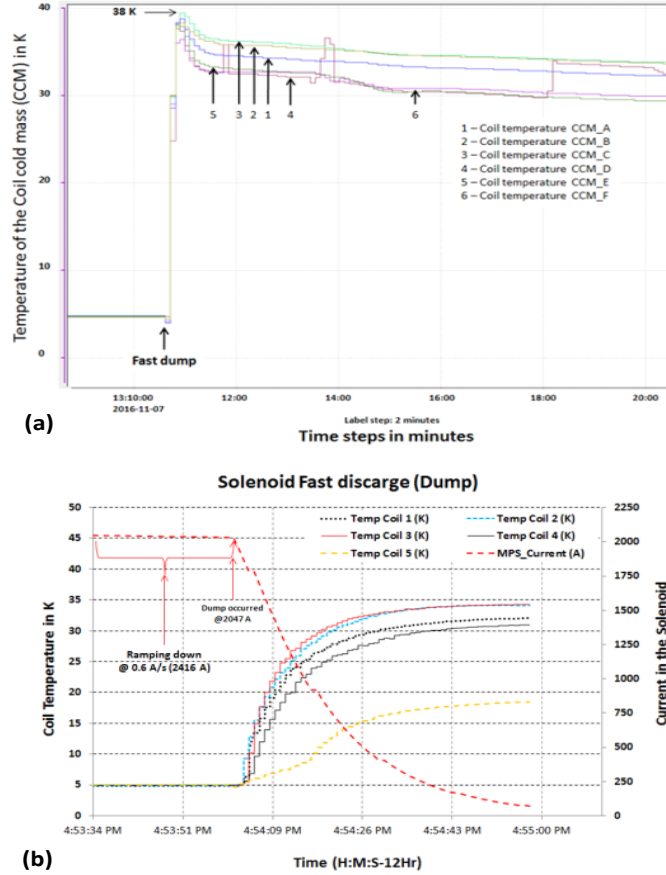


Fig. 55 Coil temperature rise - during a fast dump (a) Torus (b) Solenoid

As stated before earlier in this paper there is an electromagnetic coupling between the coil of the Torus and Solenoid. With the Torus ramped to full field (3770A) the figure below (Figure 56) shows the change in the OOPS load cell readings for the Torus CCM-A and also the radial and axial load cells for the solenoid during a ramp up to the full operating current (2416A) followed by a controlled ramp down to zero amps. As expected, the force experienced by the torus coil within its vacuum jacket during energization is not high enough to initiate a controlled ramp down of the magnet - based on the load cell limits defined. This behavior is demonstrated by all the 6 torus coils with only minor variations depending on the location of the coil due to gravity-loading. This behavior was also noted to be extremely repeatable following many cycles of magnet energization and de-energization. For the solenoid, it is encouraging to note that all the forces revert back to almost the original values after de-energization illustrating that none of the coil support structures has yielded and it has also been shown from subsequent runs that this process is very repeatable.

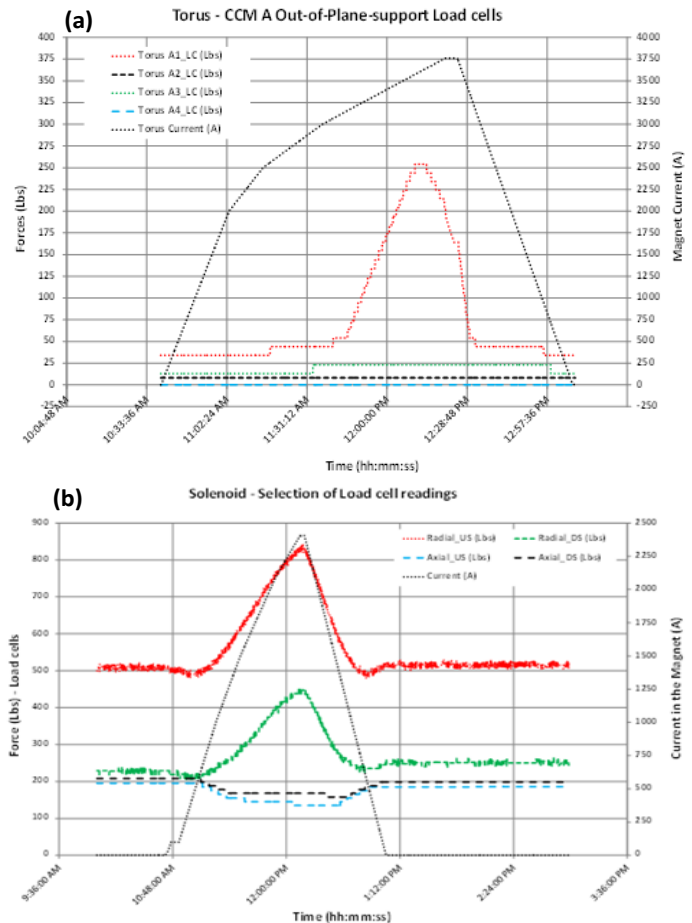


Figure 56 (a) Torus – Change in CCMA OOPS load cells during ramp up to the full operating current of 3770 A, followed by a controlled ramp down to zero amps, (b) Change in the radial and axial load cells on the solenoid during a ramp up to the full operating current of 2416 A followed by a controlled ramp down to zero amps

A. Field Mapping – Torus [26,27]

Forward tracks of charged particles (angles between 5° and 40°) are momentum analyzed by passing through the magnetic field of the torus. The magnet provides a $\int \mathbf{B} \cdot d\mathbf{l}$ of almost 3 T-m at 5° falling to about 1.0 T-m at 40° . The design requirements are given in Table XXV. Such forward tracks will first traverse the High-Threshold Cerenkov Counter (HTCC) and then enter the first drift chamber station at a distance of 2.1 m from the target. The track continues through the magnetic field region and its trajectory is measured in two more drift chambers located at 3.3 m and 4.5 m from the target, respectively. The three regions of drift chambers are expected to have spatial resolutions of about 300 μm per layer, which should allow determination of the momentum to better than 0.5 % accuracy. This sets the requirement that we know the $\int \mathbf{B} \cdot d\mathbf{l}$ to an accuracy of better than 0.3 % at small angles. Magnetic field measurement fixtures with locations are represented in Figure 57.

TABLE XXV
TORUS MAPPER SPECIFICATIONS SUMMARY

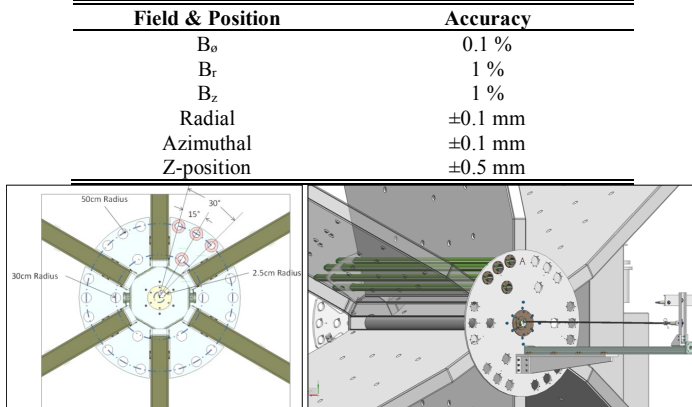


Fig 57 Magnetic field measurement locations – 4 locations in each quadrant and 7 locations in the bore (1 in the center and 6 spaced 60 degrees apart at a radius of 2.5cm) – field measured at 5 cm increments in Z (along the beam axis)

The original electromagnetic model was used to generate a field map. This model included thermal contraction but was based on the nominal coil design which did not include the real effects of “dog-boning” and compaction in the tight bend radii. The “dog-boning” of a winding of conductor is the phenomenon that occurs when multiple layers of insulated wire are wound around mandrels that have straight and circular sections such as a rectangle with rounded corners. As additional layers are added, the inner layers are compacted against the winding mandrel at the corners. This compaction tends to decrease the tension in the conductor. If enough compaction occurs then the conductor in the straight sections can go into compression, thus causing it to bow and create space between the turns. In order to avoid spaces between turns, pressure along the straight sections can in some cases re-establish the desired conductor location and spacing, the extra material then moves to the corners and this can create a shape that for long narrow coils resembles a dog-bone. As a result, this creates an uneven spacing of conductors with decreased packing density in some portion of the winding. Another cause of dog-boning is that during winding some portions of the conductor can be bent enough to yield into a permanent bend, but unless it is over-bent it will still have portions of it that are not yielded and will try to spring back into a straighter geometry. This effect produces different levels of radial stress around the winding and thus varies the compaction of the coil, which can affect the packing density.

As stated earlier in the coil fabrication discussion, spacers were added prior to the first potting to allow more accurate and consistent conductor positioning. Data from the optical surveys allowed better knowledge of the actual positioning of conductors within the coil (Figure 58). This was then used to create a new electromagnetic model of the coil. That model was compared with data from the field map.

Torus Design model and Analysis: The torus model coil design was carried out using commercial software TOSCA-Opera from Cobham and field maps were produced as the baseline for magnet field measurement (Figure 59). All design models are analyzed with cold dimensions at all times. The mapping of the field was carried out at 3000 A and the model data is scaled from 3770 A to 3000 A (3770 A being the full operating current

of the torus). The results obtained were significantly different from the original model data. The results were analyzed to calculate the “distortion field”, the difference between measured and calculated field values using Chi-squared function (χ^2) that compares the measured data deviation from the nominal modeled field data [28].

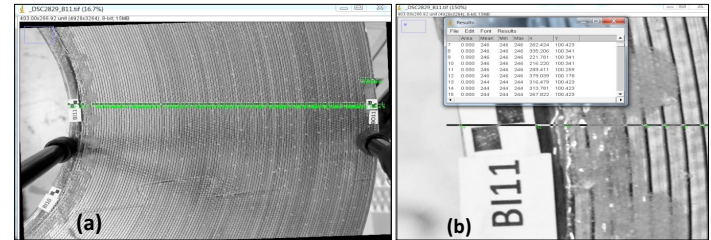


Fig 58 A close-up view of coil near one bend after 1st impregnation (a) Data capture-coil close-up mapping each turn location in the coil (b) Resulting coil co-ordinates from the mapped photos in (a).

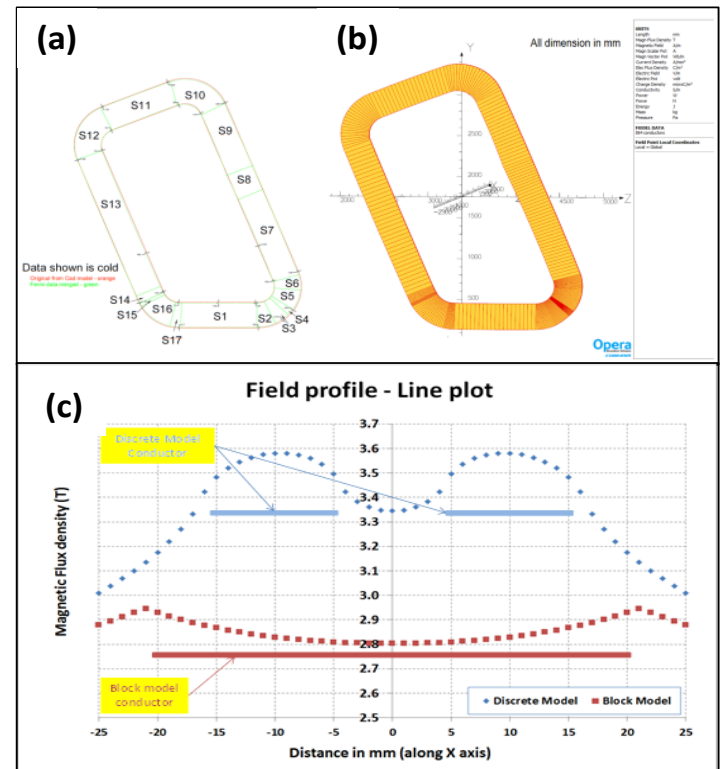


Fig 59 Single pancake of one torus coil (a) Coil survey points from 17 sections in the coil, (b) The design model prepared in Opera® with 17 sections and further discrete subsections, (c) Magnetic flux density variation near and though the coil case of the torus for a simplified version of the conductor (one large block) and refined model current is contained in 2 pancakes (Rutherford cable.)

The magnetic field modeling was improved via a 4-stage process:

- *Stage I: Symmetric “Block Model”* - Symmetric ideal coil model (nominal with cold coil dimension, 2 pancake coils simply modeled as one block);
- *Stage II: Asymmetric block model*- Block model combined with relocated coil position;
- *Stage III: Symmetric “Discrete Model”* - Symmetric coil model with surveyed conductor location (with cold coil dimension), with 2-individual pancakes; and

- Stage IV: Asymmetric Discrete Model – coil model with surveyed conductor locations combined with relocated coil positons

The absolute field data plot is presented in [Figure 60](#). The plots show that the variation in the magnetic field distribution is about +4.96 % for the block model and about -0.9 % for the discrete model in a sector (compared to the measurements).

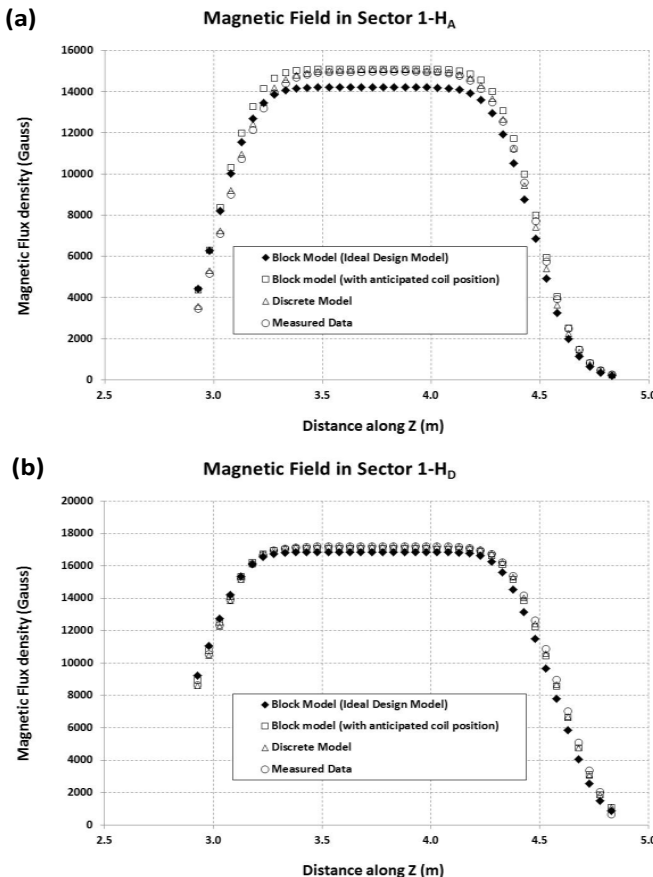


[Fig 60](#) Magnetic flux density distribution (a) sector 1 - H_A (b) sector 1 - H_D , between block model – symmetric, asymmetric and “discrete model” compared with measured data

Summary of findings - At distances far from the Hub and Coils, all models accurately represent the field, but since the detector needs a model that accurately represents the field at small angles (near the hub) as well as over the large angle in phi (from one coil to the next), only the discrete model can be used.

- a. The percentage variations cited are for one-to-one comparisons using the two-dimensional percentage analysis and the averages were calculated separately based on χ^2 .
- b. Average inner (30 cm) measurements indicate approximately a 0.5% deviation from the measured data
- c. Average outer (46.5 cm) measurements indicate approximately a 0.05% deviation from the measured data
- d. Fluctuations in the inner measurement deviations are consistent and attributed to the effect of a 1.5 mm change to the outer radius of the coil shape

Solenoid field mapping - Measurements were carried out to establish the following:

- a. To quantify the magnetic length of the solenoid.

- b. To verify the high homogeneity region (25mm diameter over 40mm length) at the center of the magnet.
- c. To measure the magnetic fringe fields at the specified detector locations.

The torus mapper was adapted for the field mapping of the solenoid magnet [29]. The mapper consisted of a digital voltmeter, 2" diameter carbon tube referenced to survey points, three single axis calibrated hall probes (one for each of the X, Y and Z axes) positioned in a cylindrical block of Teflon® spaced 5 cm apart in the Z-direction, control system (motion, data-recording, and interlocks). Commercially available Group 3 MPT-141 series transverse Hall probe with DTM-151 Teslameter was selected for the field measurement. The measurement accuracy at 25 °C with shielded cable of L300 mm x ø6.5 mm is $\pm (0.01\% \text{ of reading} + 0.006\% \text{ of full-scale})$ maximum. The hall probes are temperature compensated and were also surveyed to a positional accuracy of 0.040mm within the hall probe holder.

The sensor block is placed within a carbon-tube in order to zero the Z-position of the slide before the start of the Z-map for the particular location in question. The Z-map consisted of driving the sensor block in 5 cm steps along Z and pausing for 5 s for the Hall probes to settle before recording the probe data for each of the 3-sensors. The external fixture holds the 2" diameter carbon fiber tubes at precise X-Y positions and uses a linear stage drive to move the probes in the Z-direction as shown in [Figure 61a](#). [Figure 61b](#) shows the typical arrangement for solenoid magnet field measurement along the bore & off-center locations.

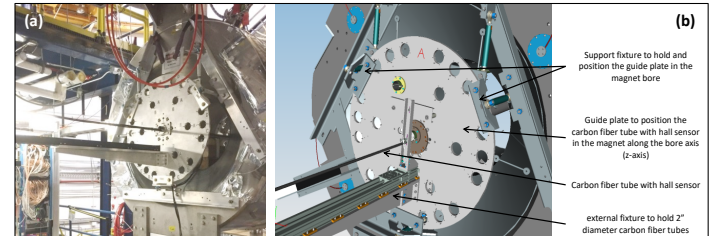


[Fig 61](#) Typical arrangement for solenoid magnet field measurement along the bore & off-center locations

During commissioning of the solenoid magnet, the field mapping was carried out at different operating currents in order to confirm the design specifications. Field mapping was performed along the Z direction at 9 locations; one at the geometrical center of the magnet and at 8 to 45 deg positions at a radius of 12.5 mm. The magnetic field was also measured along the z-axis at a 30 cm radius at a 60 deg angle from horizontal. For verifying the field homogeneity of the magnet, measurements were taken only in the central part of the magnet at 10 mm intervals along the z-axis.

The magnet length, L , $B_0^{-1} \int B dl$ measured 1.41 m. The measured homogeneity, $\Delta B/B_0$ in cylinder L40 mm length x ø25 mm is better than 300 ppm and acceptable for meeting Physics requirements. The measured magnetic fields at detector locations along with the magnetic length are summarized in Table 1. The fringe field measurement was done using a template board and a hand held field probe at representative detector locations. The central field at the solenoid is 5T, but Hall sensors were calibrated only to 3T, therefore, field mapping was limited to 3T

(1450 A operating current). The central field at higher current was verified using an NMR probe.

Another limitation of this mapper was the extent it can map in the Z-direction, because the linear stage is limited to about 1.9 m. The measured field in this length is compared with the model data to find the effective length of the magnet. Field mapping results are summarized in the Table XXVI below.

TABLE XXVI
SOLENOID – REQUIRED AND MEASURED PERFORMANCE PARAMETERS

Performance parameter	Broad Specification	Actual measured
B_0	5T	5.0 T
$L = B_0^{-1} \int B \cdot dl$ (B_0 field at the center (0,0,0) of solenoid)	$L = 1$ to 1.4 m	1.41 m
Field Uniformity in Target Area	$\Delta B/B_0 < 10^{-4}$ in cylinder 0.04 mm length x 0.025 mm (100 ppm)	318 ppm (to be improved using superconducting corrector coils around the target)
Field at HTCC PMTs location	$B < 35$ Gauss - for the four HTCC PMT locations	$B = 6\text{--}22$ Gauss
Field at TOF PMTs location	$B < 1200$ Gauss - for the two TOF PMT locations	$B = 43\text{--}1041$ Gauss

The mapped data was compared with the as-wound coil model data which also allowed for thermal contraction of the coils at 4.5K. There is still a slight discrepancy between the two data sets for the central field and the field at a radius of 30 cm. The ‘June model’ uses 5 conductors only (i.e. each of the 5 coils is treated as a single block of conductor). The ‘September model’ uses 208 block conductors, as follows - each layer for the inner and intermediate coils is assumed to be one block conductor while each layer for the shield coil has been split into 2 block conductors:

- 2*42 layers for inner coils (84 block conductors)
- 2* 46 layers for intermediate coils (92 block conductors)
- The shield coil has 16 layers, but each layer was divided into 2 block conductors (32 block conductors)

Each layer of the inner and intermediate coil is made up of as wound conductor data and in the shield coil each layer is divided in 2 conductors. The discrepancy between the model and measured data could be attributed to coil positioning errors or coil movement during energization. The theoretical model is being improved to better match the mapped data. One of these improvement iterations involves moving the inner and intermediate coils radially or axially - these results are shown in Figures 62, 63 and 64. This work is still in progress.

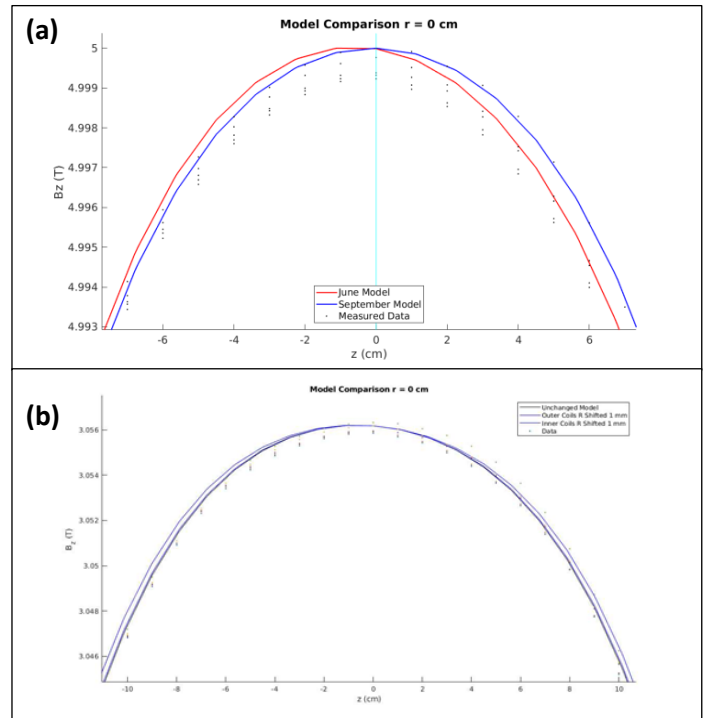


Fig 62 (a) Comparison of model and mapped data at the solenoid center, (b) Comparison of model and mapped data at $r=0$ cm with coils moved radially

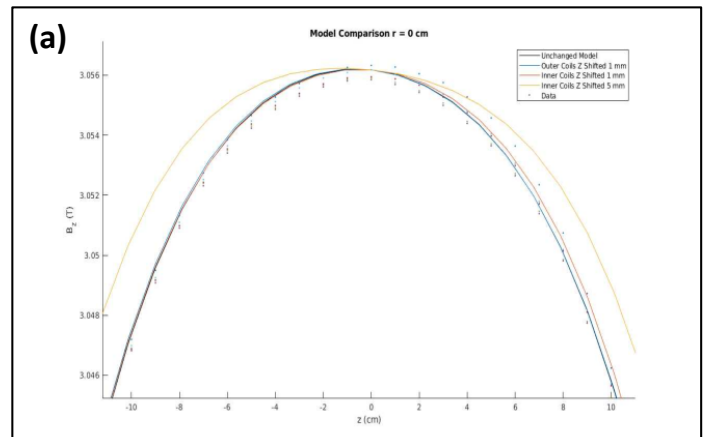


Fig 63 (a) Comparison of model and mapped data at $r=0$ cm with coils moved axially, (b) Comparison of model and mapped data at $r=30$ cm

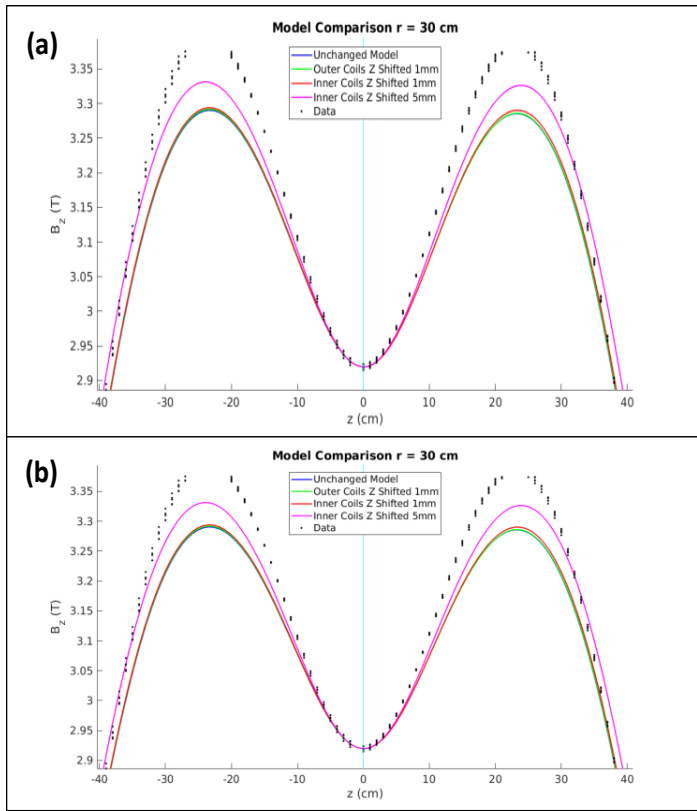


Fig 64 (a) Comparison of model and mapped data at $r=30$ cm with coils moved axially, (b) Comparison of model and mapped data at $r=30$ cm with coils moved radially

Summary

As with any typical project, the key drivers were technical reliability, schedule and cost. These drivers encouraged the team to adopt the FMEA methodology, initially to assist with the magnet design and instrumentation choices. In practice, the use of this methodology was expanded to also include the manufacturing, installation and commissioning stages for both magnets to great advantage. The skills and resourcefulness of the members of the 12GeV Magnet Task Force coupled with the commitment of the laboratory enabled Hall B to flex its planning, management and execution strategies to overcome all manner of obstacles which included sub-standard potting of torus coils, vendor quality issues on the distribution box, cool down issues involving vertical supports for the torus, the later than expected delivery of the solenoid to name the key ones.

Acknowledgements

The authors would like to acknowledge the contributions and support from all Hall B staff, the Detector Support Group and technicians at JLab. The authors would like to thank reviewers, and authors..... This material is based upon work supported by the U.S. Department of Energy, Office of Science, Office of Nuclear Physics under contract DE-AC05-06OR23177. The U.S. Government retains a non-exclusive, paid-up, irrevocable, world-wide license to publish or reproduce the published form of this manuscript, or allow others to do so, for United States Government purposes.

REFERENCES

- Fair, R. J. & Young, G. L., "Superconducting Magnets for the 12 GeV Upgrade at Jefferson Laboratory", *IEEE Transactions on Applied Superconductivity*, V25 (3), 2015, DOI - 10.1109/TASC.2014.2365737.
- Luongo, C., Ballard, J., Biallas, G., Elouadhriri, L., Fair, R., Ghoshal, P., et al., "The CLAS12 Torus Detector Magnet at Jefferson Lab.", *IEEE Transactions on Applied Superconductivity*, V26 (4), 2016, DOI - 10.1109/TASC.2015.2510336.
- Krave, S., Velev, G., Makarov, A., Nobrega, F., Kiemschies, O., Robotham, B., et al., "Overview of Torus magnet coil production at Fermilab for the Jefferson Lab 12-GeV Hall B upgrade", *IEEE Transactions on Applied Superconductivity*, V26 (4), 2016, DOI 10.1109/TASC.2016.2533264.
- Ghoshal, P. K., Biallas, G., Fair, R. J., Rajput-Ghoshal, R., Schneider, W., Legg, R., et al., "FMEA on the Superconducting Torus for the Jefferson Lab 12GeV Accelerator Upgrade", *IEEE Transactions on Applied Superconductivity*, V25 (3), 4901005, 2015, DOI - 10.1109/TASC.2015.2388591.
- Ghoshal, P., Pastor, O., Kashy, D., Schneider, W., Wiseman, M., Zarecky, M., et al., "Electromagnetic and Mechanical Analysis of the Coil Structure for the CLAS12 Torus for 12 GeV Upgrade", *IEEE Transactions on Applied Superconductivity*, V25(3), 4500705, 2015, DOI 10.1109/TASC.2014.2382604.
- de Hoog, F. R., Cozijsen, M., Yuen, W. Y. D. and Huynh, H. N., "Predicting Winding Stresses for Wound Coils of Linear Orthotropic material", in *Proc. Instrumentation Mech. Engineers, Part C, J. Mechanical Engineering Science*, 218 (C1), 13–25, 2004.
- Li, S and Cao, J., "A Hybrid Approach for Qualifying the Winding Process and Material Effects on Sheet Coil Deformation", *J. Engineering Materials and Technology*, V126, pp. 303-313, July 2004.
- Knight, C. E., "Residual Stress and Strength Loss in Filament-wound Composites", *Composite Materials: Testing and Design (Eighth Conference)*, Editor: J. D. Whitcomb, ASTM, 1988.
- Arp, V., "Stresses in Superconducting Magnets", *Journal of Applied Physics*, V48, No. 5, pp. 2026-2036, May 1977
- Pojer, M., Devred, A & Scandale, W., "A Finite Element Model for Mechanical Analysis of LHC Main Dipole Magnet Coils", *LHC Project Report 1001, Applied Superconductivity Conference (ASC 2006)*, 2006.
- Pastor, O., Willard, T., Ghoshal, P., Kashy, D., Wiseman, M., Kashikhin, V., Young, G., Elouadhriri, L., & Rode, C., "Structural Analysis of Thermal Shields During a Quench of a Torus Magnet for the 12 GeV Upgrade", *IEEE Transactions on Applied Superconductivity*, V25 (3), 2015, DOI-10.1109/TASC.2014.2371820.
- Kashikhin, V., Elouadhriri, L., Ghoshal, P., Kashy, D., Makarov, A., Pastor, et al., "Torus CLAS12-Superconducting Magnet Quench Analysis", *IEEE Transactions on Applied Superconductivity*, V24 (3), 2014, DOI - 10.1109/TASC.2014.2299531.
- Fazilleau, P., Ball, J., Hervieu, B., & Pes, C., "CLAS 12 Solenoid Magnet Technical Design Report", *Centre de Scalay, A-CRYOM-02-07-01-01-RTO5*.
- Rajput-Ghoshal, R., Ghoshal, P. K., Fair, R. J., Hogan, J., & Kashy, D., "An investigation into the electromagnetic interactions between a superconducting torus and solenoid for the Jefferson Lab 12 GeV Upgrade", *IEEE Transactions on Applied Superconductivity*, V25 (3), June 2015, DOI - 10.1109/TASC.2014.2372049.
- Ghoshal, P. K., Bachimanchi, R., Fair, R. J., Gelhaar, D., Kumar, O., Philip, S., & Todd, M., "Superconducting Magnet Power Supply and Hard Wired Quench Protection at Jefferson Lab for 12 GeV Upgrade", *IEEE Transactions on Applied Superconductivity*, V27 (8), 4703006, 2017, DOI - 10.1109/TASC.2017.2759280.
- Pfeffer, H., Flora, B., & Wolff, D., "Protection of Hardware: Powering Systems (Power Converter, Normal-Conducting, and Superconducting Magnets)", *US Particle Accelerator School, Batavia*, Aug 2016, DOI: 10.5170/CERN-2016-002.343
- Neilsen, C., "Design Report USA 502337-201, Hall B Torus/Solenoid MPS", *MPS 854 - Danfysik System 8500*, www.danfysik.com, June 2014.
- Ekelof, S., "The genesis of the Wheatstone bridge", *Engineering Science and Education Journal*, V10 (1), Feb 2001, DOI: 10.1049/esej:20010106
- Lakeshore Cryotronics - Cernox temperature sensor technical data (2017). http://www.lakeshore.com/Documents/_LSTC_appendixB_1.pdf, p168, Online at <http://www.lakeshore.com>
- Compact-sized FPGA development platform for prototyping circuit designs, <http://www.terasic.com.tw/cgi-bin/page/archive.pl?Language=English&CategoryNo=139&No=593>

21. Single Resistor Gain Programmable Precision Instrumentation Amplifier, Online link information at <http://cds.linear.com/docs/en/datasheet/1167fc.pdf>
22. Designers Guide for Applying Instrument Amplifiers Effectively, <http://www.analog.com/media/en/training-seminars/designhandbooks/designers-guide-instrument-amps-chV.pdf>
23. Wiseman, M., Elementi, L., Elouadhiri, L., Gabrielli, G., Gardner, T. J., Ghoshal, P. K., et al., "Design and Manufacture of the Conduction Cooled Torus Coils for The Jefferson Lab 12 GeV Upgrade", *IEEE Transactions on Applied Superconductivity*, V25 (3), 2015, DOI 10.1109/TASC.2014.2376964.
24. Legg, R., Kashy, D., Fair, R., Ghoshal, P., Bachimanchi, R., Bruhwel, K., et al., "Liquid Nitrogen Tests of a Torus Coil for the Jefferson Lab 12-GeV Accelerator Upgrade", *IEEE Transactions on Applied Superconductivity*, V25 (3), 2015, DOI - 10.1109/TASC.2014.2360139.
25. Ghoshal, P. K., Biallas, G., Fair, R. J., Kashy, D., Matalevich, J., & Luongo, C., "Commissioning Validation of CLAS-12 Torus Magnet Protection and Cryogenic Safety System", *IEEE Transactions on Applied Superconductivity*, V28 (6), 2018, DOI 10.1109/TASC.2018.2841928.
26. Fry, J. R., Ruggiero, G., Bergsma, F., "Precision Magnetic Field Mapping for CERN experiment NA62", *IOP Publishing, J. Phys. G: Nuclear Particle Physics* 43 (2016) 125004, DOI - 10.1088/0954-3899/43/12/125004
27. Ikeda, T., Chapman, M. D., Igarashi, Y., Imazato, J., Lee, J. M., Khabibullin, M. M., et al., "High-precision magnetic field mapping with a 3D hall probe for a T-violation experiment in $K_{\mu 3}$ decay", Elsevier Publications, *Nuclear Instruments and Methods in Physics Research, Sec A*, 401, pp243-262, 1997.
28. Ghoshal, P. K., Beck, J. M., Fair, R. J., Kashy, D., Mestayer, M. D., Meyers, J., Newton, J., Rajput-Ghoshal, R., Tremblay, K., Wiggins, C. L., "Magnetic Field Mapping of the CLAS12 Torus—A Comparative Study Between the Engineering Model and Measurements at JLab", *IEEE Transactions on Applied Superconductivity*, V29 (4), 4000310, 2019, DOI - 0.1109/TASC.2018.2884968.
29. Rajput-Ghoshal, R., Fair, R., Meyers, J., Beck, M., Brakman, D., Mestayer, M., et al., "Field Mapper for Superconducting Torus Magnet for the Jefferson Lab 12GeV Upgrade", *International Magnetic Meas. Workshop, IMMW-20*, Oxford (UK), June 2017 (Talk).